UNIVERSITY OF MISKOLC
FACULTY OF MECHANICAL ENGINEERING AND INFORMATICS



Tribological Behaviour of Hybrid Metal Matrix Composite Based Iron-Al_2O3-ZrO_2 Reinforced with Nanoparticles of Gr and MoS_2.

PHD THESES

Prepared by

Sulaiman Mustafa AL- Timmimi
Die and Tool Engineering (BSc),
Die Engineering (MSc)

ISTVÁN SÁLYI DOCTORAL SCHOOL OF MECHANICAL ENGINEERING SCIENCES
TOPIC FIELD OF DESIGN OF MACHINES AND STRUCTURES
TOPIC GROUP: PRODUCT DEVELOPMENT AND DESIGN

Head of Doctoral School

Dr. Gabriella Bognár
DSc, Full Professor

Head of Topic Group

Dr. Gabriella Bognár

Scientific Supervisor

Dr. Szávai Szabolcs
Associate Professor

Miskolc
2026

Table of Contents

List of Figures 4

List of Tables 6

Chapter One/Introduction ***7***

1.1 Metal Matrix Composites (MMCs) *7*

1.2 Powder Metallurgy (PM) *9*

1.3 Tribology of Metal Matrix Composites *11*

1.4 Wear and Friction *12*

1.5 Self-Lubricating Metal Matrix Composites *16*

Chapter Two / Literature review: 22

2.1 Introduction *22*

2.2 Summary of the Previous Survey *30*

2.3 Research gap and objectives *32*

Chapter Three / Raw Materials and Experimental Part 34

3.1 Raw Materials *34*

3.1.1 Matrix Raw Material 34

3.1.2 Reinforcement materials 34

3.1.3 Additive nano-materials 35

2.2 Preparation of Hybrid Metal Matrix Composite *37*

3.3 Design and Fabrication of Compacting Dies *39*

3.4 Techniques for Characterising the Hybrid Metal Matrix Composite *42*

3.4.1 Compressive strength test 42

3.4.2 Coefficient of friction 43

3.4.3 Wear Rate results of hybrid iron matrix composite 44

3.4.4 Hardness of the hybrid iron matrix composite 44

3.4.5 Scanning Electron Microscope of the hybrid iron matrix composite 45

Chapter Four /Results and discussion 46

4.1.1 Compressive strength of the hybrid iron matrix composite with the addition of nano-graphite 46

4.1.2 Coefficient of friction of the hybrid iron matrix composite with the addition of nano-graphite 47

4.1.3 Wear rate of the hybrid iron matrix composite with the addition of nano-graphite 51

4.1.4 Hardness of the hybrid iron matrix composite with the addition of nano-graphite 52

4.1.5 SEM and EDX of the hybrid iron matrix composite with the addition of nano-graphite 53

4.2 Characterisation of the hybrid iron matrix composite with the addition of nano-MoS_2 ..... *64*

4.2.1 Compressive strength of the hybrid iron matrix composite with the addition of nano-MoS_2 64

4.2.2 Coefficient of friction of the hybrid iron matrix composite with the addition of nano-MoS_2 64

4.2.3 Wear rate of the hybrid iron matrix composite with the addition of nano-MoS_2 69

4.2.4 Hardness of the hybrid iron matrix composite with the addition of nano-MoS_2 69
4.2.5 SEM and EDX of the hybrid iron matrix composite with the addition of nano-MoS_2 .70

Chapter Five /Conclusions 76
4.1 Conclusions of Adding Nano-Graphite : *76*
4.2 Conclusions of Adding Nano-MoS_2 : *76*
4.3 Conclusions on Adding Nano- Graphite and Nano-MoS_2.....*77*

THESES – NEW SCIENTIFIC RESULTS 78

List of Publications.....82

References: 83

List of Figures

***Figure 1**. Typical Outline of the Powder Metallurgy Process* ____ **9**

***Figure 2**.Schematic diagram of uniaxial die compaction* ____ **10**

***Figure 3.** MMC classifications* ____ **10**

***Figure 4**.At a sliding velocity of 1.85 m/s and an applied load of 10 N, wear rate variations* _ **13**

***Figure 5.** Illustration depicting how hard second-phase particles shield the ductile matrix* ___ **14**

***Figure 6**. Microscale mechanisms of frictional energy dissipation* ____ **16**

***Figure 7**.A diagram of the selection process for the ingredient of self-lubricating MMCs* ____ **16**

***Figure 8.** The chart presents the research conducted on different solid lubricants* ____ **17**

***Figure 9.** a) Nano graphite distribution in the matrix, b) graphite distribution in the matrix, c) contact profile of the nano graphite composite, d) contact profile of the graphite composite, e) and f) nano graphite reinforced composite conceptual wear generation model, g) and h) typical wear debris at 48 N and 0.77 m/s for copper nano graphite and copper graphite* ____ **19**

***Figure 10.** SEM of composite materials formed from MoS_2 and iron-based matrices* ____ **20**

***Figure 11.** Illustrated schematically for lamellar compounds MoS_2* ____ **20**

***Figure 12.** SEM micrographs of Fe at different magnifications.* ____ **34**

***Figure 13**. SEM micrographs of Alumina at 500 x magnification.* ____ **34**

***Figure 14**. SEM micrographs of ZrO_2 at different magnifications* ____ **35**

***Figure 15.** SEM micrographs of Nano Graphite at different magnifications.* ____ **36**

***Figure 16** .SEM micrographs of Nano Molybdenum disulfide (MoS_2)* ____ **36**

***Figure 17**. Scheme for the preparation of a hybrid metal matrix composite.* ____ **38**

***Figure 19**. Sample image before and after sintering* ____ **39**

***Figure 20.** Old Die of the compression test specimen* ____ **40**

***Figure 21**.Specimen made from a normal die* ____ **40**

***Figure 22**.Parts of the new die* ____ **41**

***Figure 23**.Assembly of new die.* ____ **41**

***Figure 24**. Specimen made by a new die* ____ **42**

***Figure 25.** The compressive strength instrument and sample images* ____ **42**

***Figure 26**.Friction and wear test* ____ **44**

***Figure 27**.Hardness test* ____ **45**

***Figure 28**. Compressive strength of iron, master composite and iron matrix composite* ____ **46**

***Figure 29**. Coefficient of friction during the time of iron, master composite and iron matrix composites with varying concentrations (0.5, 1, and 1.5 vol.%) of nano-Gr* ____ **48**

***Figure 30.** Coefficient of friction for iron, master composite and iron matrix composites* ____ **50**

***Figure 31**.Graphite structure* ____ **51**

***Figure 32**. wear rate of iron, master composite and iron matrix composites with varying co* **52**

***Figure 33.** Hardness of iron, master composite and iron matrix composites* **52**

***Figure 34** . The SEM micrographs of the pure iron reference sample at various* **54**

***Figure 35**.The elemental purity and presence of a baseline native oxide phase of the compacted and sintered pure iron* **55**

***Figure 36**. EDS spectrum of the iron-metal matrix composite (Fe-MMC) obtained from Site 8 for a total of 36,431 counts* **56**

***Figure 37.** Compacted iron-metal matrix composite micrographs* **56**

***Figure 38.** The SEM images of the compacted and sintered hybrid metal matrix composite* **58**

***Figure 39.** Surface energy-dispersive X-ray spectroscopy (EDS) spectrum of the sintered hybrid metal matrix composite (Fe - Al_2O_3 - ZrO_2 / 0.5 vol.% nano-graphite),* **59**

***Figure 40.**The SEM images of the compacted and sintered hybrid metal matrix composite specimen at various magnifications* **60**

***Figure 41.** Surface energy-dispersive X-ray spectroscopy (EDS) spectrum of the sintered hybrid metal matrix composite (Fe - Al_2O_3 - ZrO_2 / 1.0 vol.% nano-graphite)* **61**

***Figure 42**. Compacted and sintered SEM images of the hybrid metal matrix composite (1.5 vol. % nano-graphite) at various magnifications* **62**

***Figure 43**. Energy-dispersive X-ray spectroscopy (EDS) spectrum recorded from the surface of the sintered hybrid metal matrix composite with 1.5 vol. % nano-graphite addition* **63**

***Figure 44.** Compressive strength of iron, master composite and iron matrix composites with varying concentrations (0.5, 1, and 1.5 vol.%) of nano-MoS_2* **64**

***Figure 45**. Coefficient of friction over time of iron, master composite and iron matrix composites with varying concentrations (0.5, 1, and 1.5 vol.%) of nano-MoS_2* **66**

***Figure 46**.Coefficient of friction of iron, master composite and iron matrix composites with varying concentrations (0.5, 1, and 1.5 vol.%) of nano-MoS_2* **67**

***Figure 47.** Crystal structure of monolayer MoS_2* **68**

***Figure 48**.Wear rate of iron, master composite and iron matrix composites with varying concentrations (0.5, 1, and 1.5 vol.%) of nano-MoS_2* **69**

***Figure 49**. Hardness of iron, master composite and iron matrix composites with varying concentrations (0.5, 1, and 1.5 vol.%) of nano-MoS_2* **70**

***Figure 50**. The depiction of the Fe-Al_2O_3-ZrO_2 / 0.5 vol.% Nano-MoS_2 hybrid metal matrix composite at different magnifications.* **70**

***Figure 51.** The energy-dispersive X-ray spectroscopy (EDS) spectrum of the compacted and sintered Fe-Al_2O_3-ZrO_2 / 0.5 vol % Nano-MoS_2 hybrid metal matrix composite* **71**

Figure 52**. Scanning electron microscopy (SEM) micrographs of the Fe-Al_2O_3-ZrO_2 / 1.0 vol.% nano-MoS_2 hybrid metal matrix composite at various magnifications* ***72

Figure 53.** The energy-dispersive X-ray spectroscopy (EDS) spectrum of the compacted and sintered Fe-Al_2O_3-ZrO_2 / 1.0 vol.% nano-MoS_2* ***73

Figure 54**. Scanning electron microscopy (SEM) micrographs of the Fe-Al_2O_3-ZrO_2 / 1.5 vol.% nano-MoS_2 hybrid metal matrix composite at various magnifications* ***74

Figure 55.** The energy-dispersive X-ray spectroscopy (EDS) spectrum of the compacted and sintered Fe-Al_2O_3-ZrO_2 / 1.5 vol.% nano-MoS_2 hybrid metal.* ***75

List of Tables

Table 1:** A comparison of metallic matrix materials and their potential limitation* ***7

Table 2**. Mechanical, structural, and characteristics of hard particle reinforcements* ***8

Table 3.** Compacting Pressures for Various Applications of Powder Materials* ***8

Table 4.** Typical sintering temperatures for some common metals and materials* ***10

Table 5.** Summary of Literature Survey* ***30

Table 6.** Nano Molybdenum disulfide (MoS_2) properties.* ***37

Table 7.** Composition of Metal matrix composite (Master Matrix)* ***37

Table 8.** Composition of Metal matrix composite with nano-graphite and nano-MoS2* ***37

Table 9.** Sintering Conditions* ***38

Table 10**. Chemical Composition of Steel (DIN EN 1006-2)* ***39

Chapter One/Introduction

1.1 Metal Matrix Composites (MMCs)

Metal matrix composites (MMCs) represent a cutting-edge class of materials that combine metals with reinforcing elements, typically ceramics or other high-performance substances, to deliver properties far superior to those of conventional metals. These composites offer a distinct range of advantages, including increased strength, improved stiffness, enhanced wear resistance, and greater thermal stability, all while retaining the lightweight nature of the metal matrix. The ability to customize these properties makes MMCs particularly valuable for industries with rigorous performance requirements, such as aerospace and automotive, where materials must withstand extreme heat, pressure, and mechanical stress. MMCs excel in offering tailored property combinations, including greater toughness and corrosion resistance, solidifying their role as a pivotal advancement in modern materials engineering [1,2].

The matrix in a metal matrix composite (MMC) is a continuous, uniform substance that serves as the framework that holds and supports the reinforcing elements. To form MMCs, a reinforcing material, often hard ceramic particulates or fibres like silicon carbide (SiC) or graphite (Gr), or alumina (Al_2O_3), is dispersed within the metal matrix [3,4]. These MMCs, usually composed of low-density metals like aluminium or magnesium, offer superior performance compared to unreinforced metals. They excel in properties such as specific stiffness, strength-to-weight ratio, higher working temperatures, and resistance to wear and corrosion. Furthermore, these properties can be precisely tailored to meet the requirements of specific applications (see Table 1).

Table 1: A comparison of metallic matrix materials and their potential limitations[5]

Matrix material	Density (g/cm^3)	Major drawbacks to be filled by reinforcements
Al	2.70	1. Temperature range restricts its potential application in high temperatures. 2. Low hardness and strength. 3. Low wear and corrosion resistance, rapid creep rate, and chemical reactivity. 4. Low tensile and compressive strength, as well as low creep resistance. 5. Low hardness. 6. Problem with powder formation and diffusion bonding due to chemical reactivity and oxide development. 7. Low tensile yield strength, low hardness and wear and corrosion resistance.
Mg	1.74	
Cu	8.92	
Fe	7.87	

For example, aluminium, being one of the least dense materials after magnesium, offers excellent strength while remaining lightweight, making it ideal for many lightweight engineering applications [4].

The size, shape, percentage, and distribution of particulate reinforcement to metal matrix significantly influence the performance of the resulting composite, making them a key factor in the design of advanced MMCs for industries like aerospace, automotive, and manufacturing.

Hybrid composites utilise two or more types of dispersed phases within the same matrix, offering enhanced performance compared to single-reinforced composites. For example, combinations such as silicon carbide (SiC) with aluminium oxide (Al_2O_3), aluminium oxide with graphite (Gr), or a blend of SiC, Al_2O_3, and graphite can be employed. This multifaceted approach allows for the synergistic effects of different reinforcements, leading to improved mechanical properties, thermal stability, and wear resistance. By strategically selecting and combining various reinforcement materials, hybrid composites can be tailored to meet specific application requirements, making them particularly valuable in industries that demand high-performance materials [6],[7]. Table 2 presents an overview of the most commonly used ceramic particles in metal matrix composites (MMCs), along with their physicomechanical properties [8],[9].

Table 2. Mechanical, structural, and characteristics of hard particle reinforcements in MMC_S [8 ,9].

Property	SiC	B_4C	Al_2O_3	TiC	ZrB_2	TiB_2	AlN
Density (g/cm^3)	3.2	3.52	3.96	4.93	6.09	4.52	3.26
Metaling pt.(°C)	2730	2350	2054	3076	3010	3225	2200
HV (GPa)	35-45	----	11-20	24-32	22-26	25-35	11.8
E (GPa)	450	308	390	395	350	550	330
CTE,α (10^{-6}/K)	4.3	5.0	8.1	8.05	5.3	7.4-8.6	5.27
TC σ (W/nK)	12-22	17-40	28-32	17-30	23	60-120	280
Crystal Structure	H	R	H	C	H	H	W
E is elastic modulus, HV is Vickers hardness, H is hexagonal, C is cubic, R is Rhombohedral, and W is wurtzite.							

1.2 Powder Metallurgy (PM)

Powder metallurgy (PM) is an advanced manufacturing process that involves producing metal components from powdered metal. It is a highly efficient and versatile technique widely used in industries ranging from automotive to aerospace, electronics, and medical devices. Compressing metal powders into desired shapes and then sintering them at high temperatures allows powder metallurgy to create complex, high-performance parts with minimal material waste. This process is known for its ability to produce components with precise dimensions, tailored material properties, and cost-effective production, making it an essential method in modern engineering and manufacturing [10]. Fine metal powders undergo a series of carefully controlled steps in powder metallurgy to create composite materials, as shown in Figure 1.

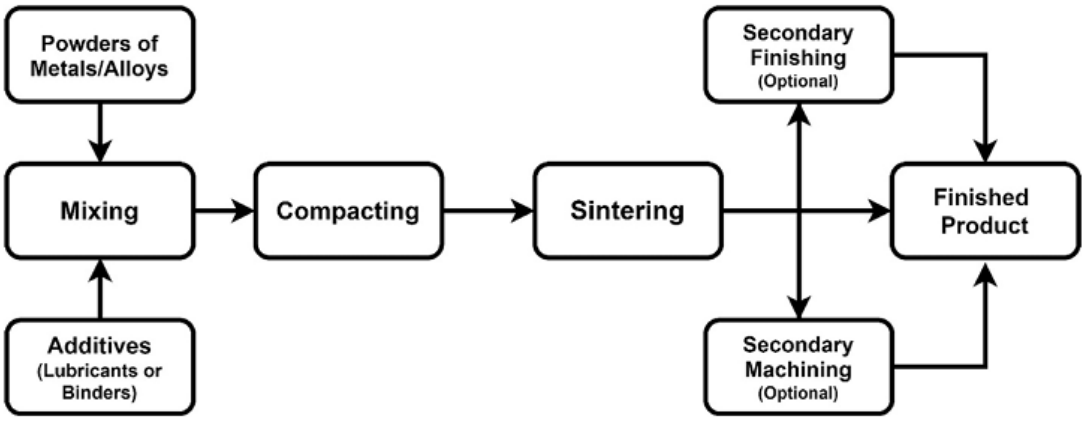


Figure 1. Typical Outline of the Powder Metallurgy Process [8].

The manufacturing process with the powder metallurgy process steps:

1. Mixing – Blending and mixing powders are essential for the uniformity of the product. Binders and /or lubricants are added to the blend before mixing powders. The function of a lubricant is to minimise wear and to reduce friction. Different powders in correct proportions are thoroughly mixed either wet or in a ball mill [11].
2. Compacting is a process that involves filling a die with powder, compressing the powder using rigid punches to form a dense compact, and ejection from the die [12]. Uniaxial die compaction is a compaction process of a powder within a die cavity by the action of an upper punch at a constant velocity, while the lower punch does not move within the mechanical assembly, as shown in Figure 2. The mixed powder composite is then compacted to shape a rigid steel die or carbide die at pressures of (150-900 MPa). At this stage, the compacts preserve their shape by features of cold-welding of the powder

composite grains within the mass [13]. Table 3 shows typical compacting pressures for various materials.

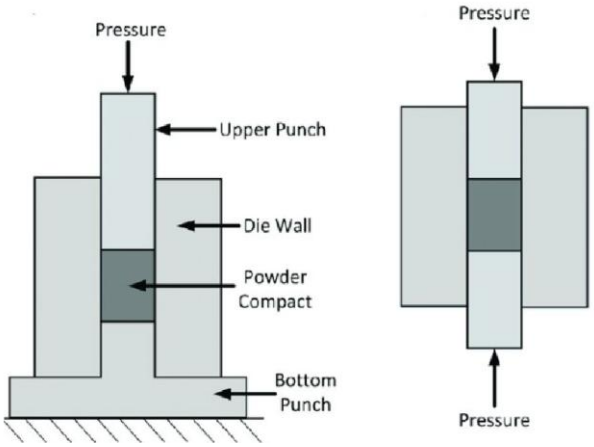


Figure 2.Schematic diagram of uniaxial die compaction [14].

Table 3.Compacting Pressures for Various Applications of Powder Materials [15, 16].

Applications	Pressure (N/mm²)	Pressure (Tons/in²)
High-density iron and steel parts	690-1650	50-120
High-density copper and aluminum parts	250-275	18-20
Machine parts(medium-density iron and steel)	275-690	20-50
Porous bearings	146-350	10-25
Refractory metals and carbides	70-200	5-15
Porous metals with filters	40-70	3-5

3-Sintering – "Sintering is a key part of the PM process". Table 4 shows typical sintering temperatures for some common metals and materials. " It is during this step that the consolidated powder compact acquires the strength needed to fulfill its intended use as an engineering product; for example, as sintered structural parts and gears for automotive and other applications, sintered self-lubricating bearings, sintered magnets, and a host of other types of PM materials. The ISO definition of the term "sintering" reads: "The thermal treatment of a powder composite or compact at a temperature under the melting point, for increasing strength by bonding particles together" [17, 18].

Table 4. Typical sintering temperatures for some common metals and materials [17]

Metal	**Sintering Temperature (°C)**
Aluminum alloys	560-620
Brass	850-950
Copper	750-1000
Iron/steel	1100-1200
Stainless steel	1200-1280
Cemented carbides	1350-1450
Molybdenum	1600-1700

1.3 Tribology of Metal Matrix Composites

Metal matrix composites (MMCs) represent a cutting-edge class of materials that combine metals with reinforcing elements, typically ceramics or other high-performance substances, to deliver properties far superior to those of conventional metals. These composites offer a distinct range of advantages, including increased strength, improved stiffness, enhanced wear resistance, and greater thermal stability, all while retaining the lightweight nature of the metal matrix. The ability to customise these properties makes MMCs particularly valuable for industries with rigorous performance requirements, such as aerospace and automotive, where materials must withstand extreme heat, pressure, and mechanical stress. MMCs excel in offering tailored property combinations, including greater toughness and corrosion resistance, solidifying their role as a pivotal advancement in modern materials engineering [18,19].

The matrix in a metal matrix composite (MMC) is a continuous and uniform substance and serves as the framework that holds and supports the reinforcing elements. To form MMCs, a reinforcing material, often hard ceramic particulates or fibres like silicon carbide (SiC) graphite (Gr), or alumina (Al_2O_3) is dispersed within the metal matrix [20]. These MMCs, usually composed of low-density metals like aluminium or magnesium, offer superior performance compared to unreinforced metals. They excel in properties such as specific stiffness, strength-to-weight ratio, higher working temperatures, and resistance to wear and corrosion. Furthermore, these properties can be precisely tailored to meet the requirements of specific applications. For example, aluminium, being one of the least dense materials after magnesium, offers excellent strength while maintaining low weight, making it ideal for many lightweight engineering applications [21]. MMCs are classified as shown in Figure 3.

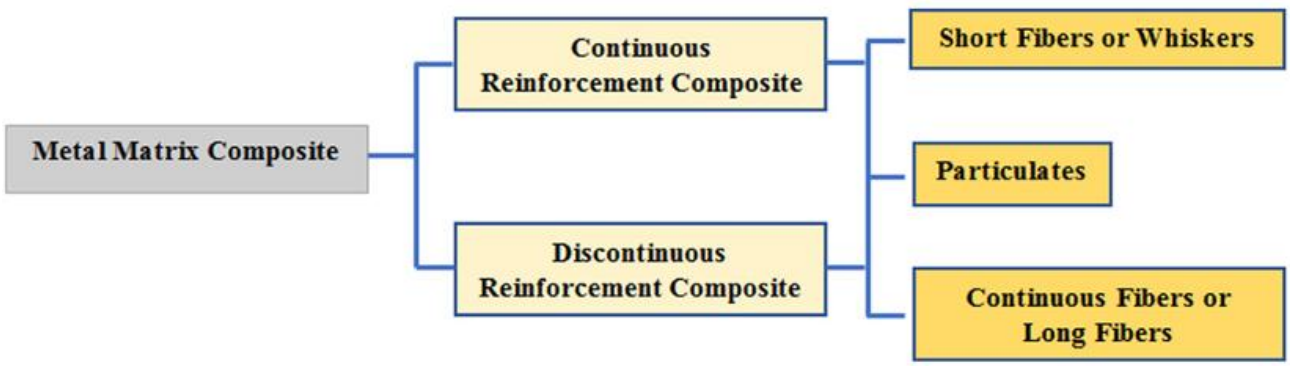


Figure 3. MMCs classified [22].

The wear and friction performance of Metal Matrix Composites (MMCs) is a function of the amount, size, shape and distribution of the embedded fibres or hard/soft particles in the matrix. Moreover, the strength of the interfacial bonding between the reinforcements and the matrix is a critical factor in determining the mechanical and tribological properties of MMCs. It has been reported that incorporating hard particles as reinforcement increases the strength and wear resistance of MMCs. However, this improvement is associated with reduced ductility. In contrast, soft particles act as solid lubricants, which reduce the coefficient of friction of MMCs. Nevertheless, there are times when incorporating reinforcements and solid lubricants into the composites can result in unforeseen material behaviour and varying performance [23].

Friction and wear are typical phenomena that take place during the movement of solid surfaces, resulting in energy loss and material degradation. However, before engaging in the lubrication of contacting surfaces, it is always checked if the materials in question are not those that have a naturally low coefficient of friction and high wear rates. Such materials are known as self-lubricating materials.

1.4 Wear and Friction

Wear is the descriptive term for the progressive loss of material by way of relative motion between the surface and the contacting substance(s). A great number of studies have been performed on the tribological properties of Metal Matrix Composites (MMCs) and most of the studies available report that MMCs have better wear resistance than the unreinforced matrices. For instance, results show that MMCs have better wear resistance than their unreinforced counterparts, as shown in Figure 4. For example, a SiC particle-reinforced Al6061 MMC was found to have better wear characteristics than the unreinforced Al6061 alloy. However, in specific cases, the wear resistance of the MMCs may be comparable to or even worse than that of the unreinforced materials, which underscores the role of material composition, operating conditions, and reinforcement parameters on the wear behaviour [24].

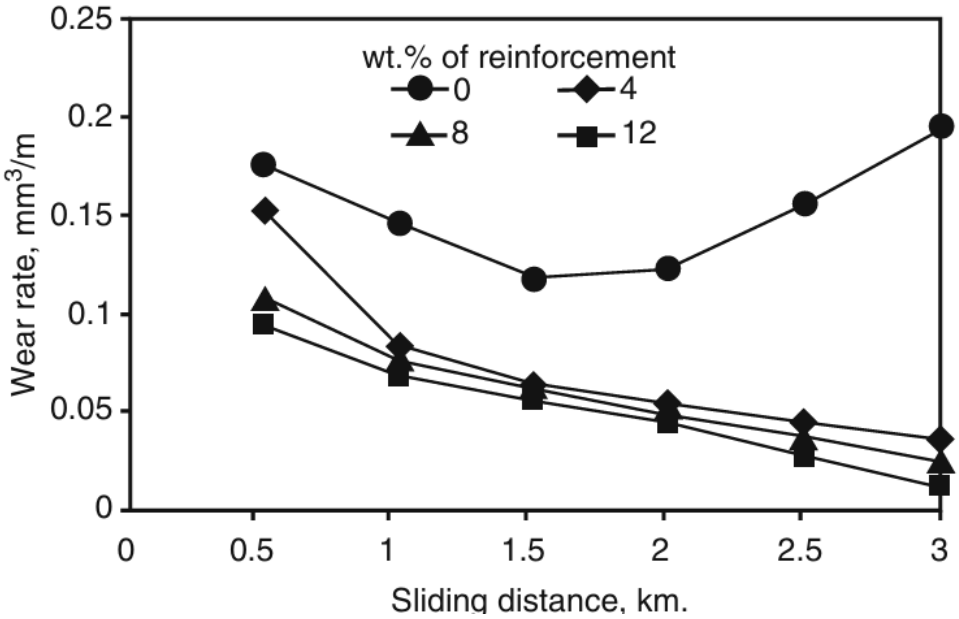


Figure 4.At a sliding velocity of 1.85 m/s and an applied load of 10 N, wear rate variations with sliding distance for Al6061-based MMC [25].

Different wear mechanisms can happen during the relative motion of surfaces in contact. These mechanisms are adhesive wear, abrasive wear, delamination wear, erosive wear, fretting wear, fatigue wear, and corrosive/oxidative wear. Out of these, the most frequent wear mechanisms in Metal Matrix Composites (MMCs) are adhesive wear, abrasive wear, fatigue wear, and corrosive/oxidative wear. Adhesive wear is the process of sticking two metallic surfaces together when they move relatively against each other under an applied load. The action of the normal force is to distribute the load to the asperities, which results in very high pressure being exerted over a very small area. This results in plastic deformation at the asperities to increase the real area of contact to support the load. Finally, the high-quality short-range forces come into play, and adhesive junctions may form at the real contact area. During relative motion, these adhered junctions are sheared. The term 'adhesive' is due to the formation of very strong metallic bonds at the asperities of the contacting surfaces. Abrasive wear occurs when a coarser and harder surface is pushed past a softer tone. It can also occur when hard particles which are interposed between the surfaces act as a medium of abrasion. Although abrasive wear can be caused by metallic and non-metallic particles, non-metallic particles are the most common cause of abrasion in MMCs. The environment and the mating material surfaces play a key role in the wear process dynamically. Corrosive wear is a form of wear that occurs when the contacting surfaces come into contact with the environment, resulting in the formation of reaction products at the asperities. In the case of sliding interactions, the wear of these reaction

products takes place using cracking or by abrasive action. In other words, corrosive wear is a combination of corrosion and rubbing, which removes the reaction products from the material surfaces in contact[25],[26]. Fatigue wear occurs on the surface of materials that are operated under cyclic loading conditions such as ball bearings and gears, which are prone to fatigue wear due to the existence of cyclic stresses during service. The opposite force that resists motion, known as friction, is defined by the coefficient of friction (μ), a scalar value without a magnitude. This coefficient is defined as the ratio of the force of friction (F) to the normal force (P) that is used to press two bodies together and does not have any units as it is a dimensionless scalar. It is usually written in the following form:

$$\mu = F / P$$

Different factors are effective in the wear and friction behavior of Metal Matrix Composites (MMCs). The three key groups of tribological parameters that govern wear and friction can be categorized as follows [25, 27]:

1. Material Factors (intrinsic to the material): These are characteristics of the reinforcement, such as the type of reinforcement, its size, shape, volume fraction, and the microstructure of the matrix. These material properties are responsible for how the composite behaves when it is in contact with other surfaces during relative motion.

2. Mechanical Factors (extrinsic to the material): These factors are relative to the application conditions of the material, i.e., normal load, sliding velocity, and sliding distance. It is these mechanical conditions that are the principal controller of the friction and wear of the material. 3. Physical Factors (extrinsic to the material): Other environmental factors, e.g., temperature, are also key in the tribological behaviour of MMCs. A temperature change and the surrounding atmosphere can be detrimental or beneficial to the material's friction and wear properties, thus affecting its performance.

The incorporation of reinforcement particles is critical in determining the wear resistance of Metal Matrix Composites (MMCs). It is a general observation that increasing the reinforcement level enhances the wear resistance of these materials. This improvement is mainly ascribed to the rise in the material properties like hardness and strength that are observed with increasing the volume fraction of the reinforcement. This trend has been reported in several MMCs, which include Al–Fe composites, AZ91D-0.8% Ce alloys reinforced with Al_2O_3 short fibres and graphite, nickel matrix composites reinforced with graphite and MoS_2, and steel matrix composites reinforced with (W, Ti)C particles. When two surfaces are brought into contact, under sliding conditions, the hard second-phase

particles act as a shield to the metal matrix and avoid its wear [28]. On the flip side, the particles can detach from the matrix and then the matrix will suffer from higher wear rates due to the abrasive particles. At a certain volume fraction, the reinforcement particles give the best protection to the matrix material. In Figure 5, this protection mechanism is shown where hard second-phase particles shield the ductile matrix from abrasive particles. Also, the increase in the volume fraction of the reinforcement decreases the amount of plastic deformation in the layer immediately below the worn surface and hence the adhesive wear in the composite [26, 28].

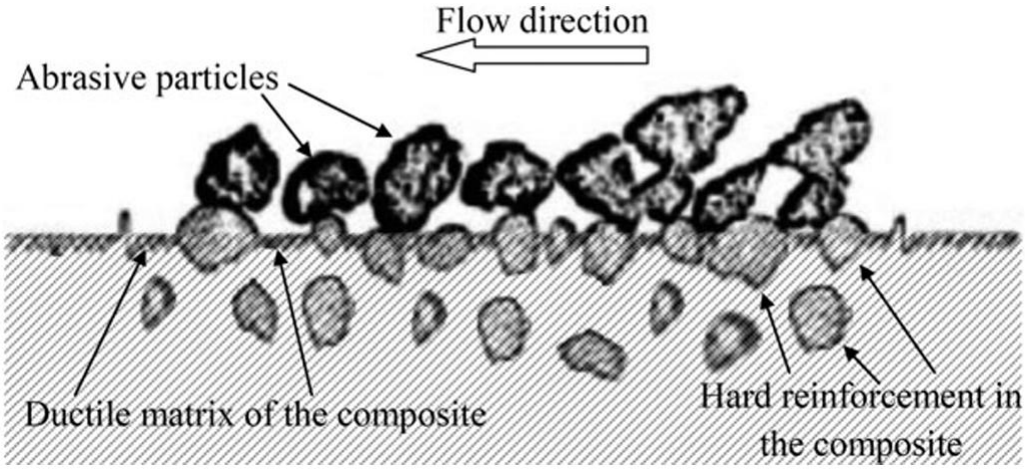


Figure 5.illustration depicting how hard second-phase particles shield the ductile matrix from abrasion [29].

Commonly, friction is evaluated using the coefficient of friction and wear rate. The effective minimising of frictional losses is crucial to understanding the fundamental atomistic mechanisms that contribute to these losses. Friction arises from heat generation due to a combination of physical, mechanical, and chemical interactions occurring at the interface of sliding surfaces. While, the complexity of these interactions, along with the absence of a unified theoretical model, makes it challenging to quantify the individual contributions of each factor. The various established mechanisms responsible for heat generation at the atomic during sliding [30]. The mechanisms of a deeper theoretical understanding of friction are provided [22], as shown in Figure 6.

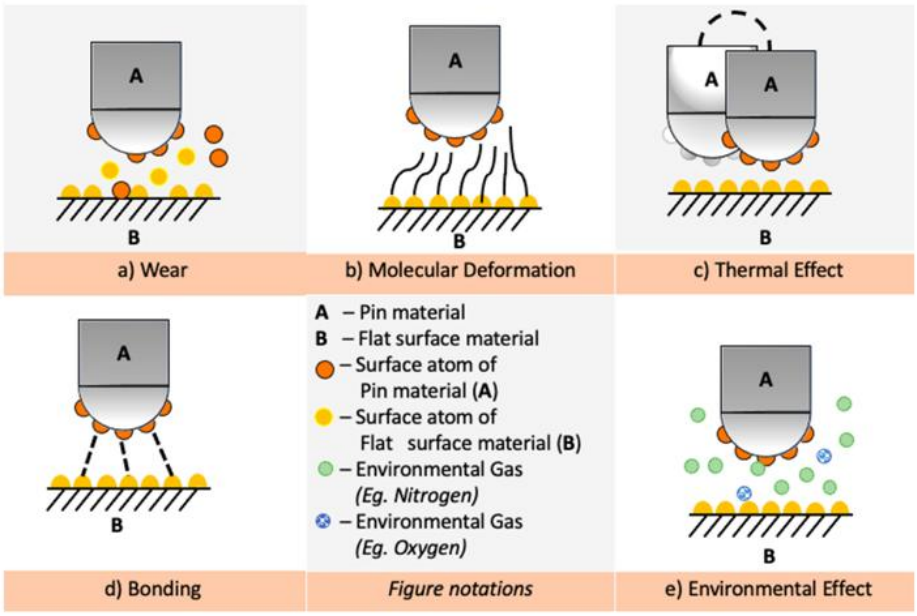


Figure 6. Microscale mechanisms of frictional energy dissipation: (a) Wear mechanism; (b) Molecular deformation; (c) Thermal Effect; (d) Bonding; and (e) Environmental effect[22], [30].

1.5 Self-Lubricating Metal Matrix Composites

The reinforcement and metal matrix selection present a challenge in the design and fabrication of self-lubricating metal-based materials, as shows in Figure 7.

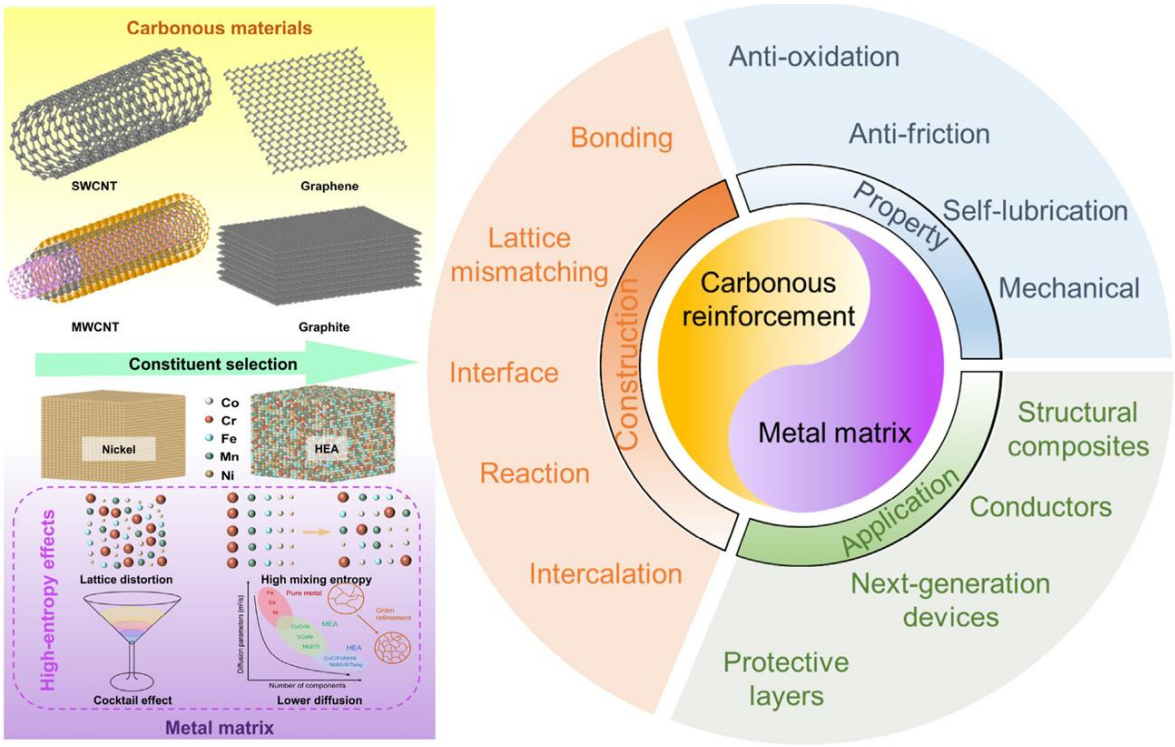


Figure 7.A diagram of the selection process for the ingredient of self-lubricating MMCs [31].

While the lubricating phase is crucial, the choice of metal matrix is equally significant for the performance of self-lubricating MMCs. Currently, lightweight metal MMCs are extensively utilized across various industrial applications due to their advantageous properties. Additionally, high-entropy alloys (HEAs) have garnered significant attention for their exceptional characteristics, including the high-entropy effect, cocktail effect, slow diffusion, and lattice distortion. Their compositional tunability makes them a promising candidate for the development of self-lubricating metal matrices [31].

In sliding applications, liquid or grease-based lubricants are commonly employed to facilitate relative motion between components while minimizing friction and wear. These lubricants create a separation between surfaces, preventing direct contact and asperity junction formation [32]. However, their effectiveness diminishes under extreme environmental conditions such as vacuum, high radiation, extreme pressure, and fluctuating temperatures. In such challenging conditions, solid lubricants—including molybdenum disulfide (MoS_2), hexagonal boron nitride, graphene, and graphite—offer a viable alternative [32, 33].

Despite their advantages, directly applying solid lubricants poses challenges, as maintaining a consistent and uniform lubricant layer between sliding components is difficult. To address this limitation, SLCs materials have been developed. SLCs are hybrid composite materials that incorporate multiple types of reinforcements within a matrix. Typically, a hard-phase reinforcement, often ceramic, enhances the matrix's mechanical properties such as strength and stiffness, while a soft-phase reinforcement (solid lubricant) improves lubrication, reducing friction and wear. Solid lubricants have demonstrated significant improvements in tribological performance across metal, polymer, and ceramic matrices [31, 33].

During sliding, the embedded solid lubricant particles gradually become exposed, forming a lubricating layer on the surface and thereby reducing direct material wear against the counter surface. A unique feature of SLCs is that wear particles generated during operation can further act as lubricants, contributing to a lower friction coefficient and reduced wear rate. Various fabrication techniques, including casting and powder metallurgy, are employed to manufacture self-lubricating metal matrix composites (MMCs). A classic example of an SLC is grey cast iron, which integrates a hard iron matrix with dispersed graphite flakes that serve as solid lubricants. Common matrix materials for SLC manufacturing include aluminium, copper, nickel, magnesium, silver, and their respective alloys [32, 34].

MoS_2 due to its low coefficient of friction and layered structure molybdenum disulfide is an excellent lubricating material and wear resistance. When a material is applied with shear stress, energy is dissipated by interlayer sliding. A huge amount of research has been done to characterize MoS_2 shear strength and coefficient of friction in numerous atmospheres. As the coefficient of friction increases, molybdenum disulfide's shear strength also increases, and such a characteristic is known as superlubricity [35].

Graphite is among the materials with a higher thermal conductivity and low density and can easily be dispersed into fluids because of its flake shape. Graphite nanoparticles appear to have a higher heat-transfer coefficient as well as a cheap price among oxide nanoparticles and metalloids. The lubrication quality of graphite is an important property that many mechanical devices can benefit from. In addition, they can easily be recycled without causing any pollution. Graphite nanoparticles are conjugated π-electron systems. When a crystal of graphite falls into nanoscales, there appear edges surrounding the particles.

As shown in Figure 8 Among lubrication materials, MoS_2 and carbon-based compounds including graphite and graphene are the most investigated materials. MoS_2 is the most successful solid lubricant for aerospace applications in dry conditions, whereas graphite and some other carbon-based lubricants require a humid environment to provide good lubrication [22].

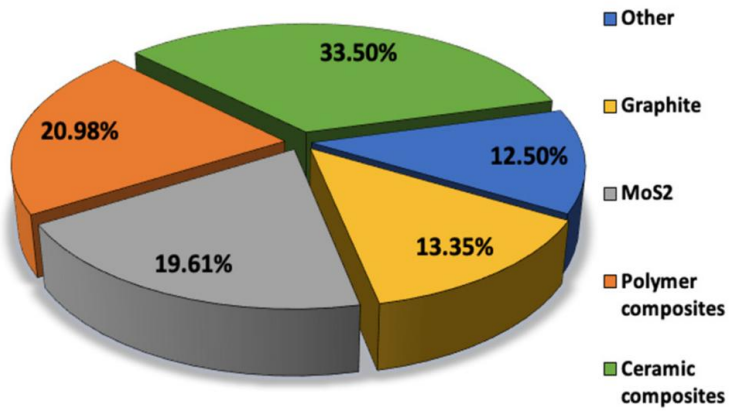


Figure 8.The chart presents the research conducted on different solid lubricants from 2000 to 2020[30].

As normal loads cause wear, under high normal loads, the nano-graphite from the composite is forced out to the contact zone, where it forms an adhering layer with fine graphite particles. Nanographite particles, being smaller than their larger counterparts, can slide deeply into the asperities of both the composite and counter surfaces. The nano-

graphite particles may have filled up the majority of the composite surface's asperities while it was sliding. Thus, at the contact between the composite pin and the steel disc, a layer of graphite formed. A thick, adherent graphite layer is the final product of the layer-forming process. The method is also applicable to graphite particles smaller than a micron, but these particles are too big to easily squeeze into the tiny grooves created by wear or the spaces between the sliding contact surfaces [36]. As shown in Figure 9**,** the distribution and particle size of the graphite on wear.

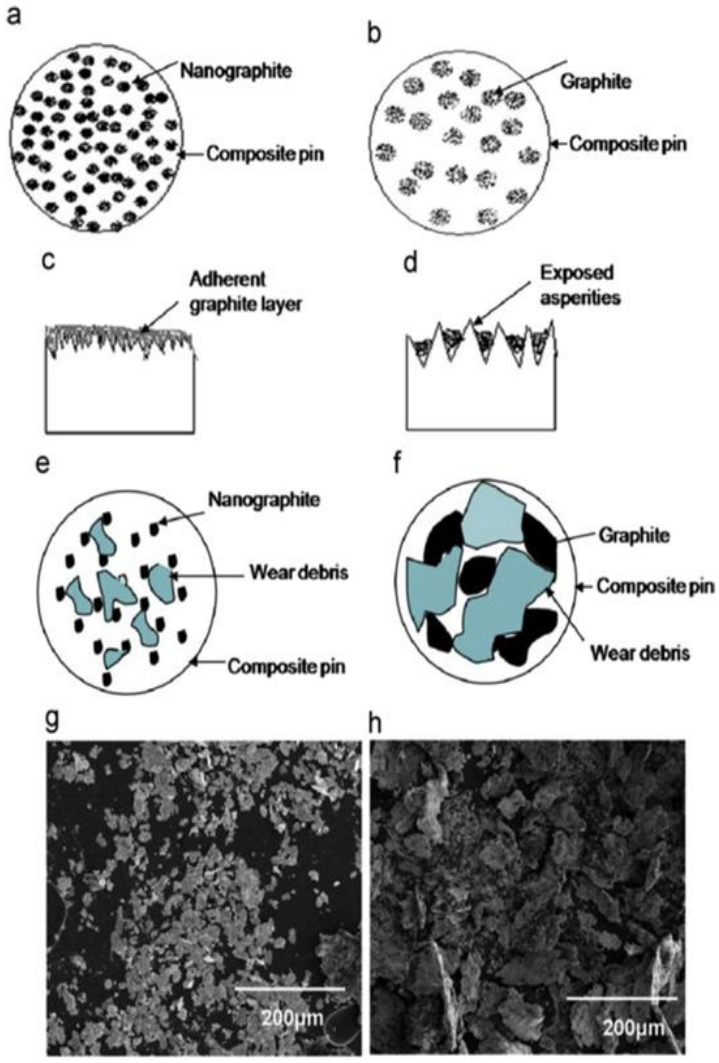


Figure 9. a) Nano graphite distribution in the matrix, b) graphite distribution in the matrix, c) contact profile of the nano graphite composite, d) contact profile of the graphite composite, e) and f) nano graphite reinforced composite conceptual wear generation model, g) and h) typical wear debris at 48 N and 0.77 m/s for copper nano graphite and copper graphite, respectively [37].

Graphite particles with sizes in the nanoscale range have a shorter mean free path Figure 9 a as compared to graphite particles with sizes in the micron range Figure 9 b for the same volume percentage. During the wearing process, this will result in smaller asperities and

less space between them compared to a micro-graphite-reinforced composite Figure 9 d , which can be filled with nano-graphite particles Figure 9 c. By creating a more uniform graphite layer, the filled nano-graphite particles lessen the amount of direct contact between the wearing bodies, which in turn lowers the frictional coefficient. SEM Figures 9 h and f confirm this, and Figure 9 e shows that the nanocomposite reduces the size of wear debris compared to micro-composites Figure 9 f [37]

The researchers provided a comprehensive analysis of the response between MoS_2 and iron-based matrices, as well as the microstructural evolution of these composites. In the initial publication, the effects of sintering temperature (750 to 1150 °C), starting MoS_2 particle size (d50=1.5 and 20 μm), and content (1 to 9 vol.%) on the characteristics and morphology of the second phase of the composites that formed after the reaction was shown in Figure 10. According to the examination of Ellingham diagrams, the reaction began sooner (850 °C) than anticipated (≈930 °C) and happened for all additional MoS_2 amounts. A eutectic point between the iron matrix and the iron sulphides (which originated from the reaction of the MoS_2 with the iron matrix) caused liquid-phase sintering when MoS_2 was present, particularly at 9 vol.%, according to sintering studies conducted at a dwell temperature of 1150 °C. This behaviour was completely different for all other MoS2 contents. The form factor, elongation, and diameter (as measured by image analysis) of the pores and the consequent iron sulphides were changed as the MoS2 content increased. In addition, the shape of the second phase had a direct impact on the mechanical properties, which include tensile strength, elongation, and Vickers microhardness. Although the microhardness rose linearly with increasing MoS_2 content, the tensile strength only rose to 3 vol.% because Mo diffused into the matrix after the reaction. We did not conduct any tribological tests [38].

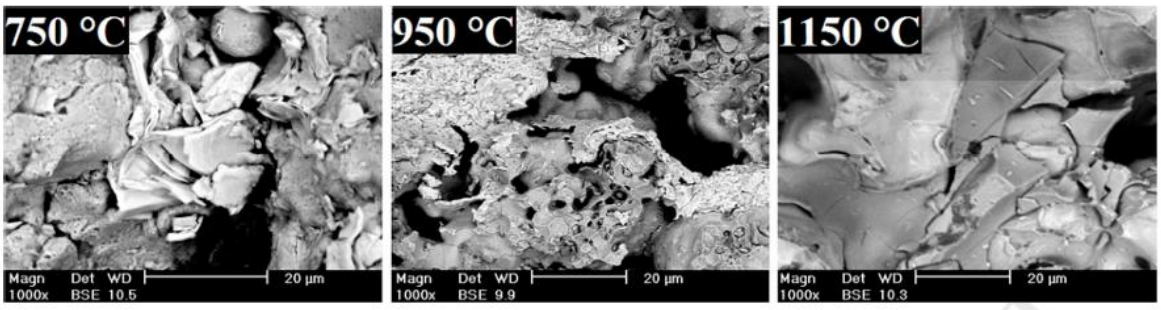


Figure 10. SEM of composite materials formed from MoS_2 and iron-based matrices, microstructural evolution of these composites by the effects of sintering temperature[38].

Figure 11 shows the lubricant's lamellar crystalline structure, which alleviates shear stress due to the weak interaction (van der Waals) between the sulphur lamellae. When sliding occurs, the lubricating action is provided by the crystalline layers of MoS_2, which will easily glide and align parallel to the direction of relative movement However, the lamellae have a great resistance to asperities penetration because to the strong ionic connection between Mo and S . Among the many uses for compounds are in the metal-forming, aerospace, and automotive industries, all of which deal with high pressure and/or temperatures. Electronic components battery cathodes [26], filters, and catalysts (often nanostructured) have all seen an uptick in their usage in the past few decades. Studies about nanostructures have also increased in recent years. As an example, a regime known as superlubricity (friction coefficient lower than 0.01) can be generated by using MoS_2 nanocrystals as a lubricant.In the tribological contact, these nanostructures function as nano-bearings, significantly lowering the system's friction coefficient. This mechanism is also present in fullerene structures and nanotubes. Recent advances include coating particles with atomic layer deposition and depositing self-lubricating coatings [38],[39].

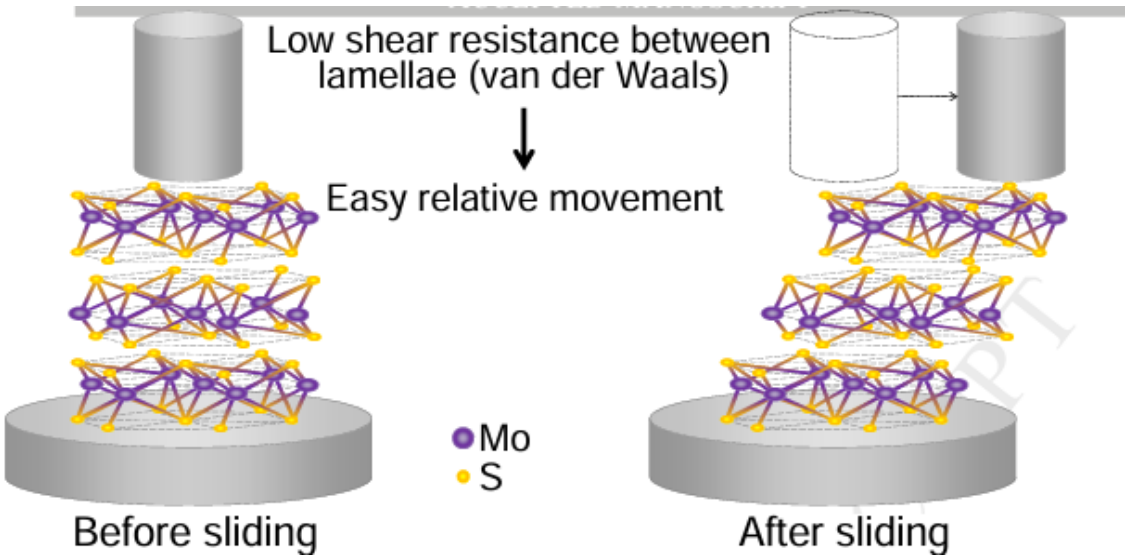


Figure 11. illustrated schematically for lamellar compounds MoS_2 [38]

Chapter Two / Literature review:

2.1 Introduction

A "composite material" is a material consisting of two or more components; one constituent is called the "reinforcing phase" while the second is called " matrix" an they combined at a macroscopic level. The "matrix phase materials" are generally continuous and are divided into metals, polymers and ceramics according to the material of the matrix. The "reinforcing phase material" is divided into flakes, fibres, or particles according to the shape of the "reinforcing phase ". Metal Matrix Composite (MMC) is one kind of composite material, and " it is prepared by combining two or more materials that display better properties than found from individual materials (i.e., parents of composites) and one of these materials is a metal and represents a matrix phase in the composite"[1]. In Metal Matrix Composite (MMC), reinforcing materials are mostly ceramics in the shape of whiskers, continuous or discontinuous fibres, and particulates [40],[41], therefore, it's called Ceramic particle reinforced metal matrix composite (CPRMMC). The reinforcements used conventionally are ZrO2, B4C, AlN, TiC, Al2O3, Si3N4 and SiC [24]. Several researchers investigated the manufacturing process, mechanical properties and tribological properties of metal matrix composite iron-based reinforced with ceramic particles.

Kaishuang Luo and Bingzhe Bai [11] designed Three medium carbon low alloyed MnCrB cast steels containing different Cr contents (0.3%, 0.6%, and 1.2%) and investigated the Cr contents effect (0.3%, 0.6%, and 1.2%) on the microstructure, mechanical properties and high stress abrasive wear behavior of the cast steels after (850 ^{o}C) air-cooling and (220 ^{o}C) tempering. They found that (1) the MnCrB cast steels have an excellent hardenability, (2) The granular bainite and lower bainite/martensite multiphase are found in the microstructure of the cast steels with (0.3% or 0.6%) Cr , (3) The formability of martensite , the hardness and wear-resistance are improved by increasing Cr content, (4) the impact toughness decreased in that more bainite was replaced by martensite by increasing Cr content, and (5) excellent combination of material properties (strength, hardness, ductility, and impact toughness) is found in the air-cooled MnCrB cast steel containing 0.6% Cr .

J. Li et. al [42] fabricated iron MC reinforced by various types of ceramic particles (SiC, Cr3C2, TiC and Ti(C, N)) by the dynamic temperature control direct current heating technology. They studied experimentally the mechanical properties of Iron-MC such as strength, Young's modulus and hardness, and they simulated the stress–strain curves of the composites and stress in reinforcing particles using Eshelby method. They found that (1)

SiC particles give higher enhancing in the strength comparing with other ceramic particles experimentally, (2). Increasing the matrix strength leads to enhance fracture toughness and hardness as a results to theoretical analysis, (3) The maximum strength of the four composites happens at (10%) volume fraction because the glomeration of particulate reinforcements happens the volume fraction is larger than 10%, (4) there are a good agreement between theoretical stress–strain curves with those of the experiments on TiC/Fe and Ti(C, N)/Fe composites only.

Adebisi et al. [43] introduced a historical background on the development and application of metal matrix composites (MMC) for automotive brake rotors. Also, they discussed and reviewed the development of material and processing techniques to get lighter weight, lower cost and higher performance brake rotors as a result of a better understanding of the mechanics of MMC. They found that "the stir casting technique provides ease of operation, sustainability and, most significantly, very competitive costs without sacrificing quality relative to other techniques; as such, it is the most attractive manufacturing process in the industry".

X.H. Zhang et. al [44] studied the influence of copper volume fraction on mechanical properties and microstructures of in situ "TiC particulates reinforced Fe-based composites". They showed that the copper content causes moving eutectoid point to the left in (Fe–C) equilibrium diagram and improving the refinement of pearlite interlamelar spacing. They explained the effect of copper as "Copper could effectively prevent the transition and deposition from carbon to graphite and also improve the activity of Ti and C element which was beneficial to synthesize more of TiC particulates".

Shouren Wang et. al [45] fabricated the blades of shot-blasting machine by high-chromium cast irons using investment cast processing to control different cooled rate in order to achieve solidification in one direction. They used deep itching methods to model and reveal the microstructure of oriented-M7C3 carbides. According to the observation of direction and shape of M7C3 carbides, they found that " when the long axis of the carbide rods is paralleling to the shots flow direction, high-chromium cast irons possess higher hardness and fracture toughness than that of perpendicular to the shots flow direction". They found that the blades possessing oriented M7C3 carbides in longitudinal direction exhibit excellent impact-abrasive wear resistance than that of in transverse and vertical direction.

M. Mohammadnezhad et. al [46] studied the influence of vanadium on the mechanical properties (impact energy, hardness) ,wear-resistance and microstructure of Ni-Hard4

white cast iron. They used the optical microscopy, the scanning electron microscopy, and the energy dispersive X-ray spectrometry to study the microstructure of 6- laboratory alloys with different vanadium contents. Their observation found that the chromium carbides were refined and carbides volume fraction decreases with increasing the content of vanadium. If the Volume fraction of vanadium was more than (2%), wear resistance and hardness were enhanced without decrease of fracture toughness, and the microstructure of Ni-Hard4 white cast iron became finer. They found that " the wear resistance of Ni-Hard4 white cast iron was modified by 2%, and vanadium liners were 40% better than the basic Ni-Hard4".

Matti Lindroos et. al [47] investigated experimentally the tribological performance and abrasive properties of a chromium-alloyed high-manganese Hadfield steel using three body abrasion tests using several different natural abrasives. Also, they studied the wear and hardening mechanisms in jaw crusher as a real application. They used scratch testing to study the impacts of plastic strain and normal loading on the surface hardening on wear rate. While they used High-velocity impact testing to investigate the effect of pre-strain on the wear behavior. They showed that "the dynamic loading affects both the yield behavior and the strain hardening rate of the studied steel". They connected between pre-strain, hardness, and wear rate in abrasion behavior. In impact behavior, they found that " the plastic straining of the surface layer first has a positive effect on the wear resistance, but when strain hardening reached the observed ductility limit, it showed an adverse effect on the material’s performance".

Jun Du et. al [48] used the finite element method to simulate the mold filling process of high chromium cast iron matrix composites reinforced by (ZTA) by infiltration casting. They applied in their simulation Volume of fluid (VOF) method and porous medium model to create the multiphase flow and heat transfer equations. They checked the accuracy of their model by comparing the theoretical results with the experimental observations. They found that" the methods developed may afford essential implication for the simulation and optimization of processing parameters in various infiltration casting systems".

C. Exare et. al [49] investigated the structural properties such as "phases stability, lattice parameters, homogeneous and non-homogeneous strains, particlesand crystallites sizes" of ZTA-composites for various vontents of zirconia and yttria at the main stages of the process. They found that three factors (yttria-doping, strain and size effect) effect on the structural states. They showed that "the yttria-doping and size effect have been shown to

stabilize the tetragonal phase relatively to the monoclinicphase, and to destabilize the tetragonal phase relatively to the cubic phase whereas strain is doing the opposite".

Wei Wang et. al [50] casted a new multiphase steel and a conventional Hadfield steel (Mn13Cr2) using high-frequency induction furnace to investigate impact-abrasive wear behaviors, wear mechanisms and phase transformation of the two kinds of steel. They used Field-emission scanning electron microscope (FE-SEM), transmission electron microscope (TEM), X-ray diffraction (XRD) and thermal dilatometer in their work. They showed that the grain refinement , transformation of retained austenite to martensite and high density dislocations for the multiphase steel in additional to the interaction of twining and dislocation walls are the main strengthening mechanisms. They concluded that "the multiphase steel with a triplex microstructure (bainite, martensite and retained austenite) had higher tensile strength, micro-hardness and impact-abrasive wear resistance than Mn13Cr2". In wear mechanisms, “press-in particle”, “micro-voids” and “delaminated crater” were found in the multiphase steel, however those of Mn13Cr2 were called as “adhesion”, “crater” and “micro-crack”. Also, they found that "impact-abrasive wear features grain deformation, orientated features, crack propagation, voids linking and the block effect of bulk retained austenite to crack branching" were observed in the affected layer of the multiphase steel".

Chenxin Jin et. al [12] used 3-grades of stainless steel binder (304L, 316L and 410L) to prepare TiC based cermets by vacuum melt infiltration, at 1500 °C, which allows the steel binder content to be readily varied from (5 – 30) vol%. They used Vickers test to investigate the hardness and fracture resistance pf cermets. They used a ball on flat geometry, with a WC-Co counter face sphere to study reciprocating wear response. They found that the coefficient of friction rises when the steel binder content, load and wear time, are increase. Also, increasing steel binder content and applied load leads to increase the specific wear rate.

Juan Chen et. al [14] fabricated ZTA ceramics (20 wt.% ZrO2) with various sintering temperatures (1450, 1500 and 1550 °C) by SPS and HP processes, respectively to study the effect of sintering process on the material properties of ZTA ceramics at 298 K and 77 K. Their results showed that: (1) improving bending strength and fracture toughness of the specimens fabricated by two processes at cryogenic temperature, (2) confirming stress-induced martensitic transformation toughening mechanism by the in-situ Raman technique. Also, they concluded that " It's easy to transform the tetragonal ZrO2 because of the

transformation toughening effect would become stronger, result in the increase of mechanical properties."

Yudong Sui et. al [51] studied experimentally the reaction product in the interfacial layer of zirconia toughened alumina (ZTA) ceramic particles reinforced high chromium cast iron (HCCI). They studied phases formed in the interfacial layer during solidification using TEM and HRTEM and they found that " they are the amorphous Na_4SiO_4 phases and diffusion of Al is faster than that of other elements in the interfacial layer". Also they found that the hardness of interfacial layer was (1877.5 HV) while the modulus was (299.8 GPa). Finally, they showed that "the phase transformation (t-ZrO2/m-ZrO2 and q-Al2O3/a-Al2O3) occurred during the composite preparation".

A. Grairia et. al [52] used powder metallurgy method to produce metal matrix composites based on iron and reinforced by WC particles. They analysed the composition and microstructure of the specimens and then investigated the wear resistance of the specimens against alumina and WC balls using SEM/EDS analyses also, they used optical profilometry to evaluate the wear rate of specimens. They used SEM to recognise two wear mechanisms (oxidation and abrasion) during dry sliding wear of tungsten carbide-reinforced iron matrix. They found that the overall wear performance, which is obtained by considering the wear loss of the substrates, indicated less resistance against Alumina compared to WC ball contact.

Samer J Algodi et. al.[53] fabricated TiC-based cermet coatings by electrical discharge coating (EDC) using a semi-sintered TiC tool electrode to study the tribological behaviours of this coating. They found that the as-deposited coatings displayed complex microtheir challenges and limitations. They provided their paper "a broad-spectrum attitude on hybrid MMCs techniques, challenges, and future research directions".

Xiaolong Cai et al. [56] fabricated iron-MMC reinforcing by "chromium carbide with polycrystalline structure" using diffusion-controlled reaction under casting and two-step heat treatment for enhancing the mechanical properties of iron-MMC. Using Scanning electron microscopy, they found that "the structure of composites involves of several chromium-chromium carbide pillars and a number of chromium carbides those are dispersed in the matrix. These pillars are constituted by a core of residual chrome wire and a shell of chromium carbide and this shell forms a dense region and chromium carbide in the matrix generates a diffusion region.". They used X ray diffraction test and found that the composites are composed primarily of $M_{23}C_6$, M_7C_3, M_3C_2, Fe_3C, Cr and α-Fe phases

and observed presented Cr-phase in XRD graph is due to incomplete reaction and the presented Fe-phase is derived from the matrix.

structures, comprising TiC grains within an iron matrix, on both high-speed steel (HSS) and 304 stainless steel (304-SS) substrates. For both substrates, they found that increasing the wear resistance of TiC/Fe cermet coatings compared with as-polished substrates. They also found the wear resistance of EDC cermet coatings on HSS is more than that fabricated on (304-SS) and the increasing rate depends on load. Also, the results show that using of Laser surface treatments leads to increase the wear rate for all samples, with the exception of HSS samples under conditions of high loading. The reasons of this increasing in wear rate are (1) a significant reduction in the proportion of TiC within the ED coatings and (2) increase in grain size

Sulaiman Mustafa Khazaal et. al [40] fabricated hybrid iron-matric composites reinforced by constant mix (80% Al2O3 and 20% ZrO2) with (1- 4) % volume fraction using powder metallurgy to investigate the mechanical properties. They used the pressure 640 MPa and sintering temperature 1120 ◦C in the presence of argon gas to fabricate specimens of hybrid iron- matric composites. They used Dosimeter, particle size analyzer and SEM to measure the purity, density, average grain size and shape of nano-particles and fabricated specimens. They found that the specimen with the contains (97% Fe + 3% (80% Al2O3 + 20% ZrO2) has a best mechanical properties comparing with other hybrid iron-matric composites and it has properties of 61%, 37% and 7% more than the matrix properties for compression strength, hardness HRC and radial crushing strength respectively.

Radosław Maruda et. al [54] used Simplex Lattice Design (SLD) method to design the experimental study of the surface topography parameters of iron-matrix composite reinforced with graphite, alumina and zirconia nanoparticles. They machined the iron-matrix composite specimens under dry turning conditions and using PVD-coated GC1115 carbide inserts. They used Sensofar S Neox optical profilometer and Mountains Map software to analyze and study the surface topography of the specimens. They found that" reinforcing additives and their amount in the mixture unambiguously affect the geometric features of the surface after turning process of the iron- MCs. Therefore, it is possible to select such a combination of particulates that will provide the expected quality of the machined surface"

Anand Babu et. al [55] introduced a review paper dealing with hybrid MMC, materials used (reinforcement and matrix) and manufacturing techniques, physic-mechanical, corrosion, and tribological properties, and challenges associated with hybrid MMCs. They

also discussed the "overview and the status" of various matrix and reinforcement materials in manufacturing of hybrid-MMCs using different fabrication techniques Wenlong Dong et. al[57] focused on the previous papers dealing with the effect of reinforced particles on the reinforcement mechanism and mechanical properties of iron-MMC in additional to the preparation technology of this kind of metal matrix composite materials. They proved that the preparation technology is one of the most important factor effect on the material properties of iron-MMC reinforced by particles , in addition to the effect of type, size and volume fraction of the reinforcing particles. Also, they showed that " The reinforcing mechanism of this kind of iron-MMC mainly includes microstructure strengthening and micromechanical strengthening".

Yunlei Wang and Tullio Monetta [58] reviewed the previous papers dealing with metal matrix composites reinforced by SiC-particles and discussed the research progress of this novel type of structural material because of their high strength, hardness, and thermal stability. Also they discussed the preparation technology, microstructure, mechanical properties, wear resistance, and application of this type of MMCs. They compared between different preparation methods and discussed the advantages and disadvantages of them and explained the relationship between the material properties and microstructure of MMCs with SiC-particle and studied the variation of macroscopic properties due to interfacial reactions. Finally, they offered new design concepts and research methodologies to generate high-quality structural composite materials with improved their performance in the future.

Wenlong Dong et. al [59] utilized lost foam casting as a processing method to create new fabrication technique of high-strength and ultra-wear-resistant particle reinforced iron-MMC. They found that "a multiphase microstructure composed of WC-11Co, α-Fe, and carbide precipitates that extend at different length scales and the precipitation of large-sized M3W3C (M = Fe, Co) type carbides at the WC-11Co/matrix interface is well controlled". They proved that the tensile and compressive residual stresses are found as a stress between WC-11Co and the matrix and compressive residual stress is greater than tensile residual stress. Also, they showed the formation of a favorable reaction layer between WC-11Co and the matrix.

Sai Chen et. al [60] reviewed the recent advances and development of Iron-MMCs with particular and discussed design of microstructure , fabrication techniques, and material performance. They studied the effect of (1) bonding mechanism, (2) selection criteria of reinforcement and matrix properties and (3) geometry of interface layer. While they summarized and compared of fabrication techniques considering the state of material (liquid, solid, and gas-mixing processing). They discussed several material properties of Iron-MMCs such as Young's modulus, hardness , wear resistance, tensile behavior and finally fracture mechanism.

Km. Pooja et. al [61] reviewed papers dealing with Metal Matrix Composites with material matrix based on aluminum, copper, magnesium, titanium, zinc and their alloys in additional to examine their material properties, fabrication methods and recent developments. Key findings highlight their ability to overcome the weaknesses of traditional materials by enhancing various mechanical properties. They discussed enhancements in mechanical properties (tensile strength**,** Young's modulus, toughness , fracture, fatigue and creep resistance) and physical properties (density, thermal expansion coefficient, and electrical conductivity) for different reinforcement methods. They presented the method or procedure that is used to get a desired properties of MMCs with minimum cost and defects and using suitable fabrication method.

Engidayehu Mekonnen Alemu et, al [62] used powder metallurgy technique to fabricate iron-MC with vanadium aluminum carbide (V_2AlC) and graphene oxide (GO) and studied the mechanical properties of this material. they measured and evaluated density of iron-MC using Archimedes method, mechanical properties (hardness and compressive strength) according to ASTM standards and corrosion resistance using an electrochemical analyzer in addition to microstructural features using Optical Microscopy and X-ray Diffraction. In the beginning, they used Taguchi-based to fabricate nine samples (consists of 5 wt.% V_2AlC and 4 wt.% GO) with different parameters of powder metallurgy and then fabricated four additional samples with varying V_2AlC percentages (5, 8, 10, and 15)% basing on the optimal parameters of powder metallurgy. From the results , they found that the mechanical, physical and corrosion properties of the optimally fabricated iron-MC are enhanced.

2.2 Summary of the Previous Survey

The previous papers are summarized in Table (5).

Table 5. Summary of Literature Survey

No.	Author	Year	Matrix	Reinforced Material	Material Properties
1	Kaishuang Luo and Bingzhe Bai [11]	2010	low alloyed MnCrB cast steels	Cr contents (0.3%, 0.6%, and 1.2%)	Hardenability , microstructure, Tensile strength, Elongation, Hardness and Impact toughness
2	J. Li et. al [42]	2010	Iron	ceramic particles (SiC, Cr3C2, TiC and Ti(C, N))	Stress-strain curve, yield strength, tensile strength, Young's modulus and Microstructure
3	X.H. Zhang et. al [44]	2011	Fe–Ti, Fe–Si, Fe–C alloys	Cu (i.e., 0.0, 1.0, 1.5 and 2.0) wt%.	Microstructure, hardness, impact toughness and ultimate tensile strength
4	Shouren Wang et. al [45]	2013	high-chromium cast irons	oriented M_7C_3 carbides	Hardness, fracture toughness, Microstructure, Microhardness , Elastic modulus, Impact Wear Resistance and Wear Morphology
5	M. Mohammadnezhad et. al [46]	2013	Ni-Hard4 white cast iron	Vanadium with different weight percentage	Microstructure, impact energy, hardness and wear resistance
6	Matti Lindroos et. al [47]	2015	chromium-alloyed high-manganese Hadfield steel	manganese	Microstructure, Surface Hardening , Damage Mechanisms, Dynamic Hardening , Strain Hardness and High-Velocity Impact
7	C. Exare et. al [49]	2015	Zirconia Toughened Alumina (ZTA) composites	different compositions of zirconia and yttria	*Stability of the phases , size of grain*, *strain/stress effect and strain effect*
8	Wei Wang et. al [50]	2016	conventional Hadfield steel (Mn13Cr2)	----	Microstructure, ultimate tensile strength , yield strength, micro-hardness, Wear resistance, Worn surface observation and wear mechanism
9	Chenxin Jin et. al [12]	2017	stainless steel	TiC	Microstructure, Hardness , indentation fracture resistance, Reciprocating wear behavior, coefficient of friction and wear rate
10	Juan Chen et. al [14]	2017	ZTA ceramics (20 wt.% ZrO2)	various sintering temperatures (1450, 1500 and 1550 °C) by SPS and HP processes	Microstructure, Bending Strength and Fracture toughness .
11	Yudong Sui et. al [51]	2018	zirconia toughened	high chromium cast iron (HCCI)	Microstructure and Hardness .

			alumina (ZTA) ceramic particles		
12	A. Grairia et. al [52]	2018	Fe-based metal matrix composites	WC particles	Microstructure, Friction Coefficients, Wear Mechanism and Wear Rates
13	Samer J Algodi et. al [53]	2018	high speed steel and 304 stainless steel	TiC-based cermet coatings	Microstructure, Specific wear rates , wear scar profiles , Counterbody wear rate, Coefficient of friction,
14	Sulaiman Mustafa Khazaal et. al [40]	2022	iron-matric composites	mix (80% Al2O3 and 20% ZrO2) with (1- 4) % volume fraction	Microstructure, compression strength, Radial crush strength, hardness and Toughness.
15	Radosław Maruda et. al [45]	2022	iron-matric composites	graphite, alumina and zirconia nanoparticles	Topography characterization
16	Xiaolong Cai et al. [56]	2023	iron-MMC	chromium carbide with polycrystalline structure	X ray diffraction and Microstructure
17	Wenlong Dong et. al [59]	2024	iron-MMC	WC-11Co	Microstructure
18	Engidayehu Mekonnen Alemu et, al [62]	2026	iron-MC	vanadium aluminum carbide (V_2AlC) and graphene oxide (GO)	Density, Mechanical properties (hardness and compressive strength), Corrosion resistance and Microstructure

2.3 Research gap and objectives

The increasing demand for iron with enhanced mechanical strength and wear resistance has created a need for it in different engineering applications. In this study, nano-graphite and nano-MoS_2 were investigated as self-lubricating and reinforcing additives for a hybrid iron-metal matrix composite. The composite consisted of 97 vol.% iron as the matrix and 2.4 vol.% Al_2O_3 and 0.6 vol.% ZrO_2 as ceramic reinforcements, with nano-graphite and nano-MoS_2 added at concentrations of 0.5, 1, and 1.5 vol.% separately. Consequently, there is comparative information on their effects when incorporated into the same Fe–Al_2O_3–ZrO_2 hybrid composite system under identical or comparable processing and testing conditions. In particular, the combined influence of ceramic reinforcements and different nanoscale solid lubricants on compressive strength, hardness, coefficient of friction, and wear resistance has not been sufficiently clarified.

A direct comparison of nano-graphite and nano-MoS_2 in the selected Fe–Al_2O_3–ZrO_2 system is therefore useful because both materials can act as solid lubricants while having different structures and lubrication mechanisms. Investigating them within the same composite system provides a consistent basis for determining how the type and concentration of the nano-additive affect the mechanical and tribological performance. Such a comparison can also help identify the relationship between nano-additive content and the balance between strengthening and lubrication effects.

The specific objectives of the research are:

1. To fabricate and characterise an Fe–Al_2O_3–ZrO_2 hybrid metal matrix composite as the reference material.
2. To investigate the effect of different nano-graphite contents on the compressive strength, hardness, coefficient of friction, and wear resistance of the Fe–Al_2O_3–ZrO_2 composite.
3. To investigate the effect of different nano-MoS_2 contents on the same mechanical and tribological properties.
4. To compare the effects of nano-graphite and nano-MoS_2 under consistent fabrication and tribological testing conditions.
5. To determine the influence of nano-additive concentration on the balance between mechanical strengthening and tribological performance.

The research is designed to answer the following questions:

- How does the addition of nano-graphite affect the mechanical and tribological properties of the Fe–Al_2O_3–ZrO_2 composite?
- How does nano-MoS_2 affect the same properties under comparable conditions?
- How does increasing the concentration of each nano-additive influence compressive strength, hardness, coefficient of friction, and wear resistance?
- What differences exist between nano-graphite and nano-MoS_2 when incorporated into the same Fe–Al_2O_3–ZrO_2 composite system?
- How does the type and concentration of the nanoscale solid lubricant influence the overall balance between strength, hardness, friction, and wear resistance?

Research Novelty

The main contribution of this research is the systematic comparison of nano-graphite and nano-MoS_2 within the same Fe–Al_2O_3–ZrO_2 hybrid metal matrix composite system. By maintaining consistent material processing and testing conditions, the study provides a more direct assessment of the effects of the two nano-additives and their concentrations on the mechanical and tribological performance of the composite.

Chapter Three / Raw Materials and Experimental Part

3.1 Raw Materials

3.1.1 Matrix Raw Material

The iron powder used as the matrix material in the present work is a commercial 98% pure iron powder (average particle size of ~100 μm) produced by the THOMAS BAKER company in India. In Figure 14, Shawn shows the microstructures of iron powder.

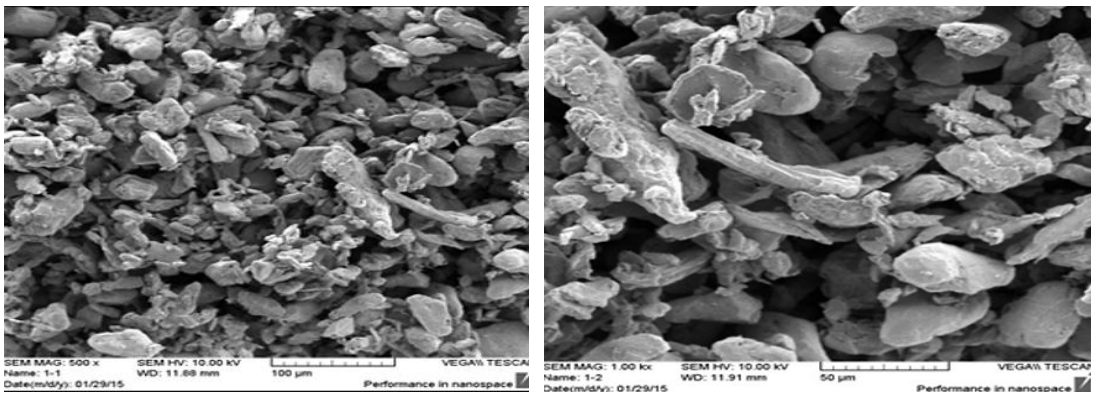


Figure 12. SEM micrographs of Fe at different magnifications.

3.1.2 Reinforcement materials

1- Aluminium oxide (Al_2O_3) powder has characteristics such as its thermal, chemical, and physical properties when compared with several ceramic materials, and is widely used for firebricks, abrasives, and integrated circuit (IC) packages. The average particle size used of ~10 μm, procured from Fix anal/Germanyabrasives, and integrated circuit (IC) packages, as shown in Figure 13**,** scanning electron microscope of alumina.

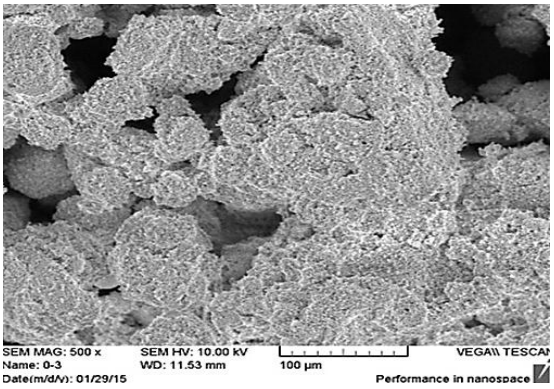


Figure 13. SEM micrographs of Alumina at 500 x magnification.

2- Zirconia is a fine powder made from zirconium dioxide, a white, hard ceramic material. It is a versatile material with a wide range of applications. It is a hard, wear-resistant material that is also resistant to corrosion. Zirconium oxide powder is an important material in a variety of industries, including abrasives, ceramics, metalworking, nuclear

power, and water filtration. The average particle size used ~10 μm, procured from Fix anal/Germany, is shown in Figure 14**,** a scanning electron microscope image of ZrO_2.

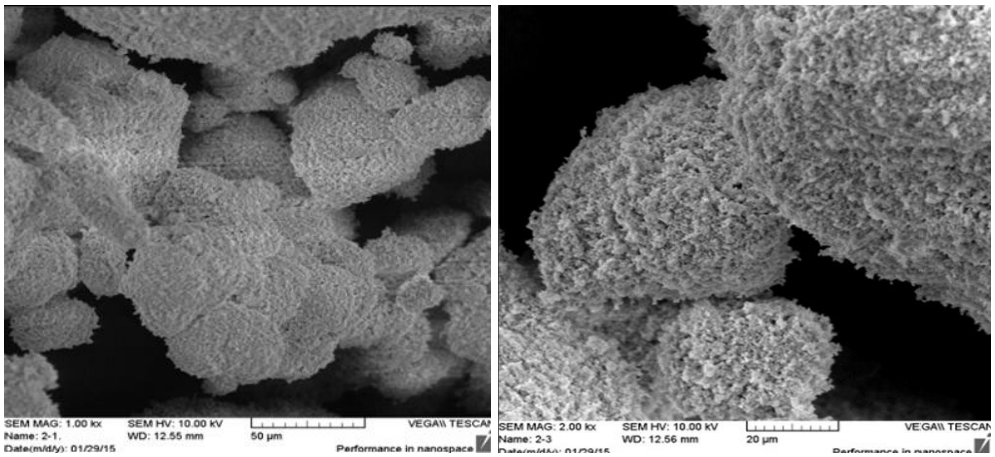


Figure 14. SEM micrographs of ZrO_2 at different magnifications (1000 X and 2000X).

3.1.3 Additive nano-materials

1- Nano Graphite (Gr)Powder. The main types of naturally occurring graphite that are found in ores and minerals are amorphous graphite, pyrolytic graphite, crystalline small flakes of graphite, and graphite fibre. Amorphous graphite is generally an extremely fine flake of graphite. Lump graphite is massively found in fissure veins or fractures and in the intergrowth of fibrous and crystalline aggregates with a hydrothermally processed origin. Crystalline small flake of graphite occurs as flat plate-like and isolated crystals with hexagonal morphology and edges. It could be claimed that graphite nanoparticles are the most investigated material because of their interesting and unique properties, such as enhanced chemical and biological compatibility, high surface area, excellent electrical and thermal conductivity, dimensional stability, corrosion resistance, and optical properties. Graphite is among the materials with a higher thermal conductivity and low density, and can easily be dispersed into fluids because of its flake shape. Graphite nanoparticles appear to have a higher heat-transfer coefficient as well as a lower price among oxide nanoparticles and metalloids. The lubrication quality of graphite is an important property that many mechanical devices can benefit from. In addition, they can easily be recycled without causing any pollution. Graphite nanoparticles are conjugated π-electron systems. When a crystal of graphite falls into the nanoscale, edges appear surrounding the particles. Nano Graphite powder was supplied by Hongwu International Group Ltd from China, with a purity of 99.95% and particle size range (40- 50) nm, as shown in Figure 15.

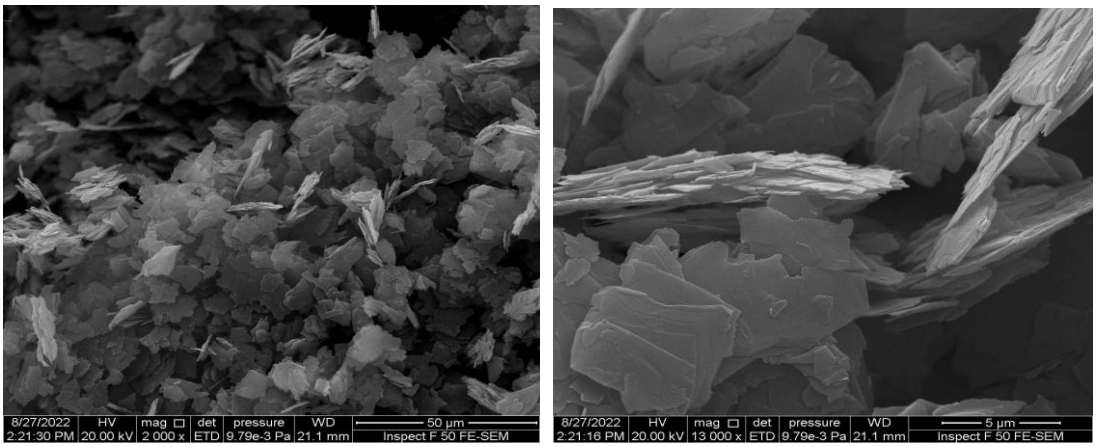


Figure 15. SEM micrographs of Nano Graphite at different magnifications.

2-Nano Molybdenum disulfide (MoS_2) powder: An inorganic compound of sulfur and molybdenum is known as molybdenum disulfide (or moly). MoS_2 is the chemical formula of molybdenum disulfide. Molybdenum disulfide is classified as a transition metal dichalcogenide. Molybdenum disulfide is a silvery black solid. Molybdenum's principal ore is MoS_2, and it takes place as the molybdenite mineral. In comparison, MoS_2 is not reactive. Oxygen and dilute acids don't affect it. It is because of its low coefficient of friction and layered structure that molybdenum disulfide is an excellent lubricating material and has wear resistance. When a material is applied with shear stress, energy is dissipated by interlayer sliding. A huge amount of research has been done to characterise MoS2 shear strength and coefficient of friction in numerous atmospheres. As the coefficient of friction increases, molybdenum disulfide's shear strength also increases, and such a characteristic is known as superlubricity. Nano Molybdenum disulfide (MoS_2) powder supplied by Hongwu International Group Ltd from China with a purity of 99.9% and particle size < 50nm as shown in Figure 16 SEM of Nano Molybdenum disulfide). Table 6 shows the properties of nano molybdenum disulfide by manufacturing. Molybdenum disulfide (MoS_2) properties.

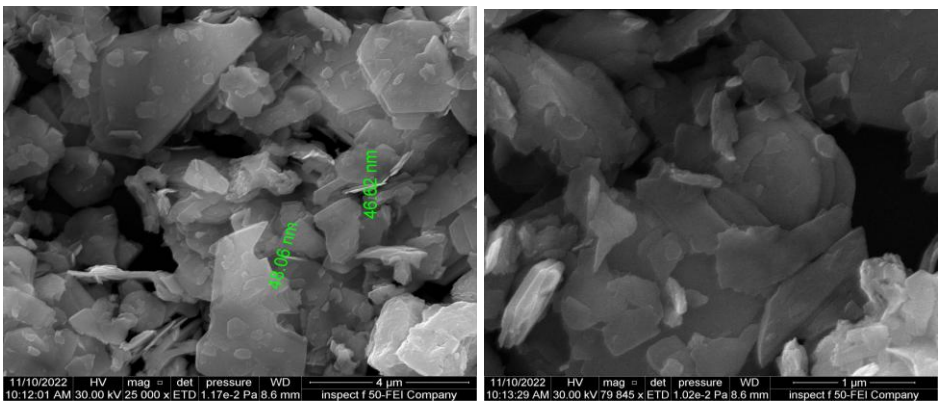


Figure 16 .SEM micrographs of Nano Molybdenum disulfide (MoS_2)at different magnifications.

Table 6. *Nano Molybdenum disulfide (MoS_2) properties.*

Properties	Value
Particle size distribution (nm)	50
Specific surface area (m^2/g)	1.2
Volume density (g/cm^3)	5
Form	Flakes
Color	Black

2.2 Preparation of Hybrid Metal Matrix Composite

Groups of samples were prepared: the first one was prepared from pure iron as a reference sample; the second group, named Master Composite, was prepared using 97 vol% pure iron powder, reinforced with 2.4 vol.% alumina and 0.6 vol.% zirconia oxides [40], as detailed in Table 7. For the other groups, the hybrid metal composite was prepared by adding nano-graphite and nano-MoS_2 in varying proportions of 0.5, 1.0, and 1.5 vol% to the basic master metal composite, as shown in Table 8.

Table 7. Composition of Metal matrix composite (Master Matrix)

Master Composite Mix	97 vol. % Fe	2.4 vol. % Al_2O_3	0.6 vol. %ZrO_2
V_f	0.97	0.024	0.006

Table 8. Composition of Metal matrix composite with nano-graphite and nano-MoS_2

Sample code	Composition (vol %)			
	Fe	Al_2O_3	ZrO_2	Addtive nano-graphite and nano-MoS_2
Fe	100	----	----	----
Comp.	97	2.4	0.6	----
Comp.+0.5 % Gr	97	2.4	0.6	0.5
Comp.+1 % Gr	97	2.4	0.6	1
Comp.+1.5 % Gr	97	2.4	0.6	1.5
Comp+0.5 MoS_2	97	2.4	0.6	0.5
Comp+1 MoS_2	97	2.4	0.6	1
Comp+1.5 MoS_2	97	2.4	0.6	1.5

To prepare the master metal composition, the powders (iron, alumina and zirconia) were mixed for 60 minutes. After this, the mixture with the nano-graphite solution in glycerin oil was combined. This solution was prepared by wet mixing nano-graphite or nano-MoS_2 using glycerin oil, which comprised approximately 2-3% of the composite's total weight. Mixing continued for 30 minutes. The wet powder was formed by the compaction method into a cylindrical sample.

The powder was compacted in a die at 650 MPa at room temperature, and the samples were sintered in a vacuum furnace to avoid oxidation during sintering. Figure 17 presents the scheme for preparing a hybrid metal matrix composite.

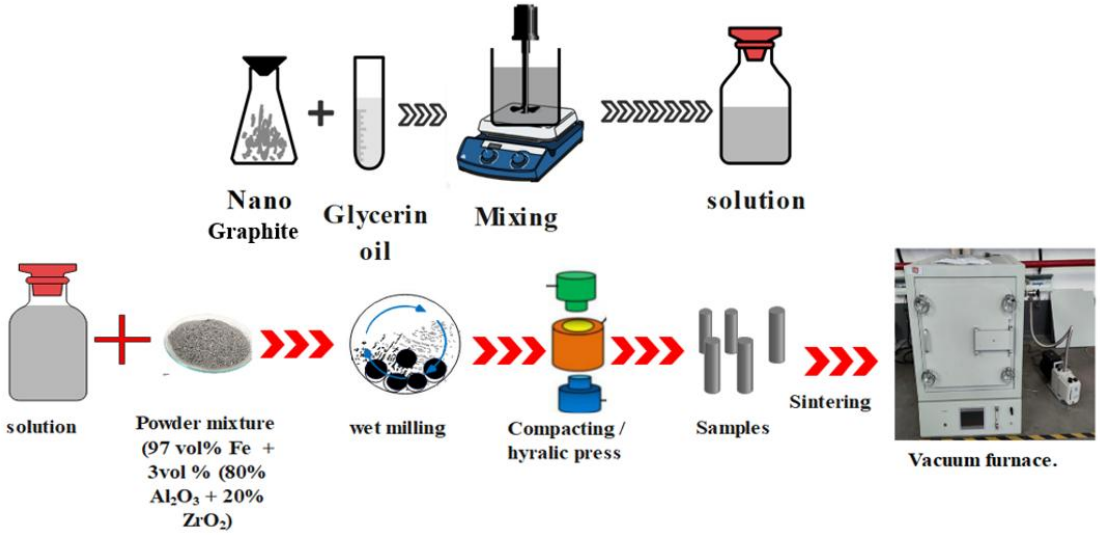


Figure 17. Scheme for the preparation of a hybrid metal matrix composite.

The samples were sintered at 1120 °C for 30 min. A furnace (Laboratory Vacuum Sintering Furnace) was used at a heating rate of 16 °C /min under pure argon at a flow rate of 10 L/min. The diagram of sintering conditions is given in Table 9 and Figure 18. Figure 19 shows sample images before and after sintering.

Table 9. Sintering Conditions

Operation	Temperature (°C)		Duration
	From	To	
Heating	Ambient (30 °C)	150 °C	24 min
Soaking	150 °C	150 °C	30 min
Heating	150 °C	1120 °C	60 min
Soaking	1120 °C	1120 °C	30 min
Cooling in Furnace	1120 °C	Ambient (30 °C)	

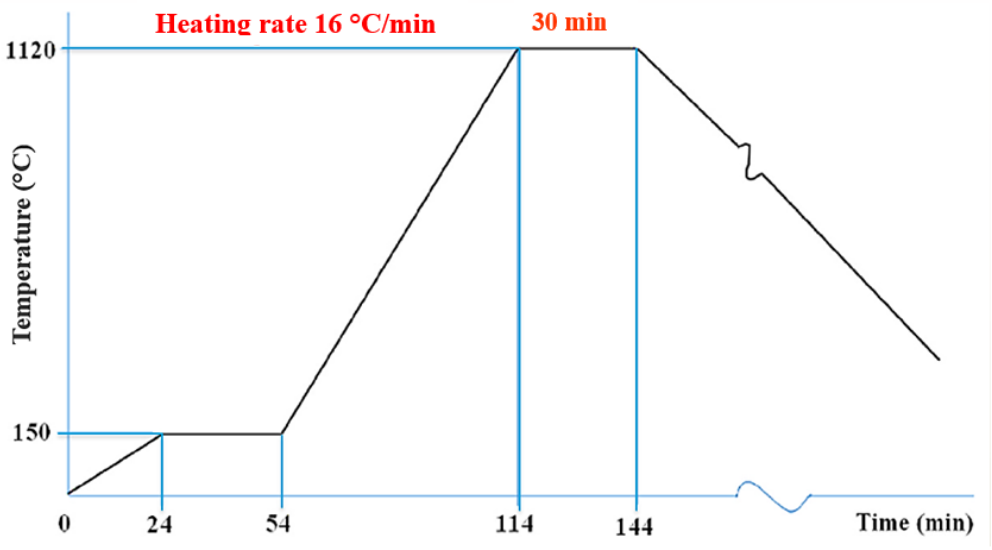


Figure 18. Sintering Conditions



Figure 19. Sample image before and after sintering

3.3 Design and Fabrication of Compacting Dies

All dies were designed in SolidWorks and fabricated from tool steel on a CNC machine at the Technical Engineering College in Baghdad. The steel (DIN EN 1006–2) [63] was selected in the design stage of compacting, and the chemical composition of the steel is illustrated in Table 10 Also, the hardness of the selected materials was 22 HRC. To improve their hardness, the materials were quenched in an oil bath and then tempered, which increased the hardness to 55 HRC.

Table 10. Chemical Composition of Steel (DIN EN 1006-2)[63].

Elements (wt%)	Fe	C	Si	Mn	Cr	S	Ni	Co	Cu
Standard	96.6	0.5	0.34	0.78	1.1	0.02	0.167	0.02	0.2
Actual	96.7	0.515	0.323	0.764	1.08	-------	0.165	-------	0.2

The die of the compression test specimen and the dimensions of the cylindrical specimen are according to ASTM E-9 [64], when a traditional single-piece die was used, as shown in Figure 20. The samples suffer from geometric limitations because they must be vertically ejected. The immense sliding friction during this rigid ejection process often scores the surface, warps dimensions, or cracks fragile, newly pressed parts. Furthermore, friction along the solid walls causes compaction pressure to drop deeper into the cavity, resulting in uneven density variations and structural weak spots throughout the finished component, as shown in Figure 21: the sample with deep cracks or a failed sample, because this defects, we developed a new die split (two-piece) design by product by using many die clamping rings; it surrounds the two pieces to fixed it and enhance to distpution the of pressure. As shown in Figures 22 and 23.

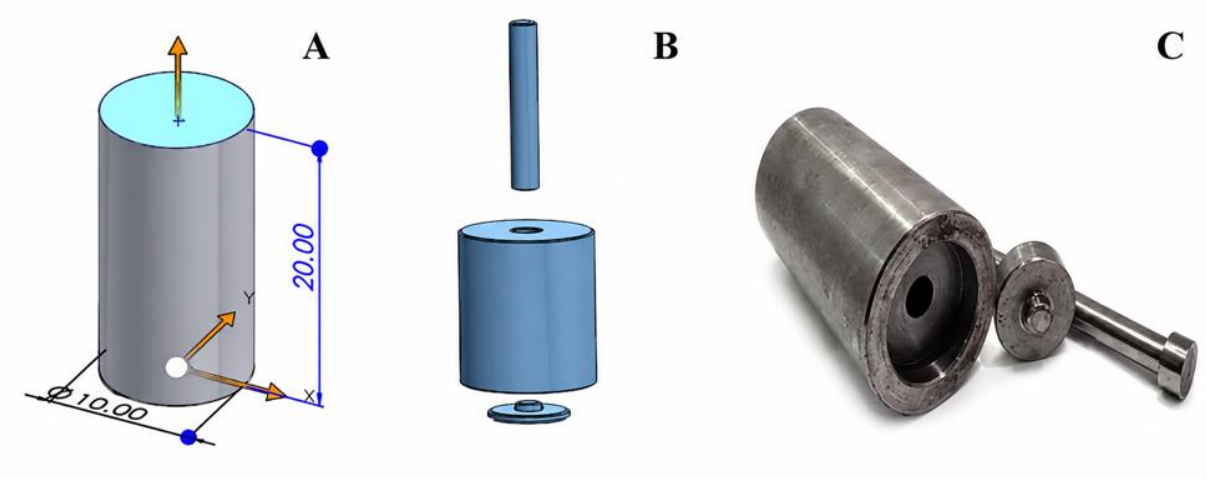


Figure 20. Old Die of the compression test specimen



Figure 21.Specimen made from a normal die



Figure 22.Parts of the new die



Figure 23.Assembly of new die.

The fundamental difference between a solid (one-piece) die and a split (two-piece) die lies in the method used to remove the compacted specimen after pressing. A split die can be opened into two halves, allowing the green compact to be released without applying an ejection force, making it particularly suitable for fragile specimens or components with complex geometries. In contrast, a solid die consists of a single rigid body, and the compact is removed by ejecting it from the die cavity using the punch. Therefore, it is generally preferred for simple, symmetrical shapes such as cylindrical and disc-shaped specimens.

The solid die (one-piece die) offers several advantages, including a simple design, lower manufacturing cost, and longer service life. However, during ejection, friction between the green

compact and the die wall can generate significant stresses, which may lead to cracking or damage, particularly in brittle materials or specimens with a high height-to-diameter ratio.

In comparison, the split die (two-piece die) facilitates specimen removal by separating the die into two halves, thereby minimizing friction and reducing mechanical stresses during extraction. This design also promotes a more uniform pressure distribution during compaction, making it ideal for long, complex, or fragile specimens. Nevertheless, split dies are more expensive and mechanically more complex than solid dies, and the parting line between the two halves may leave a slight seam or surface mark on the compacted specimen. Figure 24 shows the sample by used new die with a smooth surface without cracks.



Figure 24. Specimen made by a new die

3.4 Techniques for Characterising the Hybrid Metal Matrix Composite

3.4.1 Compressive strength test

The compressive strength test of a metal matrix composite is performed to determine the material's ability to withstand compressive loads without failure. The procedure generally follows standards such as ASTM E9 [65]. The compressive strength was measured using a LARYEE universal testing machine, model UE3450, with max load of 50 KN. The cylindrical specimens with a diameter of 1 cm and a height of 2 cm were evaluated under uniaxial loading. As shown in Figure 25**,** the image shows the instrument used to measure compressive strength and the sample shape before and after the test. Three specimens were tested for each composition, and the average compressive strength was calculated and reported.

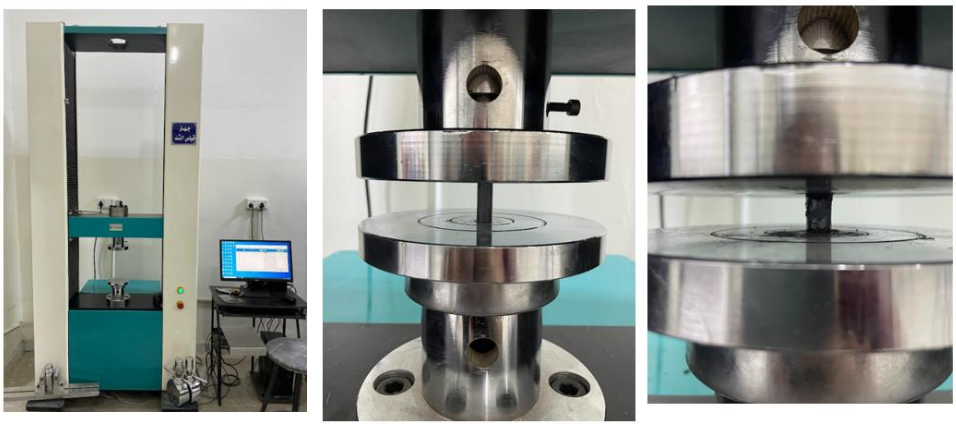


Figure 25. The compressive strength instrument and sample images were taken before and after

3.4.2 Coefficient of friction

Friction is a fundamental tribological phenomenon that governs the resistance to motion when two bodies come into contact. In engineering applications, it is generally categorized into sliding friction and rolling friction, although in practical systems these modes rarely occur in complete isolation. Even in nominal rolling contact, a certain degree of micro-sliding or creep is usually present at the interface due to surface roughness, elastic deformation, and material heterogeneity. Consequently, frictional behavior is best understood as a combined response of multiple interacting mechanisms rather than a single idealized mode.

In a typical pin-on-disc test configuration, the upper specimen (pin) is brought into contact with a rotating disc under a predefined normal load. To initiate and sustain relative motion, a tangential force F is required to overcome interfacial resistance arising from adhesion, deformation, and ploughing effects. The relationship between this tangential force and the applied normal load W is expressed through the coefficient of friction, which serves as a key parameter for evaluating interfacial performance.

$$\mu = \frac{F}{W}$$

Here, μ represents the coefficient of friction, F is the measured frictional (tangential) force, and W is the applied normal load. This parameter is highly sensitive to testing conditions, and therefore, a comprehensive interpretation of frictional behaviour must consider influencing factors such as sliding speed, surface temperature, contact pressure, environmental conditions, and material pairing. These variables collectively determine not only the steady-state friction level but also the stability and repeatability of the tribological response.

As shown in Figure 26, the pin-on-disc setup provides a controlled environment for the simultaneous evaluation of friction and wear behaviour.

The coefficient of friction was measured according to the ASTM G99 [66] standard using a Universal Friction and Wear Machine, brand: United Test, Model: MMW-1A; the wear behaviour of the iron matrix composite was evaluated using a pin-on-disc wear testing machine, as shown in the experimental setup. The test was conducted under controlled loading and sliding conditions to investigate the frictional behaviour and wear resistance of the samples. Applied load: 18.4 N; pin material: Iron matrix composite specimen; disc material: Hardened steel disc; sliding speed: 600 rpm; wear track radius: 25 mm; sliding distance: 942 m.



Figure 26.Friction and wear test

3.4.3 Wear Rate results of hybrid iron matrix composite

The wear rate is determined by monitoring the loss of mass of the specimen during the sliding process over a specified period of time. Before the test, the sample is carefully cleaned and weighed using a high-precision balance to obtain its initial mass. After the wear test is completed, the sample is cleaned again to remove loose debris and reweighed to determine the final mass. The difference between the initial and final mass represents the material loss caused by friction and wear during operation.

3.4.4 Hardness of the hybrid iron matrix composite

The hardness of the hybrid iron matrix composite was measured using the Rockwell hardness test on the C scale (HRC). A diamond cone indenter was used with a total test force of 150 kgf. Hardness measurements were performed on three samples, and the average hardness value was calculated to obtain a representative value for the material, as shown in Figure 27.



Figure 27.Hardness test

3.4.5 Scanning Electron Microscope of the hybrid iron matrix composite

The microstructural characterisation was performed using a Scanning Electron Microscope (SEM) equipped with a Secondary Electron (SE) detector. The samples were examined under high-vacuum conditions using an accelerating voltage of 20 kV, a working distance of approximately 12.3 mm, and a spot size of 30. SEM micrographs were captured at different magnifications to investigate the surface morphology, particle distribution, and microstructural features of the fabricated iron-based hybrid composites. These operating conditions provided high-resolution images suitable for detailed observation of the composite microstructure.

Chapter Four /Results and discussion

This chapter includes two parts: the first part, the characterisation of a hybrid iron matrix composite with the addition of nano-graphite, and the second part, the characterisation of a hybrid iron matrix composite with the addition of nano-MoS_2,

4.1 Characterisation of the Hybrid Iron Matrix Composite with the Addition of Nano-Graphite

4.1.1 Compressive strength of the hybrid iron matrix composite with the addition of nano-graphite

Figure 28 shows the compressive strength results with the addition of nano-graphite. It is noted that the compressive strength of the hybrid iron matrix composite is significantly higher than that of pure iron. The lowest compressive strength of pure iron was 158.40 MPa, due to its relatively soft structure and lack of reinforcements to resist deformation. The hybrid iron composite without adding nano-graphite was 178.60 MPa. Strength increases slightly due to the improved microstructure and load distribution resulting from composite formation. A major improvement is observed with the introduction of nano-graphite. The samples with 0.5 vol.% nano-graphite compressive strength that rises to 217.86 MPa, showing the strong influence of even a small amount of reinforcement. For the samples with 1.0 vol.% nano-graphite, the value slightly increases to 219.19 MPa, indicating that reinforcement continues to improve load-bearing capacity. For the sample with 1.5 vol.% nano-graphite, the compressive strength reaches the highest value of 243.07 MPa, which is ~53% higher than pure iron.

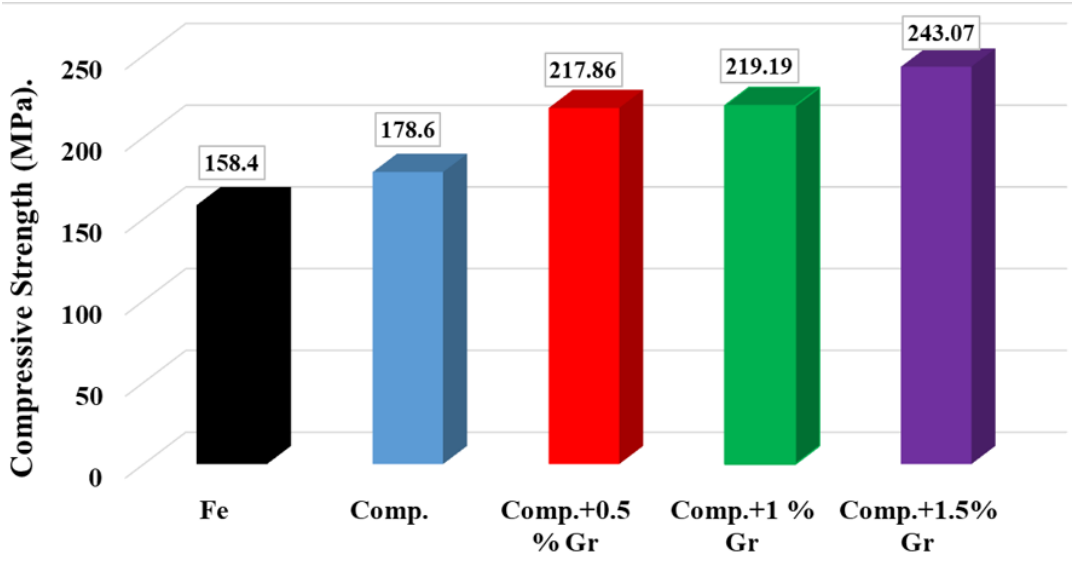
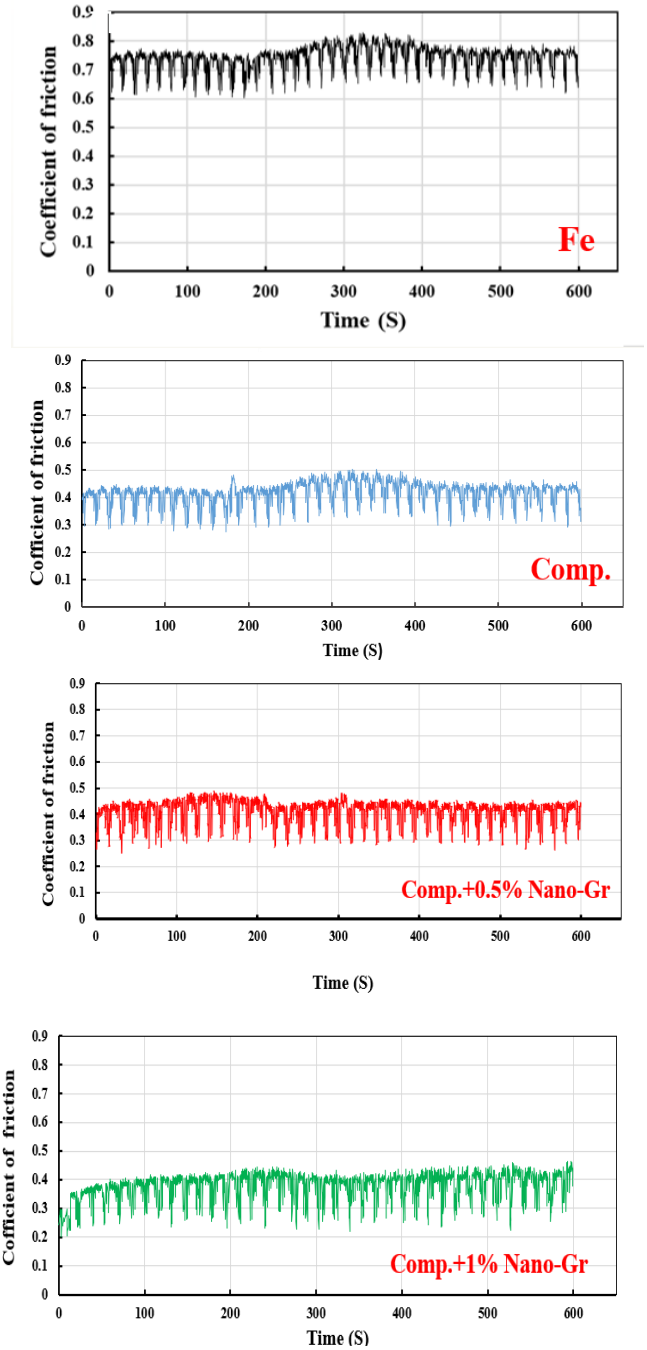


Figure 28. Compressive strength of iron, master composite and iron matrix composites with varying concentrations (0.5, 1, and 1.5 vol.%) of nano-graphite

4.1.2 Coefficient of friction of the hybrid iron matrix composite with the addition of nano-graphite

Figure 29 presents the variation of the coefficient of friction (COF) as a function of sliding time for the iron counterface, the master sample, and the hybrid iron matrix reinforced with 0.5, 1, and 1.5 vol.% nano-graphite. All specimens exhibit an initial running-in period followed by a relatively stable friction regime characterised by periodic fluctuations associated with repeated asperity interactions and wear debris formation during sliding.



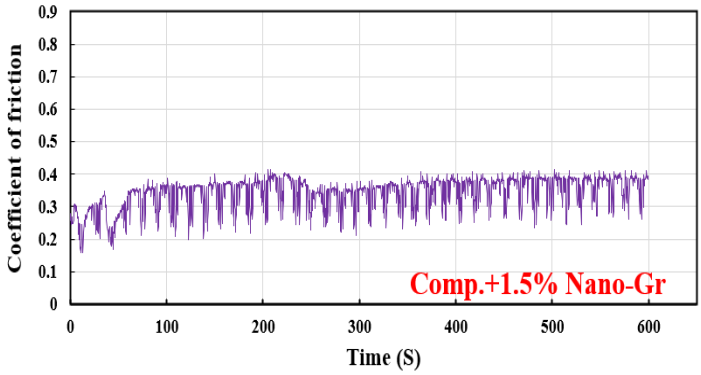


Figure 29. Coefficient of friction during the time of iron, master composite and iron matrix composites with varying concentrations (0.5, 1, and 1.5 vol.%) of nano-Gr

The iron specimen exhibits the highest friction coefficient throughout the test, with values fluctuating between 0.70 and 0.80. After approximately 250–300 s, a slight increase in COF is observed, reaching a maximum near 0.80 before stabilising. The high friction level can be attributed to direct metal-to-metal contact, surface roughening, and the absence of a lubricating tribofilm, resulting in greater adhesion and plowing effects.

The master composite exhibits a substantially lower friction coefficient, ranging from approximately 0.35 to 0.50. Following a short running-in period, the COF gradually increases and reaches a relatively stable state. The reduction in friction compared with iron is associated with the inherent characteristics of the matrix, which promotes less adhesive interaction and generates wear debris that partially separates the sliding surfaces.

For the composite containing 0.5 vol. % nano-graphite, the average friction coefficient remains in the range of 0.40–0.46. The friction behaviour is more stable than that of the master sample, with smaller long-term variations after the running-in stage. The incorporation of nano-graphene likely improves load distribution within the matrix and contributes to the formation of a lubricating transfer layer at the contact interface. However, the friction reduction is modest, suggesting that the graphene content may not be sufficient to establish a continuous lubricating film over the entire contact area.

The composite reinforced with 1 vol.% nano-graphite demonstrates the lowest friction coefficient among all tested materials, stabilising around 0.33–0.40 after the initial running-in period. Although periodic fluctuations are still present, the overall friction level is significantly reduced. This behaviour indicates that increasing the graphene content enhances the self-lubricating effect of the composite. The layered structure of graphene facilitates interlayer sliding and reduces shear resistance at the tribological interface, thereby lowering friction. Additionally, graphene nanoparticles can fill surface asperities and promote the

formation of a protective tribofilm, which minimises direct contact between opposing surfaces.

The coefficient of friction (COF) with sliding time for the composite reinforced with 1.5 vol. % nano-graphite .During the first 50–100 s of testing, the COF increases from approximately 0.20 to about 0.35, indicating progressive adaptation of the contacting surfaces and the establishment of a stable contact area. After this period, the friction coefficient remains relatively constant, fluctuating around 0.35–0.39 throughout the remainder of the test.

When compared with the results shown in the previous figure, the 1.5 vol.% nano-graphite composite exhibits friction behaviour similar to that of the 1 vol.% nano-graphite specimen. Both materials display substantially lower friction coefficients than the master composite and the iron sample, confirming the beneficial role of graphene as a solid lubricant. The average COF of the 1.5 vol. % nano-graphite composite remains within the same range as that observed for the 1 vol.% nano-graphite sample, indicating that increasing the graphite content beyond 1 vol.% does not produce a significant additional reduction in friction

As shown in Figure 30, the coefficient of friction of the hybrid iron metal composite with added nano-graphite with 0.5 ,1, and 1.5 vol.%, the coefficient of friction of pure Iron was 0.416, the highest friction value, meaning more resistance to sliding and higher wear tendency. The coefficient of friction (COF) of the composite without nano-graphite was 0.409, A slight reduction in friction compared to pure iron, due to a more stable composite structure. Composite + Nano-graphite: As nano-graphite is added, the COF decreases consistently:

- When 0.5 vol. % nano-graphite was added, the COF dropped to 0.409.
- When 1.0 vol. % nano-graphite was added, it reduced further to 0.376.
- When 1.5 vol.% nano-graphite was added, the lowest COF of 0.341 was achieved.

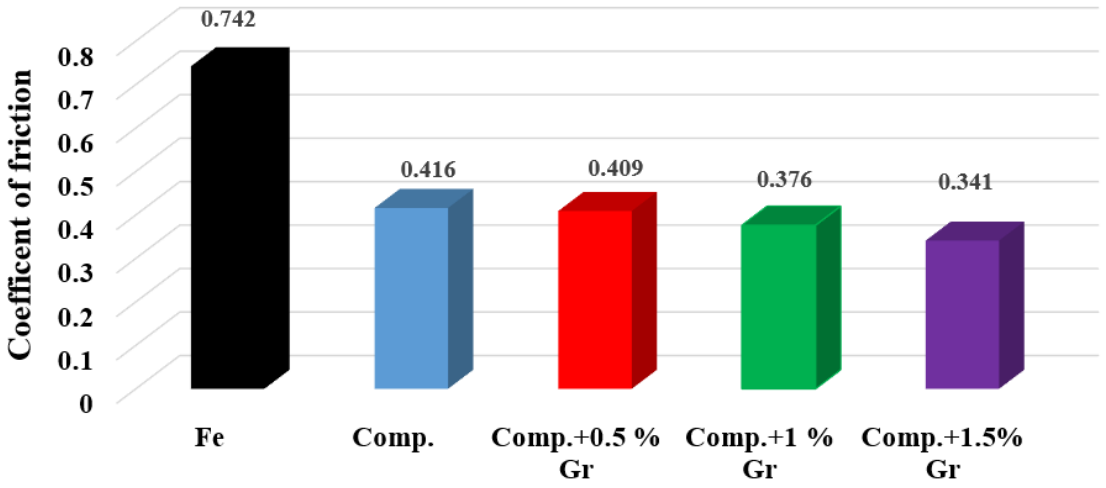


Figure 30. Coefficient of friction for iron, master composite and iron matrix composites with varying concentrations (0.5, 1, and 1.5 vol.%) of nano-Gr

The statement accurately explains the lubricating role of nano-graphite in iron-matrix composites. During the composite's production and operation, the layered crystal structure of graphite and the weak van der Waals bonds between layers allow the layers to slide past each other easily. This enables the formation of a lubricating film that reduces adhesion and wear.

Key principles of nano-graphite lubrication

- Graphite is made up of numerous layers of graphene sheets. Strong covalent bonds hold together the carbon atoms within each sheet, but the sheets themselves are linked by much weaker van der Waals forces [67].
- When friction occurs, these weak interlayer bonds allow the graphene sheets to slide over one another with minimal resistance. This provides the excellent quality that makes graphite a solid lubricant [67, 68].
- In the composite material, the nano-graphite particles are uniformly dispersed throughout the iron matrix. When the composite's surface undergoes sliding motion against another surface, the nano-graphite is released from the matrix. These particles then smear onto the contact interface, creating a protective, low-shear-strength film that prevents direct metal-to-metal contact.
- By physically separating the two sliding surfaces, this thin lubricating film significantly reduces friction. This lowers the coefficient of friction and minimises material loss, thus improving the overall wear resistance of the composite material.
    - The process of releasing and forming a lubricating film is a self-sustaining mechanism. The composite releases graphite in response to the friction and wear at the contact surface, which continuously provides lubrication as needed [67,68].

The primary self-lubrication mechanism relies on graphite's layered crystal structure, in which weak van der Waals forces hold individual carbon layers together. During sliding, these layers can easily shear relative to each other, forming a thin, lubricating film on the contact surface, as shown in **Figure 31,** the graphite structure.

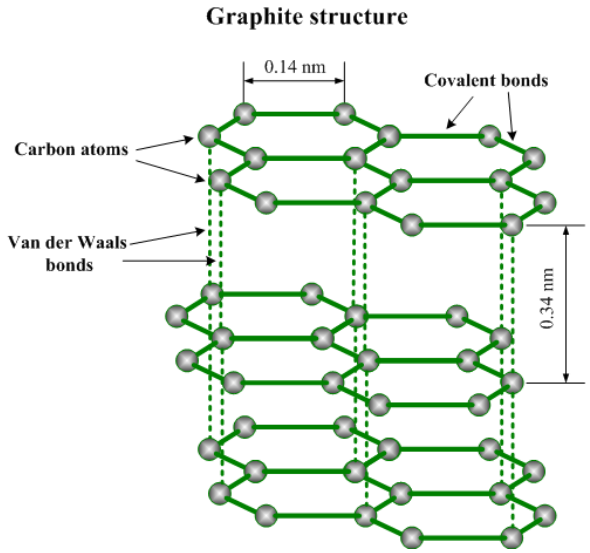


Figure 31.Graphite structure [69].

4.1.3 Wear rate of the hybrid iron matrix composite with the addition of nano-graphite

Figure 32 illustrates the wear rates (mg/s) of pure iron (Fe), a master composite, and the master composite with additions of nano- graphite 0.5, 1.0, and 1.5 vol.%. The results show a pronounced and continuous reduction in wear rate as graphite content increases. Pure iron exhibits the highest wear at 0.164 mg/s, while the base master composite alone reduces this to 0.089 mg/s—a 45.7% improvement, attributable to the intrinsic mechanical properties of the composite matrix. The addition of graphite further enhances wear resistance dramatically: 0.5 vol. % nano-graphite lowers the rate to 0.062 mg/s (a 30.3% drop from the base composite), 1.0 vol % nano-graphite brings it down to 0.029 mg/s (a 67.4% reduction), and 1.5 vol.% nano-graphite achieves the lowest value of 0.025 mg/s (a 71.9% reduction relative to the base composite, and an overall 84.8% improvement over pure iron). Notably, the incremental benefit is largest between 0.5 and 1.0 vol. % nano-graphite (a decrease of 0.033 mg/s), while the gain from 1.0 to 1.5 vol.% is smaller (only 0.004 mg/s), indicating a clear saturation effect. This behaviour is characteristic of graphite as a solid lubricant: during sliding, graphite particles are exfoliated and spread across the wear track, forming a protective, low-shear tribofilm that minimises direct metal-to-metal contact, reduces adhesion, and suppresses abrasive ploughing. Overall, the figure unequivocally demonstrates that graphite is a highly effective wear-reduction additive for this composite system, with the 1.5 vol.% nano-graphite

composition delivering the best performance, although 1.0 vol% nano-graphite already provides the vast majority of the benefit and may represent the more economical optimum.

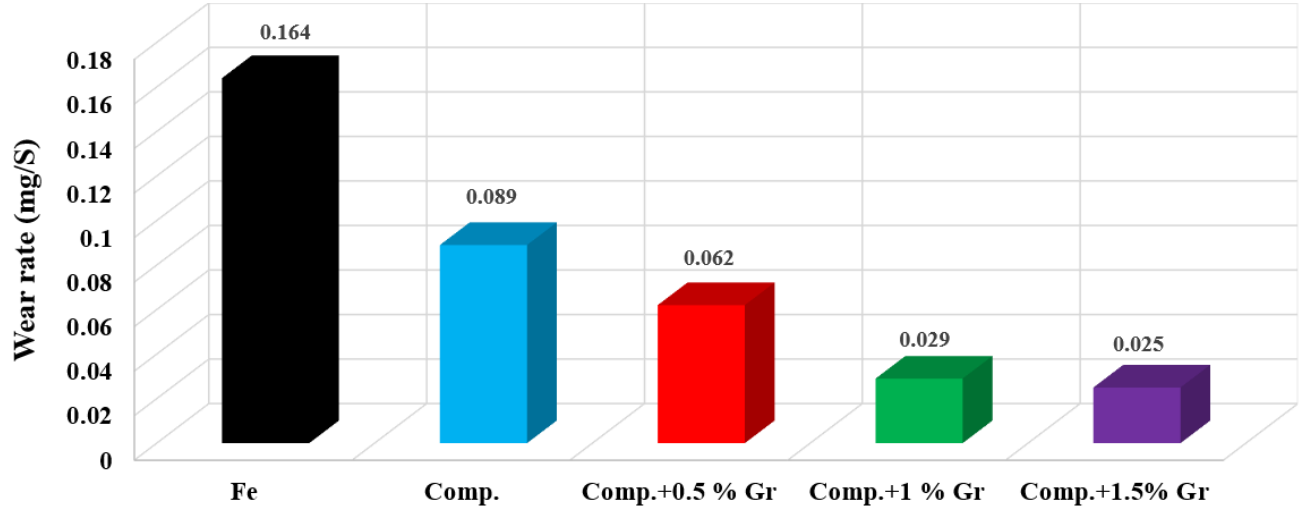


Figure 32. *wear rate of iron, master composite and iron matrix composites with varying concentrations (0.5, 1, and 1.5 vol.%) of nano-graphite.*

4.1.4 Hardness of the hybrid iron matrix composite with the addition of nano-graphite

Figure 33 shows the Rockwell hardness for iron (Fe), master composite, and composites added with different contents of nano-graphite particles. The hardness of pure iron was 77.5 HRC, which increased to 82 HRC after the addition of alumina (Al_2O_3) and zirconia (ZrO_2), indicating that the ceramic reinforcements improved the matrix's resistance to plastic deformation. This enhancement can be attributed to the inherently high hardness of Al_2O_3 and ZrO_2 particles, which act as barriers to dislocation movement and strengthen the iron matrix through dispersion strengthening.

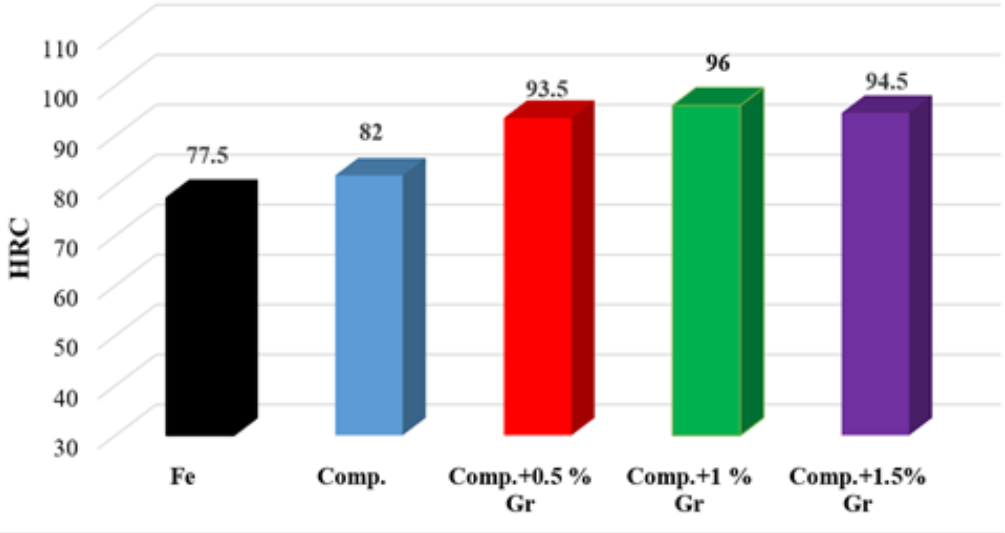


Figure 33. *Hardness of iron, master composite and iron matrix composites with varying concentrations (0.5, 1, and 1.5 vol.%) of nano-graphite*

A further increase in hardness was observed with the incorporation of nano-graphite—the composite containing 0.5 vol. % nano-graphite exhibited a hardness of 93.5 HRC, representing a significant improvement compared with the Fe–Al_2O_3–ZrO_2 composite. Increasing the graphene content to 1 vol.% nano-graphite resulted in the highest hardness value of 96 HRC, corresponding to an overall increase of approximately 23.9% relative to pure iron. This improvement is mainly due to the exceptional mechanical properties of nano-graphite, its large surface area, and its ability to effectively transfer load and hinder dislocation motion within the composite structure.

When the nano-graphite content was increased further to 1.5 vol.% nano-graphite, the hardness slightly decreased to 94.5 HRC. Although this value remained considerably higher than that of the unreinforced composite, the reduction compared with the 1 vol.% nano-graphite sample may be associated with the agglomeration of graphene nanoparticles at higher concentrations. Such agglomerates can create local stress concentrations and reduce the uniform distribution of reinforcement particles, thereby limiting the strengthening efficiency.

4.1.5 SEM and EDX of the hybrid iron matrix composite with the addition of nano-graphite

An unreinforced pure-iron matrix was characterized to be used as a comparative baseline to evaluate the effects of subsequent ceramic and nanoscale additions, as shown in Figure 34. The morphology obtained by scanning electron microscopy (SEM) at low magnification is in agreement with the typical morphology of solid-state sintering, showing equiaxed polygonal grains of iron, sharp grain boundaries, and triple junctions [70]. The major grain faces are continuous and do not have the secondary-phase blocking that is seen in hybrid metal matrix composites. This observation suggests that, in the absence of pinning by foreign dispersoids, the matrix likely underwent uninhibited grain-boundary migration and normal grain growth during the sintering cycle [71].

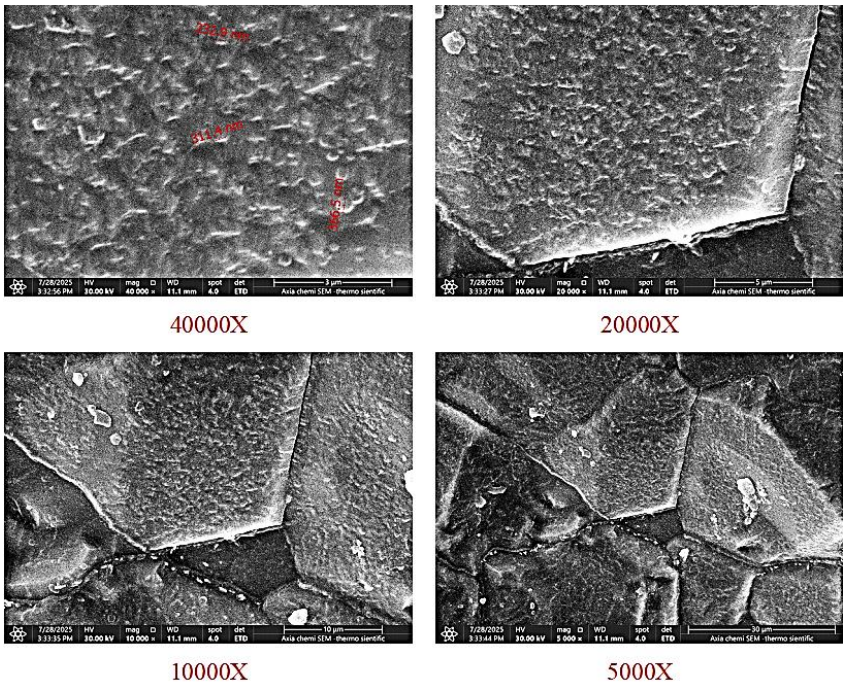


Figure 34 . The SEM micrographs of the pure iron reference sample at various magnifications (5,000×, 10,000×, 20,000× and 40,000×) show large polygonal grains of iron, well-defined grain boundaries, and fine surface thermal etchings.

Fine topographical variations (around 230–367 nm) can be seen on the surface of the grains under high-magnification SEM. Two phenomena common in high-temperature PM are believed to be responsible for these features: thermal etching, due to minimization of surface energy under high-vacuum processing [72], and the formation of superficial oxides during the cooling phase.

Spot energy-dispersive X-ray spectroscopy (EDS) of the matrix(Figure 35) shows a high-purity iron signature, dominated by the prominent Kα (6.4 keV) and Kβ (7.05 keV) emission lines. An oxygen peak is also detected at ~0.52 keV. Because no corresponding Al or Zr peaks are observed, this result is consistent with the formation of superficial native oxide nanostructures, possibly due to trace atmospheric moisture present during or after sintering [73].

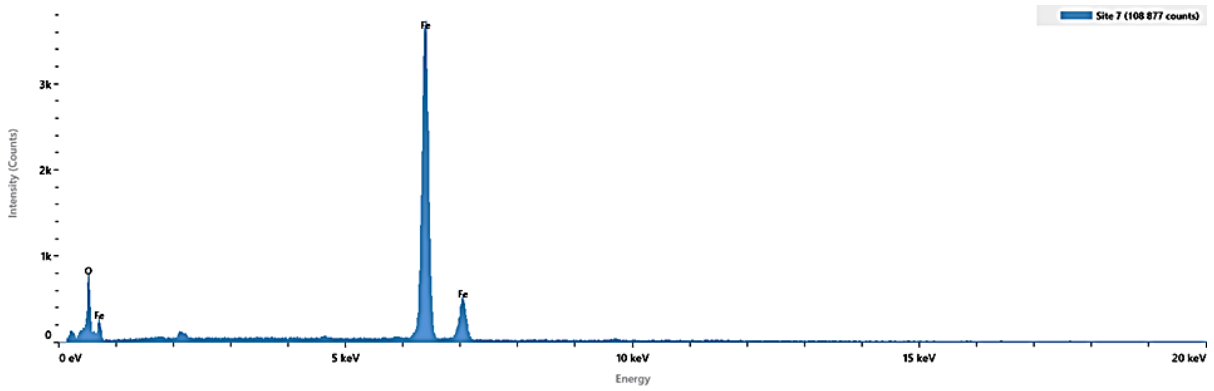


Figure 35.The elemental purity and presence of a baseline native oxide phase of the compacted and sintered pure iron (Site 7) control matrix is shown as an energy-dispersive X-ray spectroscopy (EDS) spectrum.

is overwhelmingly dominated by elemental iron (Fe). Another L_α peak is observed at low energies (close to 0.7 keV), indicating a well-defined metallic state.

Crucially, the complete absence of elements such as molybdenum (Mo), sulfur (S), aluminum (Al), and zirconium (Zr) in the EDS spectrum suggests that the raw material stock was uncontaminated and that cross-contamination protocols between batches were effective. Overall, this reference sample establishes a baseline of uninhibited polygonal grain architecture, in contrast to the restricted grain expansion and secondary-phase blockages observed in the microstructural architecture of the hybrid systems (e.g., Fe-Al_2O_3-ZrO_2/nano-MoS_2) [74].

Energy-dispersive X-ray spectroscopy (EDS) indicates that the composite matrix is predominantly iron, characterized by strong Fe Kα (6.4 keV) and Fe Kβ (7.1 keV) emission peaks, as well as a low-energy L-line (~0.7 keV) peak (Figure 36). Distinct secondary peaks corresponding to aluminum (Al L-lines at ~1.49 keV) and zirconium (Zr Lα at ~2.04 keV and Kα at 15.7 keV) are also detected. While EDS confirms the presence of these elements rather than specific crystalline phases, this result is consistent with the successful incorporation of Al- and Zr-bearing secondary reinforcements [75]. Furthermore, the relatively low intensity of these secondary peaks suggests that the reinforcing agents may be finely distributed throughout the matrix.

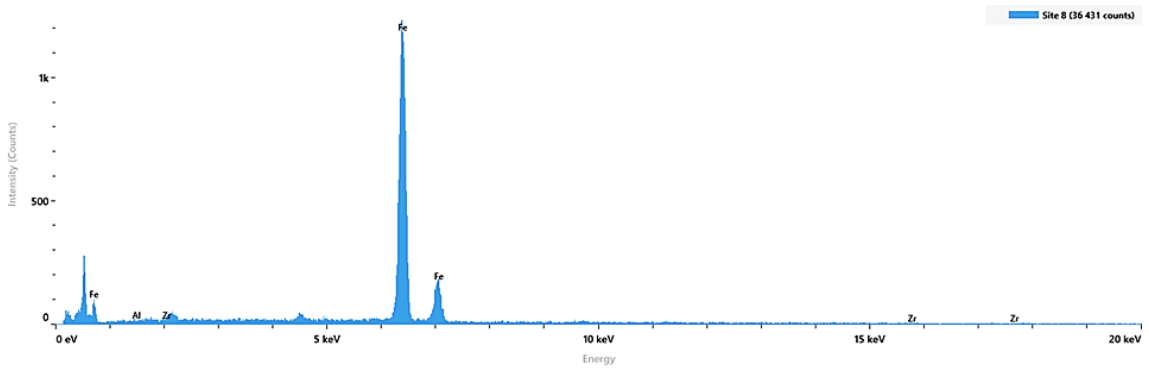


Figure 36. EDS spectrum of the iron-metal matrix composite (Fe-MMC) obtained from Site 8 for a total of 36,431 counts. The spectrum confirms a dominant elemental Fe matrix by the presence of primary emission peaks K_α and K_β, and low-energy emission peaks (L-lines), with trace distribution of reinforcing elements present as secondary peaks aluminum (Al) and zirconium (Zr).

Figure 37 shows that the SEM image of the composite exhibits a well-compacted and dense structure, with little macro-porosity. Secondary-phase particulates are seen in the intragranular spaces and segregated along the grain-boundary networks. When magnified, these particulates can be seen to have an irregular, angular shape, possibly due to mechanical milling or chemical synthesis of the dispersoids [76]

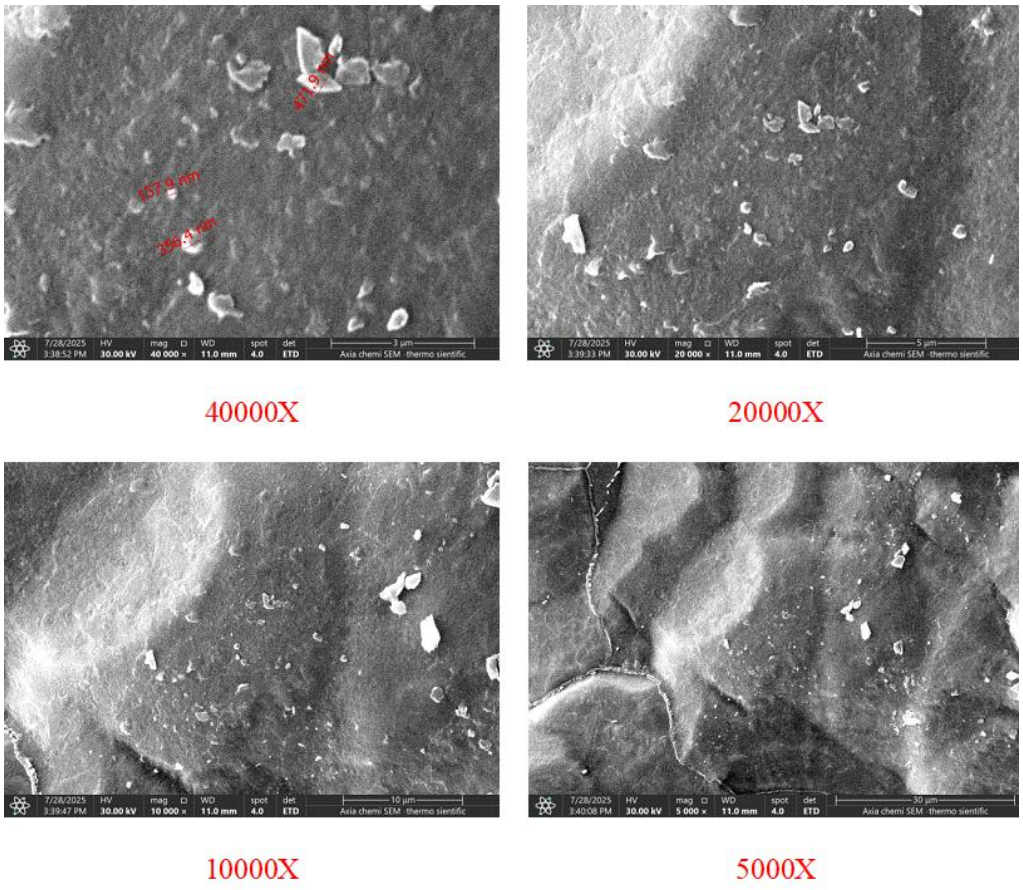


Figure 37. Compacted iron-metal matrix composite micrographs at 5000X, 10000X, 20000X and 40000X magnification by scanning electron microscopy (SEM). At high magnification

(40000X), the lateral dimensions of discrete sub-micron secondary-phase particles dispersed in the matrix are examined, providing representative particle sizes of 356.4 nm, 457.9 nm, and 471.9 nm.

The lateral dimensions of these discrete secondary particles fall within the submicron range (approximately 356-472 nm). In the high-magnification micrographs, the particles appear tightly embedded in the iron matrix with no apparent micro-voids, debonding, or micro-cracks at the interfaces. These observations suggest good wettability and mechanical interlocking achieved during compaction and sintering [78].

The distribution of these submicron particles at the iron grain boundaries may contribute to restricted grain growth during thermal processing. The observed particle radii (r ≈ 178 to 236 nm) suggest a potential enhancement in Zener pinning drag pressure $P_Z = 3\gamma F_v / 2r$. Consequently, a possible explanation for the composite's optimized mechanical performance is the combined effect of grain-boundary strengthening (the Hall-Petch effect) and dispersion strengthening. Specifically, these rigid submicron dispersoids may contribute to the Orowan bowing mechanism by acting as obstacles that impede moving dislocations [77, 79].

The microstructural characteristics of the compacted and solid-state-sintered hybrid metal matrix composite (HMMC)—intended to incorporate ceramic phases (Al_2O_3, ZrO_2) and 0.5 vol.% nano-graphite—exhibit a significant morphological shift compared to the unreinforced iron baseline. Low-magnification scanning electron microscopy (SEM) reveals a well-consolidated structure with characteristic linear features, shear-like steps, and planar slip traces (Figure 38). These observations suggest that local stresses and high constraints from the cold compaction stage may have been retained during the constrained solid-state sintering process [75].

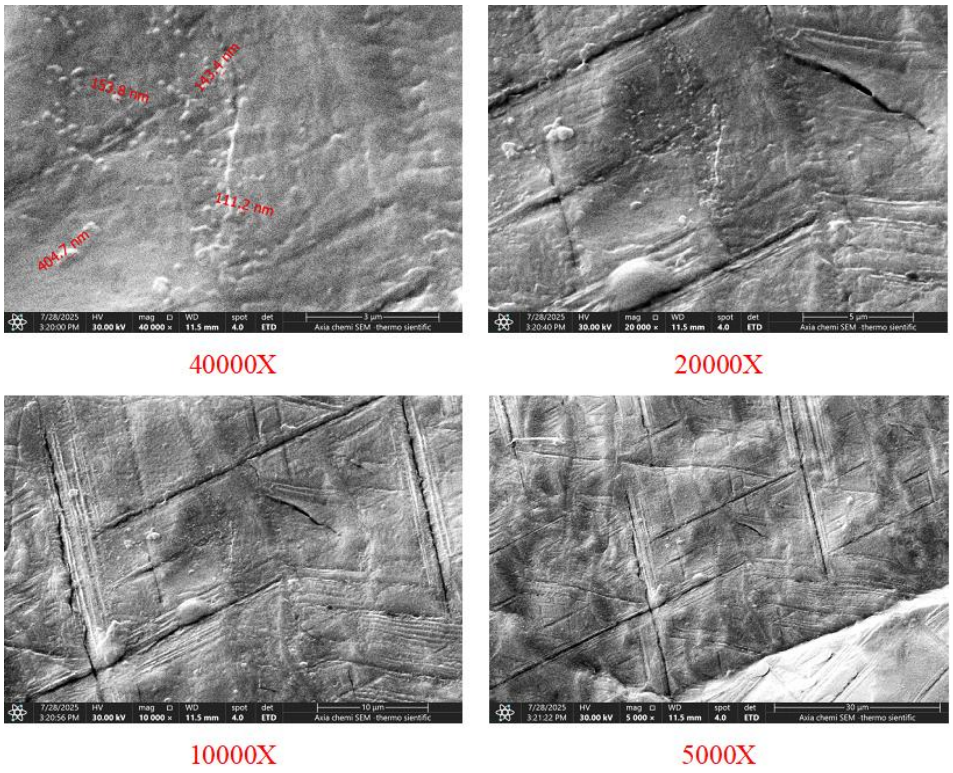


Figure 38. The SEM images of the compacted and sintered hybrid metal matrix composite specimen at various magnifications (5,000×, 10,000×, 20,000×, and 40,000×). A very different grain-surface topography is observed at high magnification, characterized by regular line slip bands, facets on the grain interfaces, and uniformly dispersed nanoscale particulate ceramic/carbonaceous reinforcements ranging from about 111.2 nm to 404.7 nm.

At high magnifications, SEM images reveal the distribution of nanoscale and sub-micron particulates (with lateral dimensions of around 111 nm to 405 nm) within and along the steps of the interfacial steps. This unique grain surface topography could be explained by the physical interpenetration of the fine ceramic and carbonaceous reinforcements in the iron matrix.

At high magnifications, SEM images reveal the distribution of nanoscale and sub-micron particulates (with lateral dimensions of around 111 nm to 405 nm) within and along the steps of the interfacial steps. This unique grain surface topography could be explained by the physical interpenetration of the fine ceramic and carbonaceous reinforcements in the iron matrix.

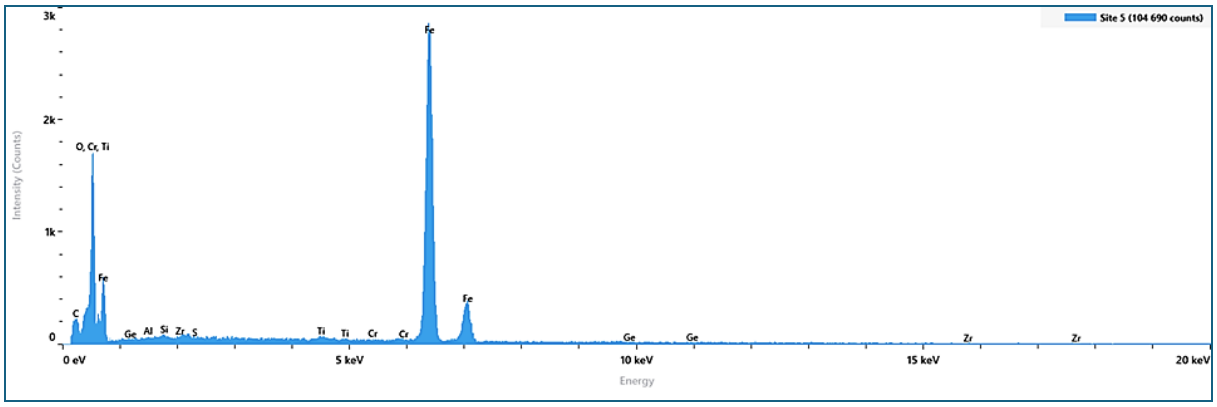


Figure 39. Surface energy-dispersive X-ray spectroscopy (EDS) spectrum of the sintered hybrid metal matrix composite (Fe - Al_2O_3 - ZrO_2 / 0.5 vol.% nano-graphite), which shows the presence of the iron matrix, characteristic peaks of C, O, Al, and Zr elements, and minor peaks of trace elements (Cr, Ti, Si, S, Ge).

The presence of these fine discrete particles in the matrix and at the grain boundaries offers promising paths for mechanical/tribological optimization. The microstructural observations imply that these secondary phases may hinder excessive iron grain growth during the isothermal sintering hold [80], and one possibility is the introduction of a Zener-pinning drag effect on the moving grain boundaries, which leads to an increased complexity of the grain-boundary network. Moreover, the results were found to be consistent with the hypothesis that rigid ceramic inclusions in the matrix can enhance mechanical behavior by Orowan strengthening and load transfer, and that the nano-graphite reinforcements possess self-lubricating properties and serve as dislocation storage barriers [81]. To summarize the above, a synergy of both configurations could result in improved wear resistance, yield strength, and integrity of the sintered compact when compared to unreinforced cases.

The 1.0 volume percent Nano-Graphite Composite was microstructurally and elementally characterized. Raising the amount of nano-graphite reinforcement to 1.0 vol. % in the Fe-Al_2O_3-ZrO_2 hybrid metal matrix composite leads to a significant change in morphology compared with the dense and continuous grain network found in lower concentrations, such as 0.5 vol. %. The matrix is highly porous with large irregularly shaped voids and high particulate agglomeration as seen in the scanning electron microscopy (SEM) image (Figure 40). At high magnifications, clean planar slip features and well-coalesced polygonal iron grains are replaced by a highly convoluted rugged topography made up of loosely bound particle aggregates. The previous observations suggest slower sintering processes and localized structural deterioration

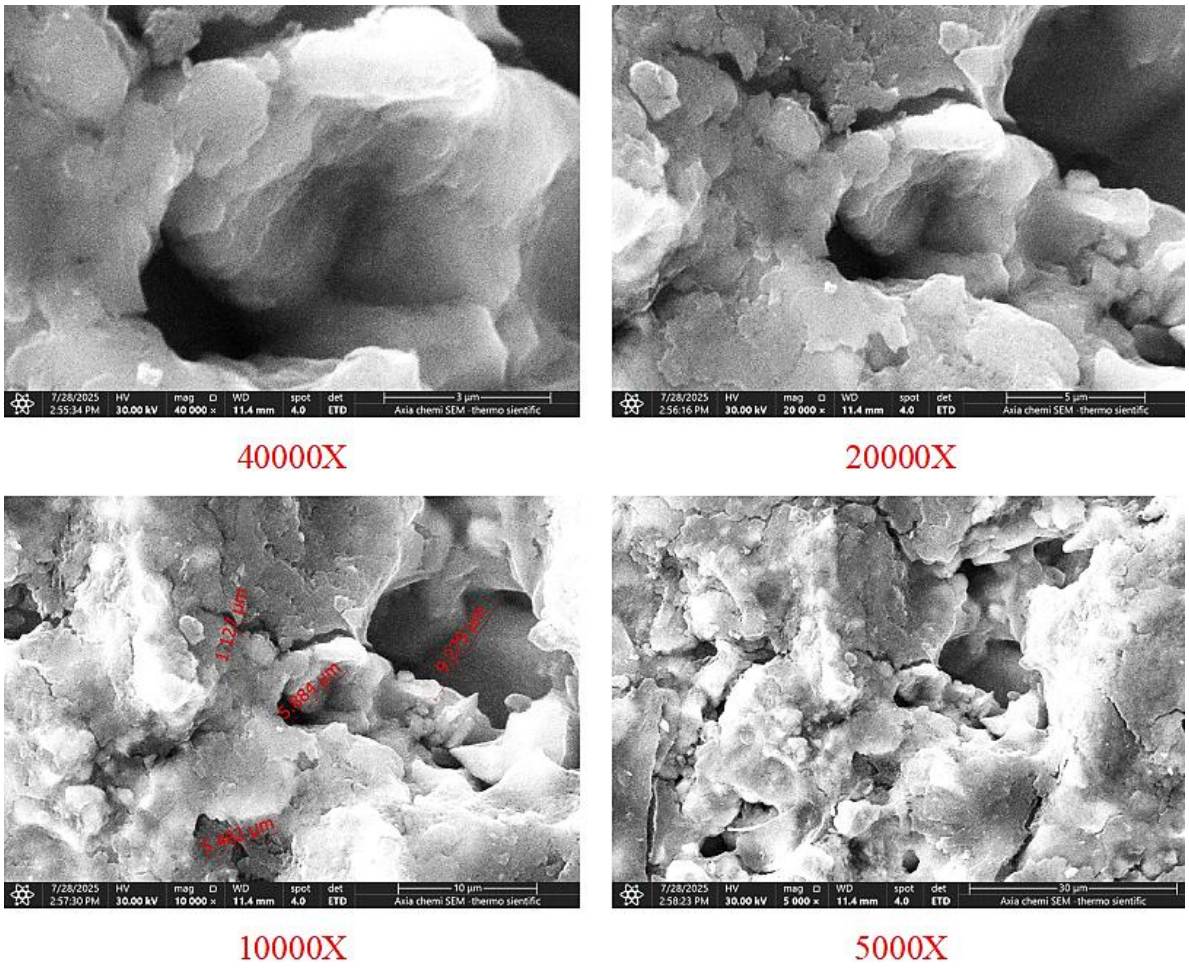


Figure 40. The SEM images of the compacted and sintered hybrid metal matrix composite specimen at various magnifications (5,000×, 10,000×, 20,000×, and 40,000×). The micrographs are used to quantify changes in particulate agglomeration and microporosity, with features measured between 1.127 µm and 9.279 µm.

The matrix has large microporosity and is extensively porous, with clusters at lower magnifications (5,000× and 10,000×). Large voids in the matrix, which are irregular in shape, and particle agglomerates that are 1.127 µm, 5.482 µm, and 5.884 µm in size, and large macro-pores of up to 9.279 µm in length are highlighted.

This unique increase in porosity and the disturbance of continuous boundaries of iron matrix grains are due to the physical behavior of carbonaceous nanomaterials in the powder metallurgy system. In cases where the sheets of nano-graphite are integrated in higher fractions, they have a strong tendency to self-attract by Van Der Waals forces [77] and tend to agglomerate. These clusters of carbonaceous material are deposited preferentially at the original interfaces between the iron particles and act as strong mechanical and steric barriers. The direct barrier posed by this boundary layer to atomic contact between iron atoms hinders

intimate contact and the growth of an interfacial neck, thereby preventing full solid-state densification through grain-boundary migration [82].

The high-magnification micrographs (20,000× and 40,000×) show a very rugged topography with a high degree of convolution. Clean, planar slip features and well-coalesced polygonal features of the iron matrix grains are no longer seen. Rather, they are substituted by aggregates of particles that are not tightly bound. This suggests the large volume fraction of elastic nano-graphite induced a large spring-back effect during cold compaction, resulting in low initial green density and directly contributing to the large volume fraction of internal voids after sintering [83].

High-resolution energy-dispersive X-ray spectroscopy (EDS) was used to make a chemical evaluation of this heterogeneous area (Figure 41). There are a lot of statistical counts (348,128), with the Fe K_α (~6.4 keV) and Fe K_β (~7.06 keV) characteristic iron matrix lines shown.

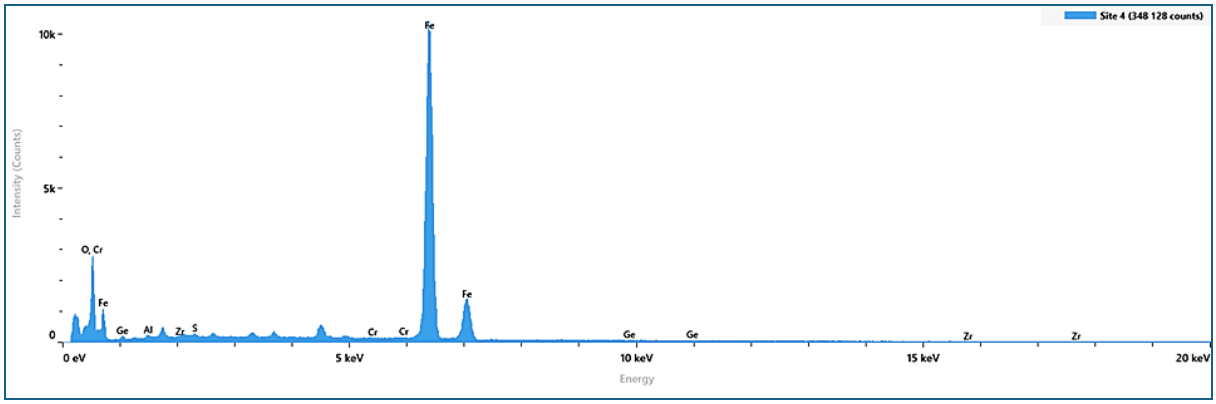


Figure 41. Surface energy-dispersive X-ray spectroscopy (EDS) spectrum of the sintered hybrid metal matrix composite (Fe - Al_2O_3 - ZrO_2 / 1.0 vol.% nano-graphite), which shows the presence of the iron matrix, characteristic peaks of C, O, Al, and Zr elements, and minor peaks of trace elements (Cr, Ti, Si, S, Ge).

Such a significant rise in porosity and the break-up of the continuous iron grain boundaries could be explained by the behavior of carbonaceous nanomaterials at higher volume fractions. There are some reports that nano-graphite sheets have a high van der Waals attraction for each other [77]. These agglomerates tend to settle at the boundaries of the initial iron particles and can become mechanical and steric barriers. This boundary layer is likely to have the effect of inhibiting intimate atomic contact and interfacial neck growth, thus preventing a complete solid-state densification by grain-boundary migration [82]. Moreover, the high volume fraction of elastic nano-graphite can lead to a spring-back effect during cold compaction, which can also directly lead to a low green density and a high volume of internal voids after the sintering process [83].

The surface energy-dispersive X-ray spectroscopy (EDS) of this very heterogeneous region (Figure 41) confirms an iron-dominated matrix, as well as the distinct signals for carbon (~0.28 keV), oxygen, aluminum (~1.49 keV), and zirconium (~2.04 keV). Although EDS cannot positively identify the exact crystal phases of the complex oxides, the results do show the presence of these elements, which is consistent with the incorporation of the ceramic and carbonaceous reinforcements. Other elements, such as trace elements (Cr, Ge, S), are also observed; it is suggested that the contamination from the precursor processing or mechanical-alloying wear is responsible [77].

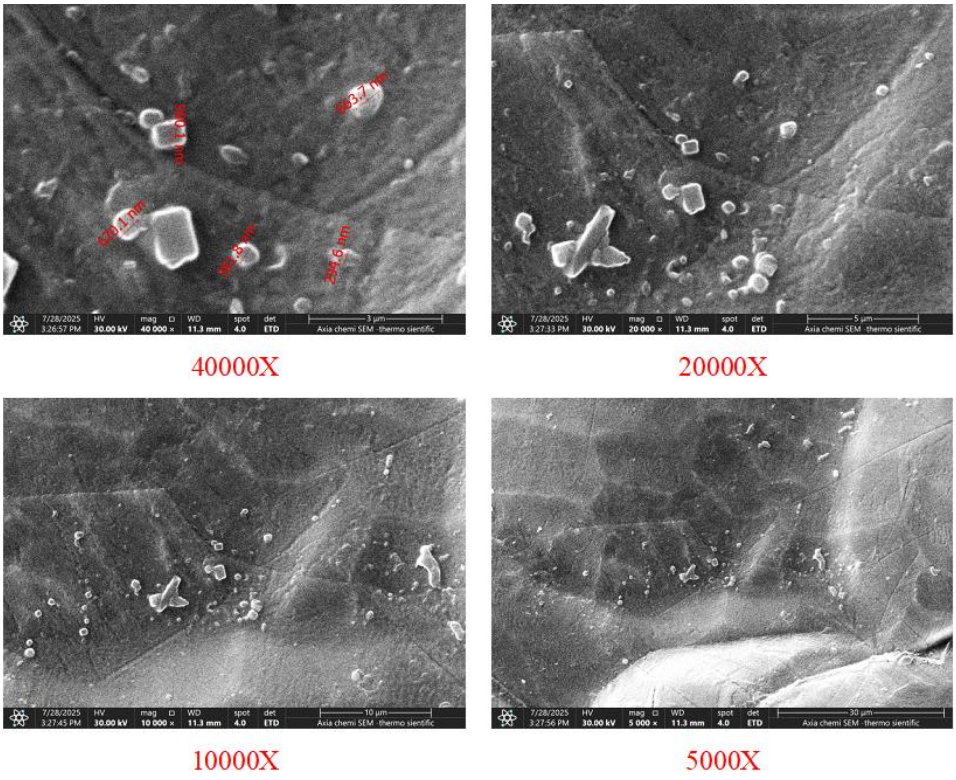


Figure 42. Compacted and sintered SEM images of the hybrid metal matrix composite (1.5 vol. % nano-graphite) at various magnifications: 5,000×, 10,000×, 20,000× and 40,000×. The high-magnification microstructural images (40,000×) show a clear morphological transition in which highly faceted, geometric micro- and nanocrystals (spanning from 294.6 to 663.7 nm) are dispersed across the matrix surfaces.

Localized energy-dispersive X-ray spectroscopy (EDS) of these geometric particulates (Figure 43) reveals a remarkably intense oxygen peak (O-Kα) relative to the iron matrix signals. The baseline also indicates aluminium and zirconium, suggesting these faceted structures are associated with the alumina and zirconia co-dispersoids. Additionally, trace elemental sulfur is detected; this observation is consistent with localized elemental segregation, which has been linked to the recrystallization of secondary phases under high carbon activity [77].

The combination of the strong oxygen signal with the blocky geometric morphologies indicates localized in situ crystallization phenomena. The presence of these features may be explained by the formation of complex hybrid oxides or by reaction with carbon (carbothermal) that nucleate preferentially at the surface interfaces, although the presence of elements is only confirmed by EDS [86].

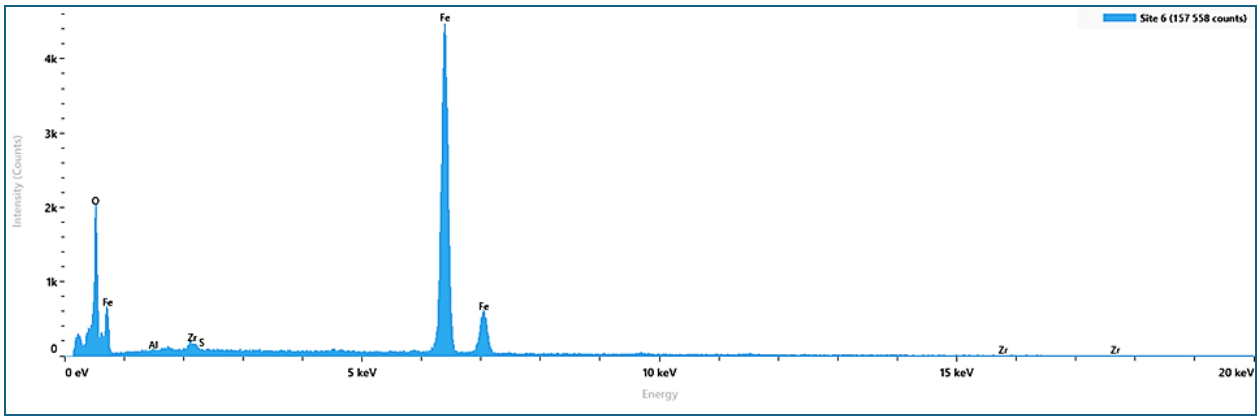


Figure 43. Energy-dispersive X-ray spectroscopy (EDS) spectrum recorded from the surface of the sintered hybrid metal matrix composite with 1.5 vol. % nano-graphite addition with a very strong oxygen (O) peak and prominent matrix lines from Fe, Al, Zr, and a trace element of sulfur (S).

The unique microstructure herein may be mechanically and tribologically suggestive of a dual-effect architecture. On the other hand, the rigid, well-anchored sub-micron crystallites might be responsible for precipitation strengthening by limiting the movement of dislocations, in a similar manner as in Orowan strengthening [87]. Conversely, the geometric sharpness of such facets may be a stress concentrator. These features may induce further micro-cleavage or intergranular delamination at the particle-matrix interfaces under cyclic or tensile loading, which may accelerate the composite's damage before occurrence and/or intensify the degradation process. These features may further induce micro-cleavage or intergranular delamination at the particle-matrix interfaces under cyclic or tensile loading, which may accelerate damage occurrence before loading and/or intensify the degradation process of the composite [88].

4.2 Characterisation of the hybrid iron matrix composite with the addition of nano-MoS_2

4.2.1 Compressive strength of the hybrid iron matrix composite with the addition of nano-MoS_2

Figure 44 shows that the compressive strength increased progressively with the addition of nano-MoS_2. Pure iron exhibited a compressive strength of 158.4 MPa, which increased to 178.6 MPa after the incorporation of Al_2O_3 and ZrO_2, due to the strengthening effect of the ceramic particles. Further addition of MoS_2 nanoparticles enhanced the compressive strength to 189.2 MPa, 195.3 MPa, and 210.5 MPa for 0.5 , 1 and 1.5 vol .% MoS_2 respectively. The improvement is attributed to better load transfer, increased resistance to deformation, and the inhibition of crack propagation by the nanoparticles. The highest compressive strength was obtained at 1.5 vol.% MoS_2, indicating that the combined reinforcement of Al_2O_3, ZrO_2, and MoS_2 effectively improved the mechanical performance of the iron matrix composite.

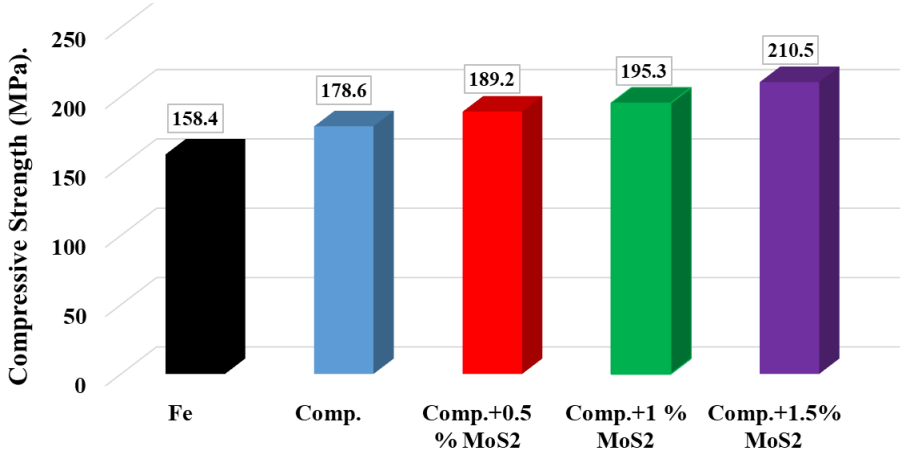
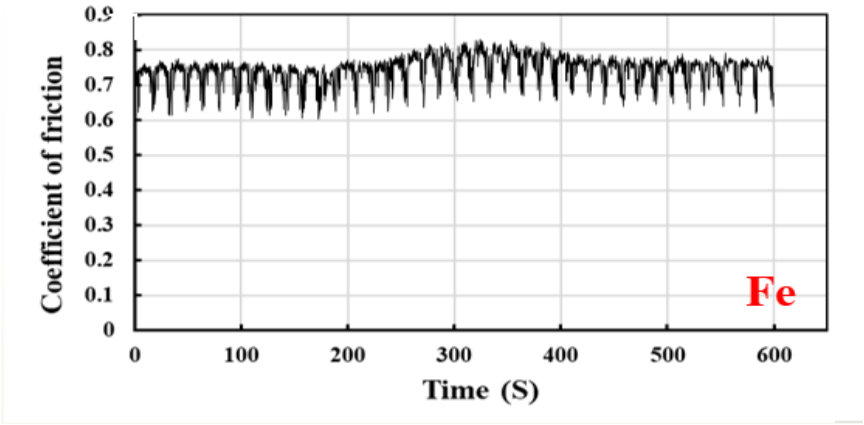
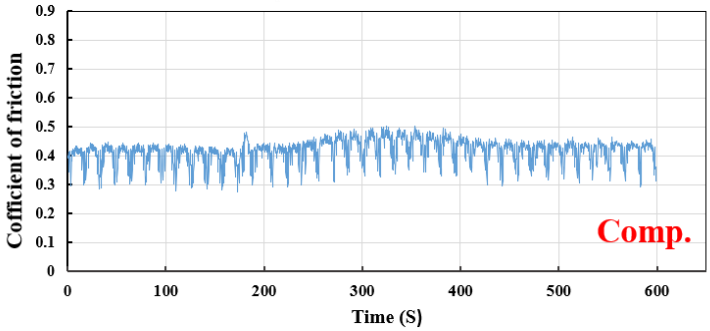


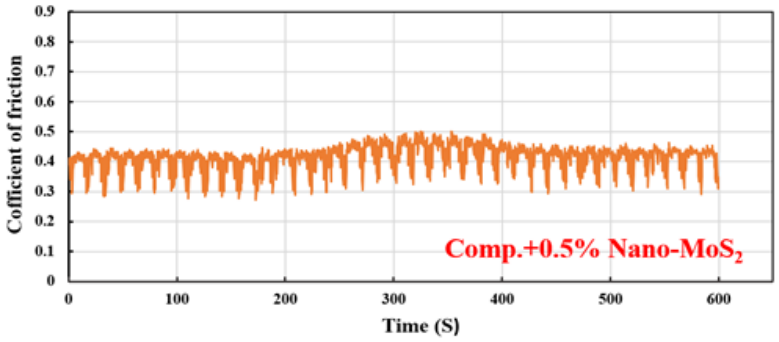
Figure 44. Compressive strength of iron, master composite and iron matrix composites with varying concentrations (0.5, 1, and 1.5 vol.%) of nano-MoS_2

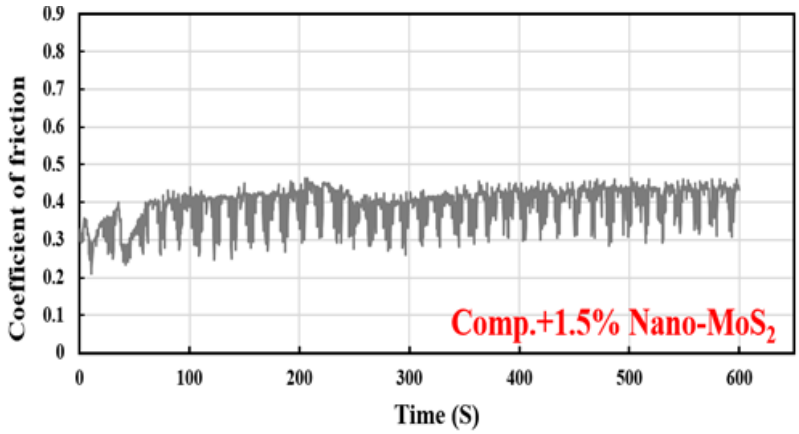
4.2.2 Coefficient of friction of the hybrid iron matrix composite with the addition of nano-MoS_2

Figure 45 presents the variation of the coefficient of friction (COF) with sliding time for the iron substrate, the master composite, and composites reinforced with 0.5 and 1 vol.% nano-MoS_2.


Coefficient of friction
0.9
0.8
0.7
0.6
0.5
0.4
0.3
0.2
0.1
0
0
100
200
300
400
500
600
Time (S)
Fe


Cofficient of friction
0.9
0.8
0.7
0.6
0.5
0.4
0.3
0.2
0.1
0
0
100
200
300
400
500
600
Time (S)
Comp.


Cofficient of friction
0.9
0.8
0.7
0.6
0.5
0.4
0.3
0.2
0.1
0
0
100
200
300
400
500
600
Time (S)
Comp.+0.5% Nano-MoS2


Coefficient of friction
0.9
0.8
0.7
0.6
0.5
0.4
0.3
0.2
0.1
0
0
100
200
300
400
500
600
Time (S)
Comp.+1.5% Nano-MoS2

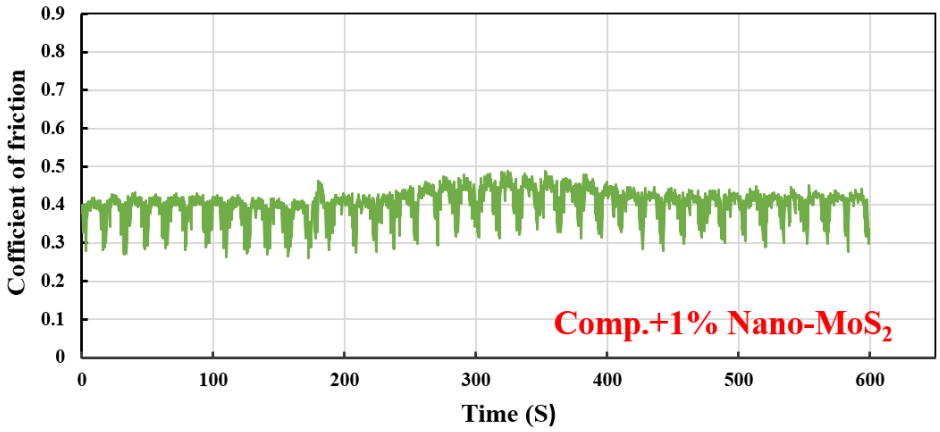


Figure 45. Coefficient of friction over time of iron, master composite and iron matrix composites with varying concentrations (0.5, 1, and 1.5 vol.%) of nano-MoS_2

All specimens exhibit periodic fluctuations throughout the 600s test duration, which are associated with repeated asperity interactions, debris formation, and tribolayer evolution during sliding. The iron sample shows the highest COF, fluctuating around 0.72–0.80, indicating greater resistance to sliding and more severe frictional interaction. In contrast, the master composite exhibits a significantly lower COF, ranging between approximately 0.38 and 0.48, demonstrating the beneficial effect of the composite matrix on friction reduction.

The incorporation of nano-MoS_2 further influences the frictional behavior. The composite containing 0.5 vol.% nano-MoS_2 maintains a relatively stable COF between 0.40 and 0.48, with a slight increase during the middle stage of the test due to temporary tribolayer instability. Similarly, the composite with 1 vol.% nano-MoS_2 shows a comparable friction profile but with slightly reduced fluctuations, suggesting improved lubrication and wear-track stability. The lowest friction values are observed for the composite with the higher nano-MoS_2 content, confirming the solid-lubricant role of MoS_2 nanoparticles. The bottom plot, representing the nano-MoS_2-rich composite, initially exhibits a running-in period followed by stabilisation around 0.40–0.45, indicating the formation of a protective lubricating film on the contact surface.

Overall, the results demonstrate that the addition of nano-MoS_2 effectively lowers the coefficient of friction compared with iron and the unreinforced composite. The enhanced tribological performance is attributed to the layered crystal structure of MoS_2, which facilitates easy shear at the sliding interface and promotes the formation of a stable lubricating tribofilm, thereby reducing direct metal-to-metal contact and improving friction stability during prolonged sliding.

Figure 46 compares the average coefficient of friction of iron, the base composite, and composites reinforced with different contents of nano-MoS_2. The iron specimen exhibited the highest COF (0.742), indicating poor tribological performance due to direct metal-to-metal contact during sliding. The introduction of the composite matrix significantly reduced the COF to 0.416, corresponding to a reduction of approximately 44% compared with iron.

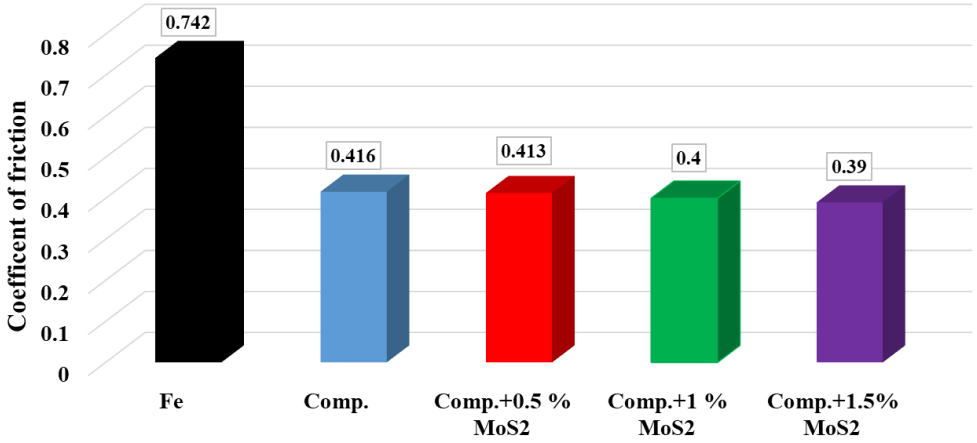


Figure 46.Coefficient of friction of iron, master composite and iron matrix composites with varying concentrations (0.5, 1, and 1.5 vol.%) of nano-MoS_2

Further addition of nano-MoS_2 resulted in a gradual decrease in friction. The COF decreased from 0.413 for the composite containing 0.5 vol.% nano-MoS_2 to 0.400 and 0.390 for the composites containing 1 and 1.5 vol.% nano-MoS_2, respectively. The lowest COF was achieved at 1.5 vol.% nano-MoS_2, representing a total reduction of about 47% relative to the unreinforced iron sample. This improvement is attributed to the excellent solid-lubricating characteristics of MoS_2, which promote the formation of a lubricating tribofilm and reduce interfacial shear stress. Overall, the results demonstrate that increasing the nano-MoS_2 content enhances the friction-reducing capability of the composite and improves its tribological performance. The lubricating property of MoS_2 is fundamentally due to its anisotropic, layered crystal structure.

- S-Mo-S Triatomic Layers: MoS_2 consists of a plane of molybdenum (Mo) atoms sandwiched between two planes of sulphur (S) atoms, as shown in Figure 47 .These triatomic layers are held together by weak van der Waals forces, giving the material a naturally low shear strength. [89]
- Easy Interlayer Slip: Under shear stress, these layers slide easily over one another, which is the primary mechanism for achieving a very low coefficient of friction (COF) [89, 90].

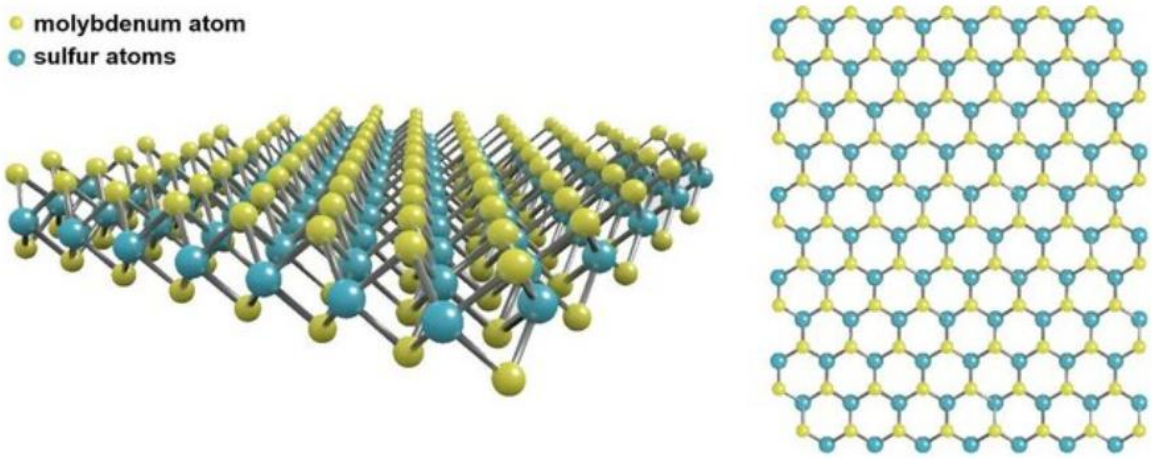


Figure 47. Crystal structure of monolayer MoS_2 [91]

At the nanoscale, the shape and dimensionality of MoS_2 particles directly dictate which lubrication mechanisms are most active. The performance is not one-size-fits-all; it can be tailored by engineering the morphology [89, 91].

A major practical challenge is that bare MoS_2 nanoparticles tend to agglomerate in lubricating oils due to their high surface energy. Therefore, a key principle for effective nano-lubrication is surface modification.[89, 92]

- Functionalization: Researchers use surface functionalization—attaching specific chemical groups to the MoS_2 surface—to improve its dispersibility and stability in base oils.
- Preventing Agglomeration: Stable dispersion ensures that the nanoparticles can be effectively delivered to the friction zone to perform their function, rather than clumping together and settling out of the oil.

Once stable and delivered to the contact area, nano-MoS_2 reduces friction and wear through several concurrent nanoscale mechanisms. These mechanisms are often described as a "triplex synergistic" process, where several actions combine for superior performance [93]:

- Film Formation (Tribofilm): The most critical mechanism. Nano-MoS_2 particles undergo tribo-chemical reactions under pressure and heat, forming a protective, low-shear film (25-40 nm thick) on the metal surfaces. This film prevents direct metal-to-metal contact and is the main source of wear protection [93, 94].
- Mending Effect: MoS_2 nanoparticles can accumulate in and fill up existing scratches or valleys on worn surfaces, effectively "repairing" the surface and making it smoother [93, 94, 95].

- Polishing Effect: Hard nanoparticles can gently smooth out surface asperities (rough peaks) through a mild abrasion process, reducing the overall surface roughness and, consequently, friction [96, 97].
- Rolling/Sliding: As mentioned above, spherical nanoparticles can act as tiny ball bearings, while nano-sheets facilitate sliding between the friction surfaces.

4.2.3 Wear rate of the hybrid iron matrix composite with the addition of nano-MoS_2

Figure 48 wear rate results demonstrate a significant improvement in wear resistance with the addition of MoS_2 to the composite. Pure Fe exhibited the highest wear rate 0.164 mg/s, while the composite without MoS_2 reduced it to 0.089 mg/s, indicating the beneficial effect of reinforcement. Further incorporation of MoS_2 progressively decreased the wear rate to 0.075, 0.048, and 0.036 mg/s for 0.5, 1.0, and 1.5 vol .% MoS_2, respectively. The lowest wear rate obtained at 1.5 vol. % MoS_2 represents an overall reduction of approximately 78% compared to pure Fe. This improvement can be attributed to the solid lubricating nature of MoS_2, which forms a protective tribo-film, minimises direct metal-to-metal contact, and reduces friction and material removal during sliding. Overall, increasing the MoS_2 content effectively enhances the wear resistance of the composite.

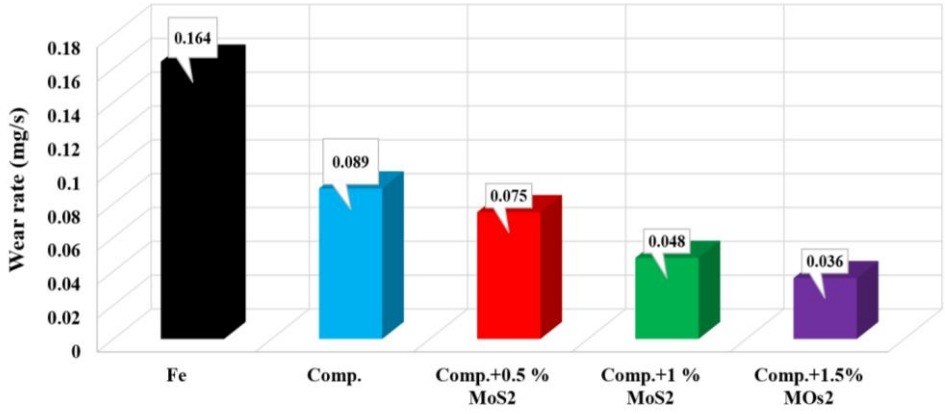


Figure 48.Wear rate of iron, master composite and iron matrix composites with varying concentrations (0.5, 1, and 1.5 vol.%) of nano-MoS_2

4.2.4 Hardness of the hybrid iron matrix composite with the addition of nano-MoS_2

Figure 49 shows the effect of nano- MoS_2 addition on the Rockwell hardness of the hybrid iron matrix composite. The hardness increases from 77.5 HRC for Fe to 82 HRC for the master composite. With increasing nano-MoS_2 content, the hardness further improves to 93 HRC, 94 HRC, and 94.5 HRC for 0.5, 1.0, and 1.5 vol.% MoS_2, respectively. Overall, MoS_2 addition enhances the hardness of the composite, with the highest value obtained at 1.5 vol.% MoS_2, although the improvement beyond 0.5 vol. % is relatively small

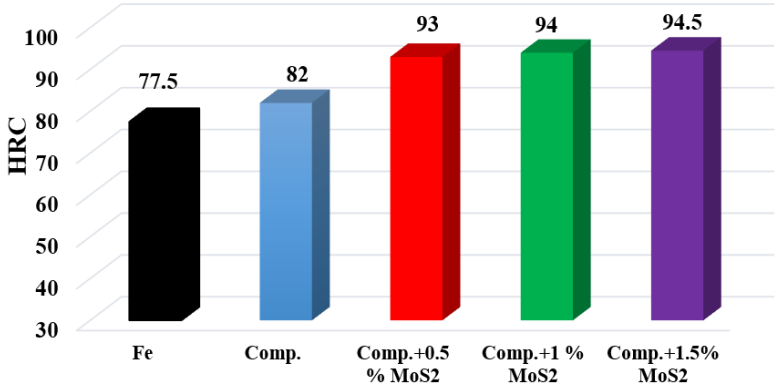


Figure 49. Hardness of iron, master composite and iron matrix composites with varying concentrations (0.5, 1, and 1.5 vol.%) of nano-MoS_2

4.2.5 SEM and EDX of the hybrid iron matrix composite with the addition of nano-MoS_2

Scanning electron microscopy (SEM) of the compacted and sintered Fe-Al_2O_3-ZrO_2/0.5 vol.% nano-MoS_2 hybrid metal matrix composite reveals a well-densified matrix with continuous grain boundaries (Figure 50). At lower magnifications (5,000× and 10,000×), complex subgrain architectures reminiscent of dendritic or faceted structures are visible. These observations suggest strong solid-state diffusion and possible local partial liquid-phase sintering pathways during high-temperature processing.

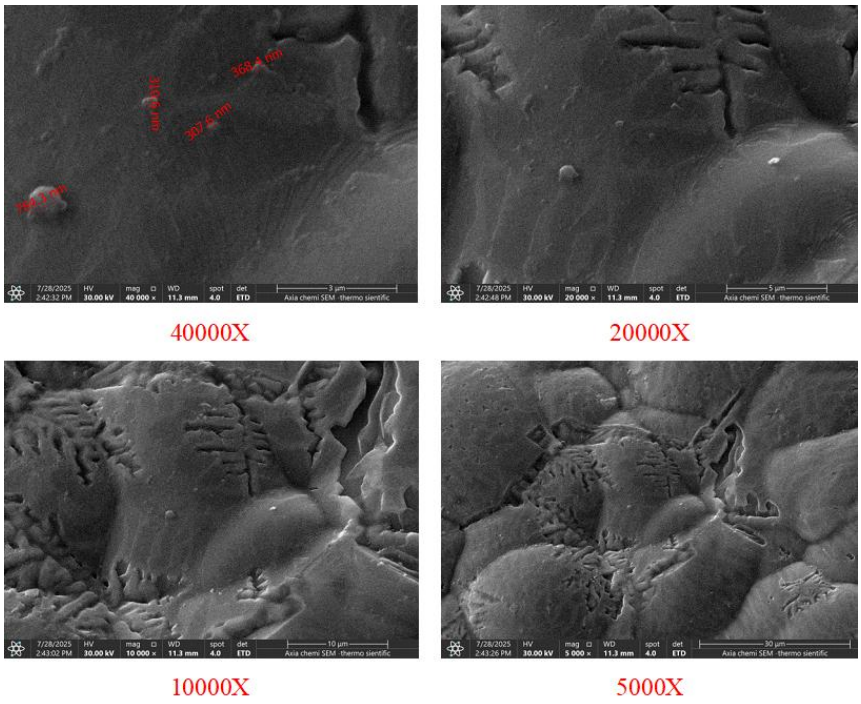


Figure 50. The depiction of the Fe-Al_2O_3-ZrO_2 / 0.5 vol.% Nano-MoS_2 hybrid metal matrix composite at different magnifications (5000×, 10,000×, 20,000×, and 40000×) under scanning electron microscopy (SEM) with focus on the matrix grain morphology, dendritic/faceted structures, and localized nanoscale phase distributions.

At higher magnifications (20,000× and 40,000×), nanoscale and sub-micron structural features (approximately 308-784 nm) are localized along subgrain boundaries and triple junctions. These features may be attributed to single dispersoids or nano-agglomerates of the secondary ceramic and solid lubricant phases. The localization of these nano-phases at grain boundaries suggests they may contribute to Zener pinning, a mechanism that can effectively reduce grain growth during thermal sintering [71]. Furthermore, the clean interfacial transition zones observed between these secondary features and the iron matrix are consistent with good wettability, which may facilitate mechanical interlocking and help reduce structural macro-porosity [74].

The topographic features were correlated with the local elemental composition by using spot energy-dispersive X-ray spectroscopy (EDS) (Figure 51). The most abundant element is iron (Fe), which again indicates the continuity of the core matrix. In addition, separate peaks for oxygen (O), aluminum (Al), and zirconium (Zr) were also found, in agreement with the presence of the desired oxide ceramic reinforcements (Al_2O_3 and ZrO_2).

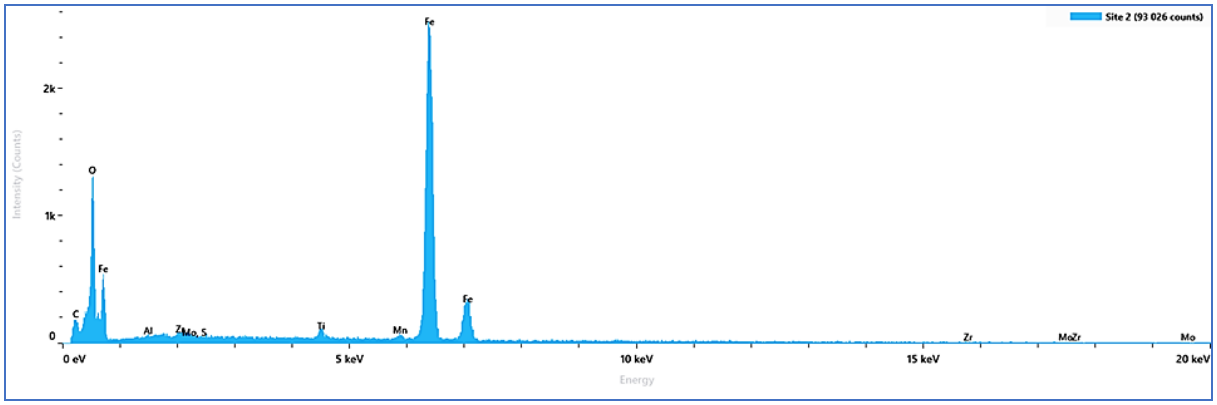


Figure 51. The energy-dispersive X-ray spectroscopy (EDS) spectrum of the compacted and sintered Fe-Al_2O_3-ZrO_2 / 0.5 vol % Nano-MoS_2 hybrid metal matrix composite with the elemental distribution of the matrix base, reinforcing ceramic phases, and solid lubricant.

Significantly, chemical signals for molybdenum (Mo) and sulfur (S) were detected. The relative stability of the sulfur signal indicated that processing conditions did not cause complete dissociation or volatilization of the sulfur source even though it is not possible to make an absolute statement, MoS_2 was likely processed to a lower extent of thermal dissociation or volatilization of the sulfur source [98]. It is suggested that this is because the MoS_2 lubricating phases were successfully retained in the sintered matrix.

Other trace elements were also identified, such as carbon (C), manganese (Mn), and titanium (Ti). The carbon signal is probably from environmental contamination or from the compaction binder that is left behind, while the Mn and Ti signals are probably from residual trace alloying elements which may be incorporated into the ferrite matrix for solid-solution

strengthening. Overall, it is believed that the correlation of the morphological structures (Figure 50) and the local EDS data (Figure 51) is indicative of an elemental distribution that is consistent with the targeted hybrid composite architecture, designed to support both structural load-bearing and self-lubricating properties.The microstructural features of the Fe-Al_2O_3-ZrO_2 hybrid metal matrix composite with 1.0 vol.% of nano-MoS_2 are presented in Figure 52. The composite shows a very well-crystallized and distinctly granular structure at lower magnifications (5,000× and 10,000×). The advanced solid-state sintering kinetics, along with the good matrix densification, is evidenced by the sharp geometric facets and the steps at the grain boundaries [70].

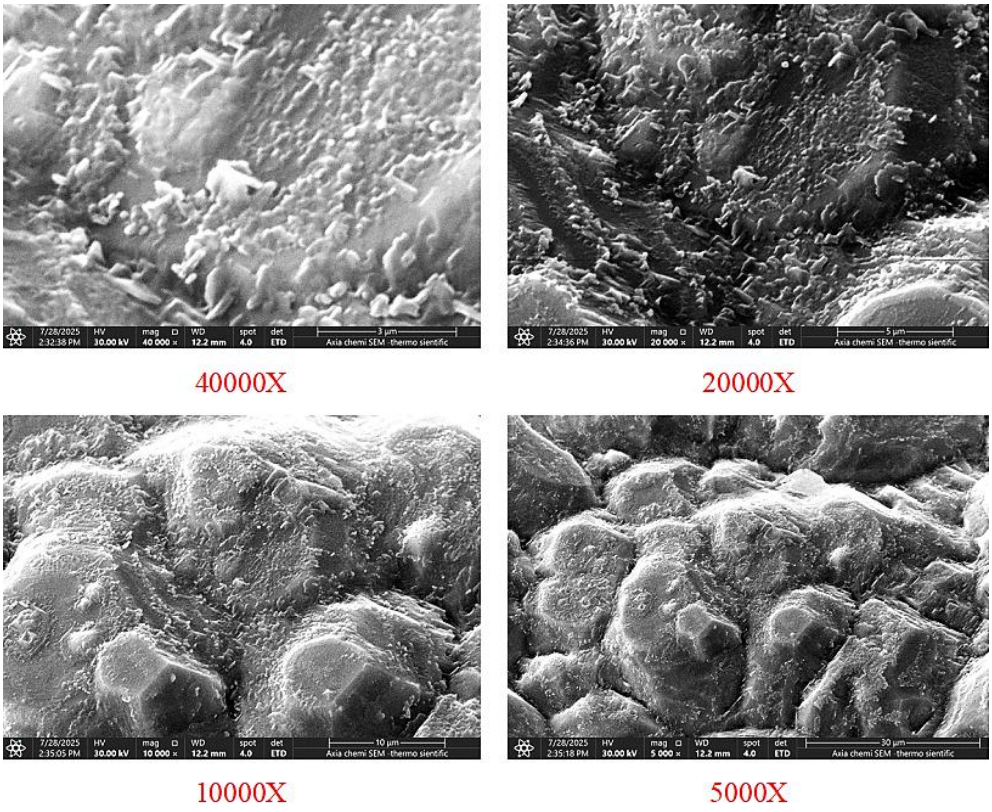


Figure 52. Scanning electron microscopy (SEM) micrographs of the Fe-Al_2O_3-ZrO_2 / 1.0 vol.% nano-MoS_2 hybrid metal matrix composite at various magnifications (5,000×, 10,000×, 20,000× and 40,000×) show highly faceted grain structures and dense surface decoration with nanoscale solid lubricant particles.

The surface of the primary matrix grains is decorated at higher magnification (20,000× and 40,000×) with submicron and even nanoscale nodular and elongated particulates. This grain cleavage/partitioned texture observed in the surface morphology may be explained by the higher weight fraction of the nano-MoS_2 phase (1.0 vol.%)) that seems to spread during processing along grain cleavage planes and grain boundaries [98]. These surface-dwelling nanoparticles have a high local concentration that could be used for two opposing structural

functions. First, the observations indicate that they may be barriers to v grain structure [71]. Second, compared to the grain faces, these nanoparticles are highly dispersed, and hence, the solid lubricant phase is easily accessible at the sliding contact, which could help to form the tribofilm under wear conditions [74].

To understand the chemical composition of this highly textured morphology, localized energy-dispersive X-ray spectroscopy (EDS) was performed (Figure 53). This produced strong Fe Kα (~6.4 keV) and Fe Kβ (~7.05 keV) peaks, which indicate the preservation of the base iron phase. The amount of oxygen (O), along with the clearly identifiable lines for aluminum (Al) and zirconium (Zr), indicates that the Al_2O_3 and ZrO_2 ceramic reinforcements were successfully introduced.

.

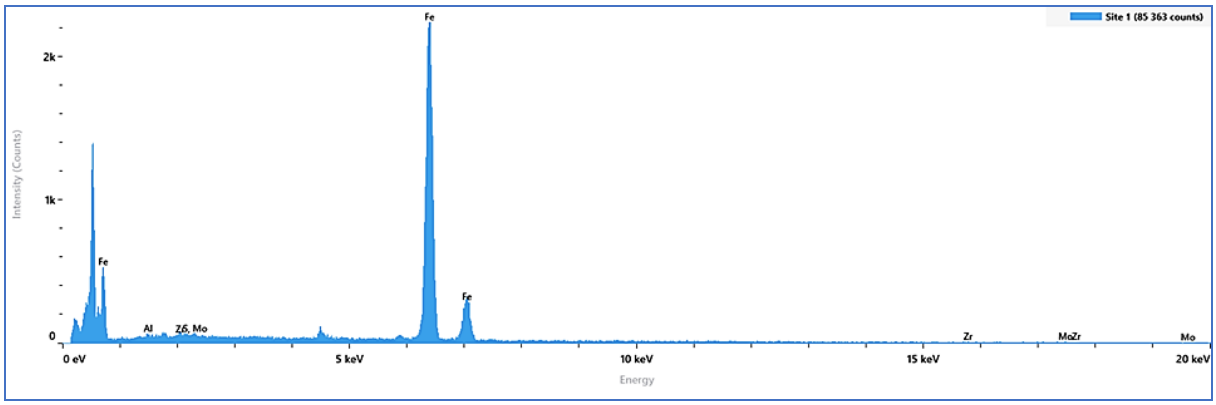


Figure 53. The energy-dispersive X-ray spectroscopy (EDS) spectrum of the compacted and sintered Fe-Al_2O_3-ZrO_2 / 1.0 vol.% nano-MoS_2 hybrid metal matrix composite with the elemental distribution of the matrix base, reinforcing ceramic phases, and solid lubricant.

Notably, the elemental markers for sulfur (S) and molybdenum (Mo) are strong near 2.3 keV and 17.5 keV, respectively. The presence of the strong sulfur and molybdenum signals in the spectra does not indicate the complete preservation of MoS_2 as a compound, but the stability of the strong sulfur and molybdenum signals implies that severe thermal dissociation and desulfurization a common technical challenge in the processing of iron-sulfide systems [99] were effectively suppressed by the local inert or reduced-sintering atmosphere. Small amounts of carbon (C), manganese (Mn), and titanium (Ti) were also detected. Mn and Ti are probably present as part of the iron powder alloy and can be included in solid-solution strengthening of the ferritic lattice [73], while the carbon signal is likely caused by ambient surface hydrocarbons or residual organic binder. Finally, the microstructural and elemental studies reveal that nano-MoS_2 when added to the composite yields a structurally coherent and highly textured hybrid composite. Features observed may be accounted for by retention of both hard

ceramic reinforcements and solid lubricant precursors in the areas of interest, which would help maintain structural integrity and provide the potential for self-lubrication characteristics.

The topography of microstructures of the Fe-Al_2O_3-ZrO_2 hybrid composite is changing after introduction of nano-MoS_2, and a heterogeneity of microstructures is noticeable (Figure 54). At lower magnifications, the binary morphology of the relatively smooth iron matrix areas and highly saturated particulate areas can be seen. The spatial distribution of the nanoparticles observed is not uniform throughout the specimen, but rather seems to be regionally segregated and clustered into nanoparticles. This localized agglomeration may be attributed to the high surface energy of the nanomaterials during the blending phase, where clusters become trapped at intergranular boundaries during compaction and solid-state sintering [70].

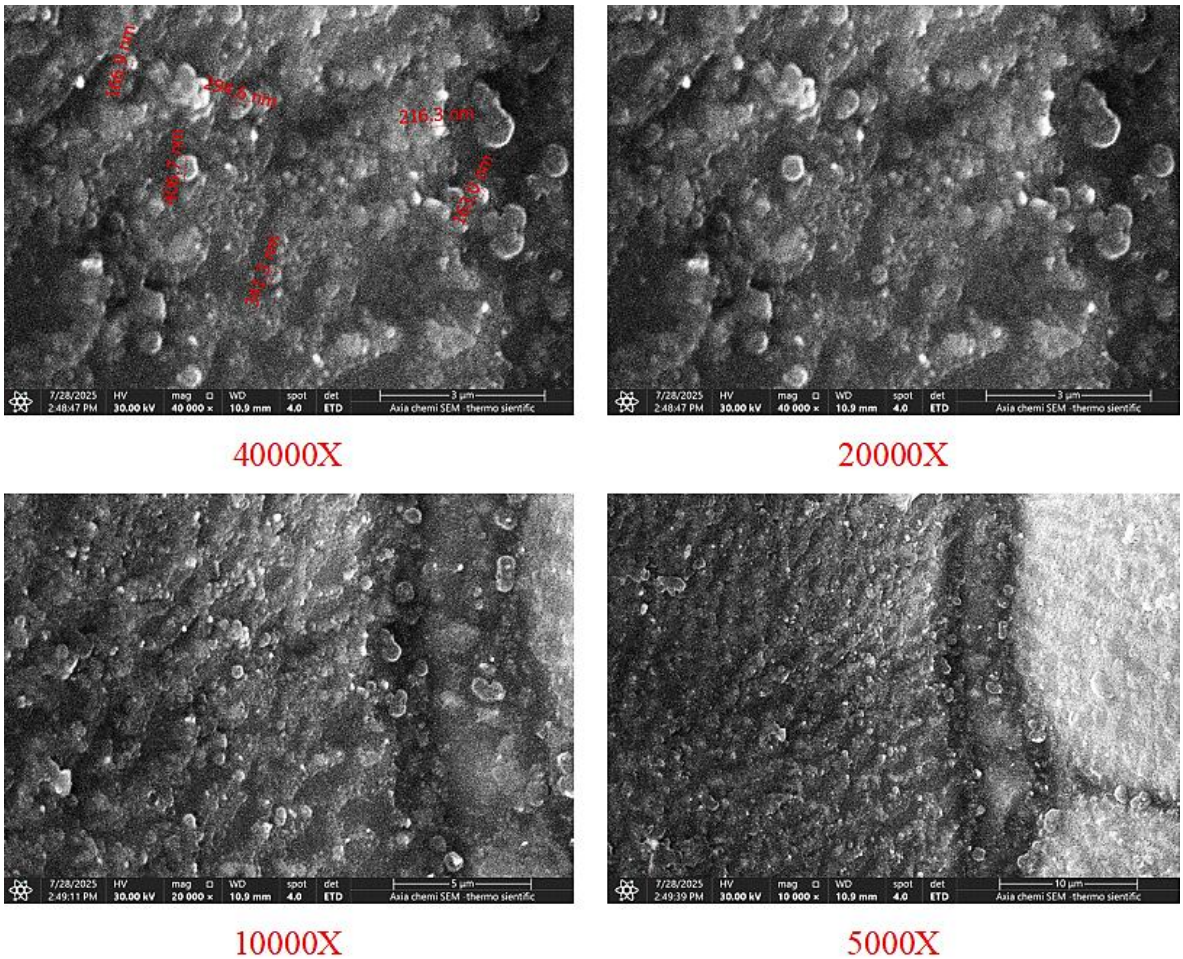


Figure 54. Scanning electron microscopy (SEM) micrographs of the Fe-Al_2O_3-ZrO_2 / 1.5 vol.% nano-MoS_2 hybrid metal matrix composite at various magnifications (5,000×, 10,000×, 20,000× and 40,000×) show highly faceted grain structures and dense surface decoration with nanoscale solid lubricant particles.

High-magnification micrographs (Figure 54, 20,000× and 40,000×) reveal abundant sub-micron globular particulates with a relatively narrow size distribution ranging from 163.0 nm

to 416.2 nm. While the close packing of such particulate arrays is generally effective for solid lubrication, high weight fractions tend to clump. A possible explanation for the reduction of bulk hardness and tensile strength in the composite is that severe agglomeration during sintering prevents localized matrix-to-matrix metallurgical bonding, thereby creating stress-concentration zones [99].

Spot EDS analysis (Figure 55) was utilized to assess the local chemical environment of these highly populated microstructural zones. The high-intensity Fe peaks (~6.4 keV and ~7.05 keV) are in agreement with the main iron matrix. Separate signals are also measured for Aluminum (Al), Zirconium (Zr), and Oxygen (O), reflecting the presence of the original oxide-reinforcing components. Also, the identification of Mo and S peaks suggests that Mo and S were retained in the matrix. This observation indicates that volatilization from the lubricant was avoided at the macroscale in the thermal processing window [98]. Small peaks for minor elements (Si, Na, C, and Ti) that are detected at low intensity could be from processing-contaminating materials (wear from the milling media, binder residues, etc. [73]) or the presence of micro-alloying components in the raw iron powder.

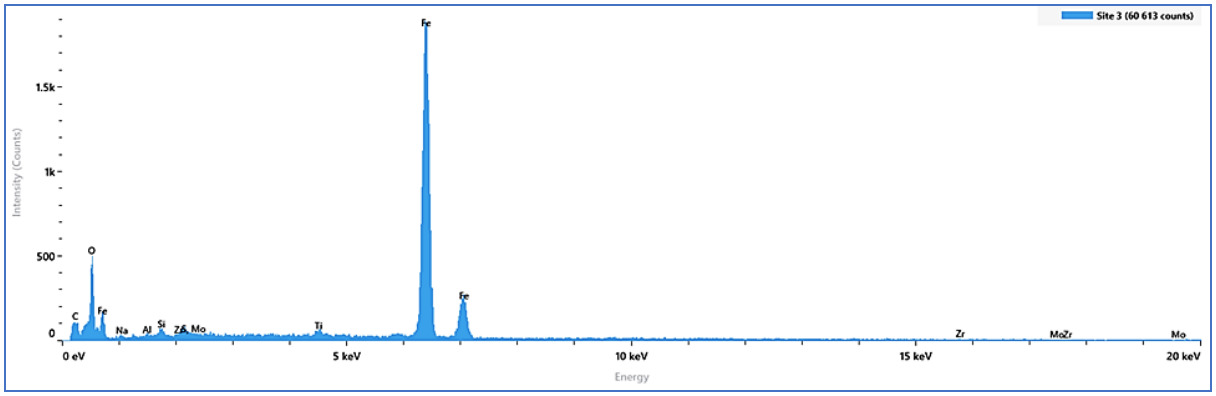


Figure 55. The energy-dispersive X-ray spectroscopy (EDS) spectrum of the compacted and sintered Fe-Al_2O_3-ZrO_2 / 1.5 vol.% nano-MoS_2 hybrid metal matrix composite, along with the elemental distribution of the matrix base, reinforcing ceramic phases, and solid lubricant.

The observations indicate that the 1.5 vol. % nano-MoS_2 formulation contains sub-micron particulates (163.0–416.2 nm) which may be able to form a lubricious surface layer, but may also have a very strong tendency to agglomerate locally. Based on this agglomeration tendency, this suggests that a volume fraction of 1.5 vol.% may be the maximum limit for lubricant addition in this particular Fe-Al_2O_3-ZrO_2 processing system without a major degradation in mechanical structural integrity.

Chapter Five /Conclusions

4.1 Conclusions of Adding Nano-Graphite :

1- The hybrid Fe–Al_2O_3–ZrO_2 composite exhibited higher compressive strength than pure iron. The addition of nano-graphite further enhanced the strength; the highest value of 243.07 MPa was obtained with 1.5 vol% nano-graphite, representing an improvement of approximately 53% compared with pure iron.

2- The incorporation of Al_2O_3 and ZrO_2 increased the hardness of iron from 77.5 HRC to 82 HRC. Adding nano-graphite produced a further increase, with the maximum hardness of 96 HRC achieved at 1 vol% nano-graphite, while a slight decrease at 1.5 vol% was attributed to nanoparticle agglomeration.

3- Nano-graphite effectively reduced the coefficient of friction from 0.742 for pure iron to 0.34 at 1.5 vol% nano-graphite, demonstrating its excellent self-lubricating behaviour and ability to reduce sliding resistance.

4- The combined addition of ceramic reinforcements (Al_2O_3 and ZrO_2) and nano-graphite produced a synergistic strengthening effect by improving load transfer, restricting dislocation motion, and enhancing the microstructural stability of the iron matrix.

5- Although 1 vol% nano-graphite provided the highest hardness, 1.5 vol% nano-graphite delivered the best overall performance by achieving the highest compressive strength and the lowest coefficient of friction, making it the optimum composition for applications requiring high mechanical strength and improved tribological performance.

4.2 Conclusions of Adding Nano-MoS_2 :

1- The addition of nano-MoS_2 further enhanced the mechanical properties, with the compressive strength increasing from 158.4 MPa for pure iron to 210.5 MPa at 1.5 vol% MoS_2.

2- Nano-MoS_2 effectively reduced the coefficient of friction from 0.742 for pure iron to 0.390 at 1.5 vol.% through the formation of a solid-lubricating film that minimised direct metal-to-metal contact.

3- The hardness increased from 77.5 HRC for pure iron to 94.5 HRC at 1.5 vol. % MoS_2, although the improvement became marginal beyond 0.5 vol% MoS_2.

4- Among the investigated compositions, 1.5 vol % nano-MoS_2 exhibited the best overall performance, providing the highest compressive strength, 210.5 MPa, the lowest coefficient of friction, 0.390 and the highest hardness, 94.5 HRC. These improvements are attributed to the combined strengthening effect of Al_2O_3 and ZrO_2 reinforcements, together with the solid-lubricating and reinforcing action of nano-MoS_2

4.3 Conclusions on Adding Nano- Graphite and Nano-MoS_2

1- Both nano-MoS_2 and nano-graphite significantly improved the mechanical and tribological properties of the hybrid iron matrix composite. Nano-graphite provided a greater improvement in compressive strength and hardness, and reduced the coefficient of friction and enhanced wear resistance because of its superior solid-lubricating behaviour.

2- The enhancement in compressive strength due to the addition of zirconia and alumina is about 12.75% compared to pure iron. The maximum enhancement in compressive strength from adding 1.5 vol% nano-Gr to iron-MC is about 53.45% compared to pure iron and about 36.1% compared to iron-MC. On the other hand, the maximum enhancement in compressive strength from adding 1.5 vol% nano-MoS_2 to iron-MC is about 32.8% compared with pure iron and about 17.86% compared with iron-MC.

3- The enhancement in the coefficient of friction due to the addition of zirconia and alumina is about 43.9% compared with pure iron (i.e. Coefficient of friction of iron-MC is smaller than that of pure iron). While the maximum enhancement in the coefficient of friction due to adding 1.5 vol % of Nano-Gr to iron-MC is about 54% compared to pure iron and about 18% compared with iron-MC. On the other hand, the maximum enhancement in the coefficient of friction due to adding a 1.5 vol % of Nano- MoS_2 to iron-MC is about 47.4% compared to pure iron and about 6.25% compared to iron-MC.

4- The wear rate enhancement due to the addition of zirconia and alumina is about 45.7% compared to pure iron (i.e., the wear rate of iron-MC is lower than that of pure iron). While the maximum wear rate enhancement due to adding 1.5 vol% of nano-Gr to iron-MC is about 84.75% compared with pure iron and about 71.9% compared to iron-MC. On the other side, the maximum wear rate enhancement due to adding a 1.5 vol% of nano- MoS_2 to iron-MC is about 78% compared with pure iron and about 59.5% compared with iron-MC.

5- The enhancement in hardness due to adding 1 vol% of nano-Gr compared to iron and master composite was (23.87 and 7.87) %, respectively. While the enhancement in

hardness of volume frication 1.5%of nano-MoS_2 compared to iron and master composite was (21.94 and 15.94) %, respectively.

THESES – NEW SCIENTIFIC RESULTS

Thesis 1. It succeeded in improving the properties of iron by preparing an iron matrix composite by replacing 3 vol.% of iron with (2.4 vol% alumina, 0.6 vol% zirconia). The samples were sintered at 1120 °C. A furnace (Laboratory Vacuum Sintering Furnace) was used at a heating rate of 16 °C /min under pure argon at a flow rate of 10 L/min. The incorporation of Al_2O_3 and ZrO_2 ceramic reinforcements into the iron matrix increased the compressive strength by 12.75%, owing to the high stiffness of the ceramic particles and their ability to transfer the applied load and restrict plastic deformation. The coefficient of friction decreased by 1.68%, indicating improved sliding behaviour resulting from the enhanced load-bearing capacity of the reinforced matrix. A much greater improvement was observed in the wear rate, which decreased by 45.73%, demonstrating that the hard ceramic particles effectively protected the iron matrix against material removal during sliding. In addition, the Rockwell hardness increased by 5.81%, confirming that the Al_2O_3 and ZrO_2 reinforcements enhanced the resistance of the iron matrix to plastic deformation and contributed to the overall improvement in mechanical and tribological performance. Table A shows the summary results compared between pure Iron and the composite.

Table A. Results compared between pure Iron and composite.

Property	Pure iron	Master composite	Improvement
Compressive strength (MPa)	158.40	178.60	+12.75 %
Coefficient of friction	0.416	0.409	-1.68 %
Wear rate (mg/s)	0.164	0.089	-45.7 %
Rockwell hardness (HRC)	77.5	82	+5.81 %

Related Pulication: Sulaiman Mustafa Khazaal**, Nasri S.M. Nimer, Sz´avai Szabolcs, Luay S. Al Ansari, Husam Jawad Abdulsamad, Study of manufacturing and material properties of the hybrid composites with metal matrix as tool materials, **Results in Engineering**, Volume 16, December 2022, 100647), https://doi.org/10.1016/j.rineng.2022.100647 **(journal rank: Q1)

***Related International conference oral presentation: Sulaiman AL-TIMMIMI**, Szabolcs SZÁVAI, Investigation of Manufacturing and Material Characteristics of Metal Matrix Hybrid Composites for Tool Applications, 12. International Summit Scientific Research Congress, Date:29.05.2024*

***Sulaiman Mustafa,** Szávai Szabolcs, Investigation of the Properties of Iron-Based Composites Reinforced with Aluminium Oxide and Zirconium Oxide, 3rd International Yeditepe Scientific Research Congress, Conference, 12 October 2025*

Thesis 2. I developed a unique hybrid iron matrix composite with a low coefficient of friction and high hardness. It was prepared by adding 0.5, 1, and 1.5 vol% of nano-graphite to the master composite (97 vol.% iron, 2.4% alumina, and 0.6 vol.% zirconia) and sintering at 1120

°C in a vacuum furnace. The addition of nano-graphite significantly enhanced the mechanical and tribological properties. Compressive strength increased with increasing nano-graphite content, reaching 243.07 MPa at 1.5 vol.% nano-graphite, while the maximum hardness, 96 HRC, was obtained at 1.0 vol.% nano-graphite. A slight reduction in hardness at 1.5 vol.% nano-graphite was attributed to possible nanoparticle agglomeration. The coefficient of friction and wear rate decreased continuously with increasing nano-graphite content, reaching minimum values of 0.341 and 0.025 mg/s, respectively, at 1.5 vol.% nano-graphite. These improvements are attributed to the synergistic effect of the hard Al_2O_3–ZrO_2 ceramic particles and the self-lubricating nano-graphite, which enhances load transfer, improves interfacial bonding, and forms a protective lubricating tribofilm during sliding. Overall, 1.5 vol.% nano-graphite provided the best overall balance of mechanical strength and tribological performance. Table B shows the summary improvement properties of the effective add nano-graphite on pure iron and master composite properties.

Table B: Effect of nano-graphite addition on the mechanical and tribological performance compared with pure iron and the master composite.

Master Composite with added	Compressive strength improvement Comparison		Coefficient of Friction Improvement Comparison		Wear rate improvement Comparison		Hardness Improvement Comparison	
	Pure iron	Master Composite	Pure iron	Master Composite	Pure iron	Master Composite	Pure iron	Master Composite
0.5 vol% nano-Gr	**+ 37.5 %**	**+ 22 %**	**- 44.9%**	**-1.68%**	**- 62.20 %**	**- 30.34%**	**+ 20.56 %**	**+5.06 %**
1 vol% nano-Gr	**+ 38.4 %**	**+ 22.7%**	**- 49.3%**	**-9.62%**	**- 83.32 %**	**- 67.42 %**	**+23.87 %**	**+7.87%**
1.5 vol% nano-Gr	**+ 53.5 %**	**+ 36.1 %**	**- 54.0%**	**-18.03%**	**- 84.76%**	**- 71.91%**	**+21.94%**	**+6.18%**

Related Publication: Sulaiman Mustafa Khazaal, *Szavai Szabolcs, Nasri S.M. Nimer, Improvement of the Mechanical and Tribological Properties of Hybrid Iron Matrix Composites by Adding Nano-graphite, Materials Design and Processing Communications, Q2 (Under Review)*

Related International conference oral presentation: Sulaiman Mustafa Khazaal, *Szávai Szabolcs, Self-lubricating metal composites using graphite nanoparticles: A review,14th International Zeugma Congress on scientific research, 9th September 2025.*

Sulaiman AL-TIMMIMI, Szabolcs SZÁVAI, Enhance the Compressive Strength of the Hybrid Metal Matrix Composite by Adding Nanoparticles,11th International Scientific Conference on Advances in Mechanical Engineering (ISCAME),7th November 2025.

Thesis 3. Enhance and study the properties of a novel hybrid iron matrix composite by adding 0.5, 1.0, and 1.5 vol% nano-MoS_2 into a master composite consisting of 97 vol% iron, 2.4 vol% alumina, and 0.6 vol% zirconia. The prepared composites were subsequently sintered in

a vacuum furnace at 1120 °C to achieve the desired microstructure and properties. The addition of nano-MoS_2 significantly enhanced the mechanical and tribological performance of the hybrid iron matrix composite. Compressive strength increased progressively with increasing MoS_2 content, reaching a maximum value of 210.5 MPa at 1.5 vol.% MoS_2, indicating improved load-bearing capacity due to the combined strengthening effect of the ceramic reinforcements and nano-MoS_2. The Rockwell hardness also increased from 82 HRC for the master composite to 94.5 HRC, demonstrating enhanced resistance to plastic deformation. Tribological properties showed marked improvement, with the coefficient of friction decreasing from 0.416 to 0.390 and the wear rate reducing from 0.089 to 0.036 mg/s as the MoS_2 content increased. These improvements are mainly attributed to the solid-lubricating behaviour of MoS_2, which forms a protective tribofilm during sliding, reducing metal-to-metal contact, minimising material removal, and improving wear resistance. Overall, 1.5 vol% nano-MoS_2 provided the best combination of mechanical strength, hardness, and tribological performance among the investigated compositions. Table C shows the summary of improved properties by add nano-MoS_2 on pure iron and the master composite properties.

Table C. Improvement in Mechanical and Tribological Properties with Nano-MoS_2 Addition Compared to Pure Iron and the Master Composite

Master Composite with added	Compressive strength improvement Comparison		Coefficient of Friction Improvement Comparison		Wear rate improvement Comparison		Hardness Improvement Comparison	
	Pure iron	Master Composite	Pure iron	Master Composite	Pure iron	Master Composite	Pure iron	Master Composite
0.5 vol% nano-MoS_2	**+ 19.44 %**	**+ 5.49 %**	**- 44.34 %**	**- 0.72 %**	**- 54.27 %**	**- 15.73 %**	**+ 20.00 %**	**+13.41 %**
1 vol% nano-MoS_2	**+23.30 %**	**+ 9.35 %**	**- 46.09 %**	**- 3.85 %**	**- 70.73 %**	**- 46.07 %**	**+21.29%**	**+ 14.63 %**
1.5 vol% nano-MoS_2	**+ 32.89 %**	**+17.86 %**	**- 47.44 %**	**- 6.25 %**	**- 78.05 %**	**- 59.55 %**	**+ 21.94%**	**+ 14.24 %**

Thesis 4. The addition of nano-graphite exhibited the highest reinforcing efficiency and tribological properties of the hybrid iron matrix composite, significantly compared with adding nano-MoS_2. From one of the most important perspectives, the economic perspective, nano-graphite is generally cheaper than nano-MoS_2 because of its lower production cost and greater commercial availability. The nano-graphite powder with a particle size below 400 nm costs approximately USD 1.93–2.29 per gram, whereas 100 nm MoS_2 nanopowder with 99.9% purity costs approximately USD 5.85–19.00 per gram

The composite reinforced with 1.5 vol.% nano-graphite exhibited the highest compressive strength, 243.07 MPa, compared with 210.5 MPa for 1.5 vol .% nano-MoS_2, indicating that

nano-graphite contributed more effectively to load transfer and strengthening of the iron matrix. In terms of hardness, the highest value of 96 HRC was achieved with 1.0 vol.% nano-graphite, whereas nano-MoS_2 reached a maximum hardness of 94.5 HRC at 1.5 vol.%, demonstrating a slightly lower strengthening effect.

Regarding tribological performance, both reinforcements markedly reduced the coefficient of friction and wear rate; however, nano-graphite exhibited superior performance. The lowest coefficient of friction 0.341 and wear rate 0.025 mg/s were obtained with 1.5 vol.% nano-graphite, compared with 0.390 and 0.036 mg/s, respectively, for 1.5 vol.% nano-MoS_2.

***Related International conference oral presentation: Sulaiman Mustafa Khazaal**, Szávai Szabolcs, Comparison of Self-lubrication in metal composites using nanoparticles MoS_2 and Graphite,14th International Zeugma Congress on Scientific Research, 9th September 2025.*

List of Publications

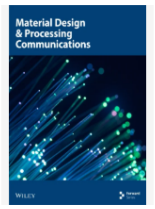
International Journal articles

1- **Sulaiman Mustafa Khazaal**, Nasri S.M. Nimer, Sz´avai Szabolcs, Luay S. Al Ansari, Husam Jawad Abdulsamad, Study of manufacturing and material properties of the hybrid composites with metal matrix as tool materials, **Results in Engineering**, Volume 16, December 2022, 100647), https://doi.org/10.1016/j.rineng.2022.100647 **(journal rank: Q1, IF:)**_

2- **Sulaiman Mustafa Khazaal** and Szávai Szabolcs, Effect of Hybrid Metal Matrix Composite Punch on the Deep Drawing Process, Journal of Composites Science: Journal, https://doi.org/10.3390/jcs7090370.**(Journal rank: Q2, IF:7.9)**

3- Hassan Hamoodi Mahdi, Sami Ali Nama, **SulaimaMustafa Khazaal** (2023). Experimental and numerical investigation on the free vibration characteristics of 3D printed springs with square cross sections. **Mathematical Modelling of Engineering Problems,** Vol. 10, No. 6, pp. 1961-1966. http://creativecommons.org/licenses/by/4.0/, **(journal ranked: Q3, IF:0.231)**

4- **Sulaiman Mustafa Khazaal,** Szavai Szabolcs, Nasri S.M. Nimer, Improvement of the Mechanical and Tribological Properties of Hybrid Iron Matrix Composites by Adding Nano-graphite, Materials Design and Processing Communications, Q2 (Under Review)



Improvement of the Mechanical and Tribological Properties of Hybrid Iron Matrix Composites by Adding Nano-graphite

Under Review

Manuscript ID: **MDP2-26-00064** Article type: **Research Article**

Publication: **Material Design & Processing Communications**

International conference oral presentation

1. **Sulaiman AL-TIMMIMI**, Szabolcs SZÁVAI, Investigation of Manufacturing and Material Characteristics of Metal Matrix Hybrid Composites for Tool Applications, 12. International Summit Scientific Research Congress, Date:29.05.2024
2. **Sulaiman AL-TIMMIMI**, Szabolcs SZÁVAI, Investigation of the Deep drawing technique used punch made from a Hybrid Metal Matrix Composite, 10th International
3. **Sulaiman AL-TIMMIMI**, Szabolcs SZÁVAI, Effect of reinforcement on Mechanical properties of iron metal matrix composites,10th International Scientific Conference on Advances in Mechanical, Engineering, Thursday, 7th of November 2024.

4. **Sulaiman Mustafa**, Szávai Szabolcs, Deep drawing steel by using a punch made from an iron matrix composite, 14th CUKUROVA International Scientific Research Conference, 29 March 2025.
5. **Sulaiman Mustafa**, Szávai Szabolcs, Tribological behavior of metal matrix composite: review, 14th CUKUROVA International Scientific Research Conference, 24 March 2025
6. **Sulaiman Mustafa Khazaal**, Szávai Szabolcs, Self-lubrication metal composites using graphite nanoparticles: A review,14th International Zeugma Congress on Scientific Research, 9th September 2025.
7. **Sulaiman Mustafa Khazaal**, Szávai Szabolcs, Comparison of Self-lubrication in metal composites using nanoparticles MoS2 and Graphite,14th International Zeugma Congress on Scientific Research, 9th September 2025.
8. **Sulaiman Mustafa,** Szávai Szabolcs, Investigation of the Properties of Iron-Based Composites Reinforced with Aluminium Oxide and Zirconium Oxide, 3rd International Yeditepe Scientific Research Congress, Conference, 12 October 2025.
9. **Sulaiman AL-TIMMIMI**, Szabolcs SZÁVAI, Enhance the Compressive Strength of the Hybrid Metal Matrix Composite by Adding Nanoparticles,11th International Scientific Conference on Advances in Mechanical Engineering (ISCAME),7th November 2025.
10. **Sulaiman Mustafa Khazaal Al-Timmimi** ,Szávai Szabolcs, Improve the coefficient of friction of the hybrid iron matrix composite by adding graphite nanoparticles, 9: International Antalya Scientific Research and Innovative Studies Congress, 20th November 2025

References:

[1] S. Das, S. Das, Properties for Polymer, Metal and Ceramic Based Composite Materials, in: Encyclopedia of Materials: Composites, Elsevier, 2021: pp. 815–821. https://doi.org/10.1016/B978-0-12-803581-8.11897-1.

[2] S.M. Sapuan, Materials Selection for Composites: Concurrent Engineering Perspective, in: Composite Materials, Elsevier, 2017: pp. 209–271. https://doi.org/10.1016/b978-0-12-802507-9.00006-4.

[3] D.A. Ashebir, G.A. Mengesha, D.K. Sinha, An Insight into Mechanical and Metallurgical Behavior of Hybrid Reinforced Aluminum Metal Matrix Composite, Advances in Materials Science and Engineering 2022 (2022). https://doi.org/10.1155/2022/7843981

[4] S. Dhanesh, K.S. Kumar, N.K.M. Fayiz, L. Yohannan, R. Sujith, Recent developments in hybrid aluminium metal matrix composites: A review, in: Mater Today Proc, Elsevier Ltd, 2021: pp. 1376–1381. https://doi.org/10.1016/j.matpr.2020.06.325.

[5] V. Khanna, V. Kumar, S.A. Bansal, Mechanical properties of aluminium-graphene/carbon nanotubes (CNTs) metal matrix composites: Advancement, opportunities and perspective, Mater Res Bull 138 (2021). https://doi.org/10.1016/j.materresbull.2021.111224.

[6] J.M. Mistry, P.P. Gohil, Research review of diversified reinforcement on aluminum metal matrix composites: Fabrication processes and mechanical characterization, Science and Engineering of Composite Materials 25 (2018) 633–647. https://doi.org/10.1515/secm-2016-0278.

[7] U.A. Essien, S. Vaudreuil, In-situ metal matrix composites development for additive manufacturing: a perspective, Journal of Achievements in Materials and Manufacturing Engineering 111 (2022) 78–85. https://doi.org/10.5604/01.3001.0015.9997.

[8] C.S. Kim, K. Cho, M.H. Manjili, M. Nezafati, Mechanical performance of particulate-reinforced Al metal-matrix composites (MMCs) and Al metal-matrix nano-composites (MMNCs), J Mater Sci 52 (2017) 13319–13349. https://doi.org/10.1007/s10853-017-1378-x.

[9] P. Samal, P.R. Vundavilli, A. Meher, M.M. Mahapatra, Recent progress in aluminum metal matrix composites: A review on processing, mechanical and wear properties, J Manuf Process 59 (2020) 131–152. https://doi.org/10.1016/j.jmapro.2020.09.010.

[10] N. Wu, W. Du, Q. Hu, S. Vupputuri, Q. Jiang, Recent development in fabrication of co nanostructures and their carbon nanocomposites for electromagnetic wave absorption, Engineered Science 13 (2021) 11–23. https://doi.org/10.30919/es8d1149.

[11] K. Luo, B. Bai, Microstructure, mechanical properties and high stress abrasive wear behavior of air-cooled MnCrB cast steels, Mater Des 31 (2010) 2510–2516. https://doi.org/10.1016/j.matdes.2009.11.040.

[12] C. Jin, C.C. Onuoha, Z.N. Farhat, G.J. Kipouros, K.P. Plucknett, Reciprocating wear behaviour of TiC-stainless steel cermets, Tribol Int 105 (2017) 250–263. https://doi.org/10.1016/j.triboint.2016.10.012.

[13] W. Wang, H. Qi, P. Liu, Y. Zhao, H. Chang, Numerical simulation of densification of Cu–Al mixed metal powder during axial compaction, Metals (Basel) 8 (2018). https://doi.org/10.3390/met8070537.

[14] J. Chen, Z. Xie, W. Zeng, W. Wu, Toughening mechanisms of ZTA ceramics at cryogenic temperature (77 K), Ceram Int 43 (2017) 3970–3974. https://doi.org/10.1016/j.ceramint.2016.11.072.

[15] D. Poquillon, V. Baco-Carles, P. Tailhades, E. Andrieu, Cold compaction of iron powders - Relations between powder morphology and mechanical properties: Part II. Bending tests: Results and analysis, Powder Technol 126 (2002) 75–84. https://doi.org/10.1016/S0032-5910(02)00035-9.

[16] A. Rodriguez-Contreras, M. Punset, J.A. Calero, F.J. Gil, E. Ruperez, J.M. Manero, Powder metallurgy with space holder for porous titanium implants: A review, J Mater Sci Technol 76 (2021) 129–149. https://doi.org/10.1016/j.jmst.2020.11.005.

[17] Z.Z. Fang, H. Wang, Sintering of ultrafine and nanosized ceramic and metallic particles, in: Ceramic Nanocomposites, Elsevier Inc., 2013: pp. 431–473. https://doi.org/10.1533/9780857093493.3.431.

[18] S. Das and S. Das, “Properties for Polymer, Metal and Ceramic Based Composite Materials,” in Encyclopedia of Materials: Composites, vol. 2, Elsevier, 2021, pp. 815–821. doi: 10.1016/B978-0-12-803581-8.11897-1.

[19] S. M. Sapuan, “Materials Selection for Composites: Concurrent Engineering Perspective,” in Composite Materials, Elsevier, 2017, pp. 209–271. doi: 10.1016/b978-0-12-802507-9.00006-4.

[20] D. A. Ashebir, G. A. Mengesha, and D. K. Sinha, “An Insight into Mechanical and Metallurgical Behavior of Hybrid Reinforced Aluminum Metal Matrix Composite,” 2022, Hindawi Limited. doi: 10.1155/2022/7843981.

[21] S. Dhanesh, K. S. Kumar, N. K. M. Fayiz, L. Yohannan, and R. Sujith, “Recent developments in hybrid aluminium metal matrix composites: A review,” in Materials Today: Proceedings, Elsevier Ltd, 2021, pp. 1376–1381. doi: 10.1016/j.matpr.2020.06.325.

[22] M. Gradzka-Dahlke, “A tribological study of composite material based on iron with addition of calcium pyrophosphate,” Wear, vol. 261, no. 11–12, pp. 1383–1389, Dec. 2006, doi: 10.1016/j.wear.2006.03.047.

[23] A. T. Alpas and J. Zhang, “Effect of Sic particulate reinforcement on the dry sliding wear of aluminium-silicon alloys (A356) _ 83,” 1992.

[24] J. Leng, L. Jiang, G. Wu, S. Tian, and G. Chen, “Effect of graphite particle reinforcement on dry sliding wear of SiC/Gr/Al composites,” Xiyou Jinshu Cailiao Yu Gongcheng/Rare Metal Materials and Engineering, vol. 38, no. 11, pp. 1894–1898, Nov. 2009, doi: 10.1016/s1875-5372(10)60059-8.

[25] P. K. Rohatgi, M. Tabandeh-Khorshid, E. Omrani, M. R. Lovell, and P. L. Menezes, “Tribology of metal matrix composites,” in Tribology for Scientists and Engineers: From Basics to Advanced Concepts, vol. 9781461419457, Springer New York, 2013, pp. 233–268. doi: 10.1007/978-1-4614-1945-7_8.

[26] W. Yang, Z. Deng, D. Zhang, P. Ke, and A. Wang, “Microstructure and tribological behavior of self-lubricating (Si:N)-DLC/MAO coatings on AZ80 magnesium substrate,” Acta Metallurgica Sinica (English Letters), vol. 26, no. 6, pp. 693–698, Dec. 2013, doi: 10.1007/s40195-013-0265-y.

[27] A. P. Sannino and H. J. Rack, “WEAR Dry sliding wear of discontinuously reinforced aluminum composites: review and discussion,” 1995.

[28] S. Srivastava and S. Mohan, “ Study of Wear and Friction of Al-Fe Metal Matrix Composite Produced by Liquid Metallurgical Method,” 2011.

[29] A.Vencl, A. RAC, I . Bobic, “Tribological Behaviour of Al-Based Mmcs and Their Application in Automotive Industry, Tribology in industry ,vol.26,2004.

[30] B. R. Manu, A. Gupta, and A. H. Jayatissa, “Tribological properties of 2D materials and composites- A review of recent advances,” Apr. 01, 2021, MDPI AG.

[31] Wenting Ye , Yeran Shi, Qing Zhou , Mingda Xie , Haifeng Wang , Benyebka Bou-Saïd and Weimin Liu, “Recent advances in self-lubricating metal matrix nanocomposites

reinforced by carbonous materials: A review," Dec. 01, 2024, KeAi Communications Co. doi: 10.1016/j.nanoms.2024.02.007

[32] D. K. Rajak and P. L. Menezes, "Application of Metal Matrix Composites in Engineering Sectors," in Encyclopedia of Materials: Composites, vol. 1, Elsevier, 2021, pp. 525–539. doi: 10.1016/B978-0-12-803581-8.11832-6.

[33] Massoud Malaki , Wenwu Xu, Ashish K. Kasar, Pradeep L. Menezes, Hajo Dieringa , Rajender S. Varma and Manoj Gupta, "Advanced metal matrix nanocomposites," Metals (Basel), vol. 9, no. 3, Mar. 2019, doi: 10.3390/met9030330.

[34] A. T. Sose, S. Y. Joshi, L. K. Kunche, F. Wang, and S. A. Deshmukh, "A review of recent advances and applications of machine learning in tribology," Jan. 26, 2023, Royal Society of Chemistry. doi: 10.1039/d2cp03692d.

[35] N. Salehi and A. Abareshi, "Study of structural, optical, and thermal properties in MoS2-based nanocomposites: iron and gold," Eur Phys J Plus, vol. 137, no. 11, Nov. 2022, doi: 10.1140/epjp/s13360-022-03502-z.

[36] H. D. Huang, J. P. Tu, L. P. Gan, and C. Z. Li, "An investigation on tribological properties of graphite nanosheets as oil additive," Wear, vol. 261, no. 2, pp. 140–144, Jul. 2006, doi: 10.1016/j.wear.2005.09.010.

[37] A. Dorri Moghadam, E. Omrani, P. L. Menezes, and P. K. Rohatgi, "Mechanical and tribological properties of self-lubricating metal matrix nanocomposites reinforced by carbon nanotubes (CNTs) and graphene - A review," Compos B Eng, vol. 77, pp. 402–420, Aug. 2015, doi: 10.1016/j.compositesb.2015.03.014.

[38] K. P. Furlan, J. D. B. de Mello, and A. N. Klein, "Self-lubricating composites containing MoS2: A review," Apr. 01, 2018, Elsevier Ltd. doi: 10.1016/j.triboint.2017.12.033.

[39] B. Sustarsic, L. Kosec, M. Kosec, B. Podgornik, and S. Dolinšek, "The influence of MoS2 additions on the densification of water-atomized HSS powders," J Mater Process Technol, vol. 173, no. 3, pp. 291–300, Apr. 2006, doi: 10.1016/j.jmatprotec.2005.04.122.

[40] Sulaiman Mustafa Khazaal , Nasri S.M. Nimer , Sz´ avai Szabolcs , luay S. Al Ansari and Husam Jawad Abdulsamad , "Study of manufacturing and material properties of the hybrid composites with metal matrix as tool materials" , Results in Engineering 16 (2022) 100647. https://doi.org/10.1016/j.rineng.2022.100647.

[41] W\.D. Callister Jr., D.G. Rethwisch, Fundamentals of Materials Science and Engineering: an Integrated Approach, John Wiley & Sons, 2020.

[42] J. Li, B.Y. Zong, Y.M. Wang, Experiment and modeling of mechanical properties on iron matrix composites reinforced by different types of ceramic particles Mat, Sci Eng A-Struct. 527 (2010), 7545–51. https://doi.org/10.1016/j.msea.2010.08.029

[43] A.A. Adebisi, M.A. Maleque, M.M. Rahman, Metal matrix composite brake rotor: historical development and product life cycle analysis, Int. J. Automot. Mech. Eng. 4 (2011) 471–480. \

[44] X. Zhang, M. Yu, H. Tang, G. Su, Effect of copper addition on microstructures and mechanical properties of in situ TiCp/Fe composites, Mater. Des. 32 (2011) 3560–3565. https://doi.org/10.1016/j.matdes.2011.01.026

[45] S. Wang, L. Song, Y. Qiao, M. Wang, Effect of carbide orientation on impact-abrasive wear resistance of High-Cr iron used in shot blast machine, Tribol. Lett. 50 (2013) 439–448. https://link.springer.com/article/10.1007/s11249-013-0140-z

[46] M. Mohammadnezhad, V. Javaheri, M. Shamanian, M. Naseri, M. Bahrami, Effects of vanadium addition on microstructure, mechanical properties and wear resistance of Ni-Hard4 white cast iron, Mater. Des. 49 (2013) 888–893. https://doi.org/10.1016/j.matdes.2013.02.043

[47] M. Lindroos, M. Apostol, V. Heino, K. Valtonen, A. Laukkanen, K. Holmberg, V. Kuokkala, The deformation, strain hardening, and wear behavior of chromiumalloyed hadfield steel in abrasive and impact conditions, Tribol. Lett. 57 (2015) 24. doi: 10.1007/s11249-015-0477-6

[48] J. Du, X.Y. Chong, Y.H. Jiang, Numerical simulation of mold filling process for high chromium cast iron matrix composite reinforced by ZTA ceramic particles, Int. J. Heat Mass Tran. 89 (2015) 872–883. https://doi.org/10.1016/j.ijheatmasstransfer.2015.05.046

[49] C. Exare, J.M. Kiat, N. Guiblin, F. Porcher, V. Petricek, Structural evolution of ZTA composites during synthesis and processing, J. Eur. Ceram. Soc. 35 (2015) 1273–1283. https://doi.org/10.1016/j.jeurceramsoc.2014.10.031

[50] W. Wang, R. Song, S. Peng, Z. Pei, Multiphase steel with improved impact-abrasive wear resistance in comparison with conventional Hadfield steel, Mater. Des. 105 (2016) 96–105.doi: 10.1016/j.matdes.2016.05.056

[51] Y.D. Sui, M.J. Zhou, Y.H. Jiang, Characterization of interfacial layer of ZTA ceramic particles reinforced iron matrix composites, J. Alloys Compd. 741 (2018) 1169–1174. https://doi.org/10.1016/j.jallcom.2018.01.199

[52] G. Amina, B.N. Eddine, Z. Moussa, Dry sliding wear investigation on tungsten carbide particles reinforced iron matrix composites, Mater. Res. Express 5 (2018) 11. DOI 10.1088/2053-1591/aade07

[53] S.J. Algodi, J.W. Murray, P.D. Brown, A.T. Clare, Wear performance of TiC/Fe cermet electrical discharge coatings, Wear 402 (2018) 109–123. https://doi.org/10.1016/j.wear.2018.02.007

[54] Radosław Maruda, Kamil Leksycki, Eugene Feldshtein, Eryk Sasiadek, Natalia Szczotkarz, Magdalena Odwazna, Kamil Ochał and Andrzej Gradzik Effects of Hard Oxides Reinforcing of Iron-Based MMCs on the Surface Topography Features after Finish Turning Advances in Science and Technology Research Journal 2023, 17(1), 15–22. https://doi.org/10.12913/22998624/157438

[55] K., Anand Babu, Jeyapaul, R., Gugulothu, Bhiksha and Varatharajulu, M. " A Retrospective Investigation on Hybrid Metal Matrix Composites: Materials, Processing Methods, and Properties of Composites" ; Iran. J. Chem. Chem. Eng. ; Vol. 42, No. 6, 2023. DOI:1021-9986/2023/6/1842-1870 29/$/7.02

[56] Xiaolong Cai , Mingzhi Shen , Baowei Cao , Mingxin Liu and Yunhua Xu "Microstructural characterization of chromium carbide-reinforced iron matrix composites prepared by combination of casting and heat treatment" Vacuum 216(5428):112477.2023. doi: 10.1016/j.vacuum.2023.112477

[57] Wenlong Dong, Xuefeng Yang, Kai Wang and Bowen Liu " Research and prospect of particle reinforced iron matrix composites " The International Journal of Advanced Manufacturing Technology Volume 128, pages 3723–3744 (2023). https://link.springer.com/article/10.1007/s00170-023-12050-4?utm_source=researchgate.net&utm_medium=article

[58] Yunlei Wang and Tullio Monetta " Systematic study of preparation technology, microstructure characteristics and mechanical behaviours for SiC particle-reinforced metal matrix composites" Journal of materials research and technology 2023; 25: 7470 -7497. https://doi.org/10.1016/j.jmrt.2023.07.145

[59] Wenlong Dong, Xuefeng Yang , Zhiqiang Zhang, Kai Wang and Bowen Liu "Microstructural evolution and performance analysis of WC-11Co reinforced iron matrix composites";Materials & Design 239 (2024) 112753 https://doi.org/10.1016/j.matdes.2024.112753

[60] Sai Chen , Shuangjie Chu and Bo Mao "Iron-Based Metal Matrix Composite: A Critical Review on the Microstructural Design, Fabrication Processes, and Mechanical Properties";Acta Metallurgica Sinica (English Letters) (2025) 38:1–44. https://doi.org/10.1007/s40195-024-01758-1

[61] Km. Pooja, Nazia Tarannum and Pallavi Chaudhary " Metal matrix composites: revolutionary materials for shaping the future"; Discover Materials (2025) 5:35. https://doi.org/10.1007/s43939-025-00226-6

[62] Engidayehu Mekonnen Alemu, Jana Petrů, Muhammad Nasir Bashir, Abdulrahman Aljabri, Joon Sang Lee , Irfan Anjum Badruddin, Bilal Akbar Chuddher, M. A. Fazal, Sami Ghazali, Abdulmalik Alkotami and Gulam Mohammed Sayeed Ahmed "Experimental investigation on mechanical properties of iron metal matrix reinforced with MAX phase V2AlC-GO" Nature - Scientific Reports ; (2026) 16:3944. https://doi.org/10.1038/s41598-025-33860-4

[63] Deutsches Institut für Normung 2009, Advanced technical ceramics - Monolithic ceramics - Guidance on the selection of test pieces for the evaluation of properties, Standard No. DIN EN 1006:2009, DIN Media, Berlin.

[64] ASTM International. 2019. Standard Test Methods of Compression Testing of Metallic Materials at Room Temperature. ASTM E9-19. West Conshohocken, PA: ASTM International.

[65] ASTM International. 2019. Standard Test Methods of Compression Testing of Metallic Materials at Room Temperature. ASTM E9-19. West Conshohocken, PA: ASTM International

[66] ASTM International, "Standard Test Method for Wear Testing with a Pin-on-Disk Apparatus," ASTM G99-23, West Conshohocken, PA, 2023. doi: 10.1520 /G0099-23

[67] Menezes, P.L., Rohatgi, P.K., Lovell, M.R. (2012). Self-Lubricating Behavior of Graphite-Reinforced Metal Matrix Composites. In: Nosonovsky, M., Bhushan, B. (eds)

Green Tribology. Green Energy and Technology. Springer, Berlin, Heidelberg. https://doi.org/10.1007/978-3-642-23681-5_17

[68] Omrani E, Moghadam AD, Kasar AK, Rohatgi P, Menezes PL. Tribological Performance of Graphite Nanoplatelets Reinforced Al and Al/Al2O3 Self-Lubricating Composites. Materials (Basel). 2021 Mar 3;14(5):1183. doi: 10.3390/ma14051183. PMID: 33802337; PMCID: PMC7959118.

[69] Khan, Z. U., Kausar, A., & Ullah, H. (2016). A Review on Composite Papers of Graphene Oxide, Carbon Nanotube, Polymer/GO, and Polymer/CNT: Processing Strategies, Properties, and Relevance. Polymer-Plastics Technology and Engineering, 55(6), 559–581. https://doi.org/10.1080/03602559.2015.1098693

[70] German, R. M. (2014). Sintering Science and Technology. John Wiley & Sons.

[71] Humphreys, F. J., & Hatherly, M. (2012). Recrystallization and Related Annealing Phenomena. Elsevier.

[72] Exner, H. E., & Arzt, E. (1996). Sintering processes. Physical Metallurgy, 1883-1943.

[73] ASM International Handbook Committee. (2015). ASM Handbook, Volume 7: Powder Metallurgy. ASM International.

[74] Tjong, S. C. (2007). Novel nanoparticle-reinforced metal matrix composites with enhanced mechanical properties. Advanced Engineering Materials, 9(8), 639-65.

[75] Tjong, S. C. (2013). Novel nanoparticle-reinforced metal matrix composites with enhanced mechanical properties. Advanced Engineering Materials, 15(11), 1032–1041.

[76] Orowan, E. (1948). Discussion on internal stresses. Symposium on Internal Stresses in Metals and Alloys, Institute of Metals, London, 451–453.

[77] Suryanarayana, C. (2019). Mechanical Alloying and Milling. Progress in Materials Science, 46(1-2), 1-184. (Excellent for explaining the hybrid milling/blending impurities and oxide integration).

[78] Torralba, J. M., da Costa, C. E., & Velasco, F. (2020). Sintering behavior and interfacial phenomena in iron-based metal matrix composites. Journal of Materials Processing Technology, 282, 116670.

[79]   Zhang, Z., & Chen, D. L. (2018). Consideration of Orowan strengthening effect in particulate-reinforced metal matrix composites: A review. Materials Science and Engineering: A, 483, 148–152.

[80] Gladman, T. (1966). On the theory of the pinning of grain boundaries by second-phase particles. Europhysics Letters, 11(12), 1045. (Classic reference for Zener pinning).

[81] Goldstein, J., et al. (2017). Scanning Electron Microscopy and X-ray Microanalysis. Springer.

[82] Neubauer, E., et al. (2010). Potential and limitations of carbon nanotubes and graphene in metal matrix composites. Composite Structures, 92(9), 2091-2095.

[83] Casati, R., & Vedani, M. (2014). Metal matrix composites reinforced by nanoparticles—a review. Metals, 4(1), 65-83.

[84] Casati, R., & Vedani, M. (2014). Metal matrix composites reinforced by nanoparticles—a review. Metals, 4(1), 65-83.

[85] Gözler, E., et al. (2018). Effect of graphene oxide and graphite nano-particles on the sintering behavior of iron matrix composites. Journal of Alloys and Compounds, 741, 685-697.

[86] Nieto, A., et al. (20160. Graphene reinforced metal and ceramic matrix composites: a review. International Materials Reviews, 62(5), 241-302.

[87] Shin, S. E., et al. (2015). Strengthening behavior in aluminum matrix composites reinforced with multi-walled carbon nanotubes. Composites Part A: Applied Science and Manufacturing, 74, 46-55. (Excellent for explaining the degradation threshold when carbon nanomaterials exceed critical volume fractions).

[88] Thümmler, F., & Oberacker, R. (1993). Introduction to Powder Metallurgy. Institute of Materials.

[89] Hengquan Jiang, Zehan Zhang, Aiyun Jiang, Zhongzheng Yang, Laigui Yu, I.N. Kavaliova, Maksim V. Prozhega, Yongxing Hao, MoS2 nanoadditives for lubrication: Morphology, surface chemistry, and mechanisms, Tribology International, Volume 214, Part A,2026,111151, ISSN 0301-679X, https://doi.org/10.1016/j.triboint.2025.111151.

[90] Chen Chen, Kaifei Wang and Lei Luo . AuNPs and 2D functional nanomaterial-assisted SPR development for the cancer detection: a critical review. Cancer Nanotechnology. (2022) 13:29. https://doi.org/10.1186/s12645-022-00138-7

[91] Hengyang Liu, Yong Xu, Enzhu Hu, Kunhong Hu,Synthesis and tribological properties of WS2/MoS2 micro-nano composite lubricant, Tribology International, Volume 204, 2025,110506, ISSN 0301-679X,https://doi.org/10.1016/j.triboint.2025.110506. (https://www.sciencedirect.com/science/article/pii/S0301679X25000015)

[92] Singh, P. ., & Sastry, S. V. A. R. (2025). Engineering Various Morphologies of 2 Dimensional Nanomaterials for Enhanced Nanolubricant Efficiency: A Review. Trends in Sciences, 22(7), 9606. https://doi.org/10.48048/tis.2025.9606

[93] Marina Benmansour, Pavel Afanasiev, Jules Galipaud, Béatrice Vacher, Lucile Joly-Pottuz, et al.. Influence of the Crystallinity on the Tribological Behavior of MoS2 Nanoparticles Stabilized by a Succinimide Dispersant. Tribology Letters, 2025, 73 (1), pp.36. ⟨10.1007/s11249-025-01972-7⟩. ⟨hal-04942851⟩

[94] Xu, Y., Peng, Y., You, T., Yao, L., Geng, J., Dearn, K., & Hu, X. (2018). Nano-MoS2 and Graphene Additives in Oil for Tribological Applications. In T. Saleh (Ed.), Nanotechnology in Oil and Gas Industries: Principles and Applications (pp. 151-191). (Topics in Mining, Metallurgy and Materials Engineering). Springer. https://doi.org/10.1007/978-3-319-60630-9_6

[95] Ru Yan, Hongyang Wang, Rui Dong, Ping Wen, Mingjin Fan,Tailorable MoS2 quantum dots nanofluids via coordination-confined growth for high-performance lubrication, Journal of Colloid and Interface Science, Volume 710, 2026, 140049,ISSN 0021-9797, https://doi.org/10.1016/j.jcis.2026.140049.

[96] Hongxing Wu, Liguo Qin, Guangneng Dong, Meng Hua, Shuncheng Yang, Junfeng Zhang, An investigation on the lubrication mechanism of MoS2 nano sheet in point contact: The manner of particle entering the contact area, Tribology International, Volume 107,2017, Pages 48-55, ISSN 0301-679X, https://doi.org/10.1016/j.triboint.2016.11.009.

[97] Renhui Zhang, Xue Yang, Jibin Pu, Zhongyi He, Liping Xiong,Extraordinary macroscale lubricity of sonication-assisted fabrication of MoS2 nano-ball and investigation of in situ formation mechanism of graphene induced by tribochemical reactions,Applied Surface Science,Volume 510,2020,145456,ISSN 0169-4332, https://doi.org/10.1016/j.apsusc.2020.145456.

[98] Mahathanabodee, S., et al. (2013). Effects of MoS2 particles on friction and wear behavior of SS316L/MoS_2 composites. Wear, 307(1-2), 164-173.

[99] Sahoo, S., et al. (2020). Synthesis and tribological performance of self-lubricating iron matrix composites: A review. Journal of Materials Research and Technology, 9(4), 9110-9125.